Electron energy distribution functions in helium, helium-neon and helium-nitrogen mixtures in low pressure discharge plasmas.

Mainwaring, E. E.

Award date:
1977

Awarding institution:
University of Bath

ELECTRON ENERGY DISTRIBUTION FUNCTIONS IN HELIUM, HELIUM-NEON AND HELIUM-NITROGEN MIXTURES IN LOW PRESSURE DISCHARGE PLASMAS.

submitted by E.E.Mainwaring for the degree
of Ph.D of the University of Bath.
1977.

E. Mainwaring

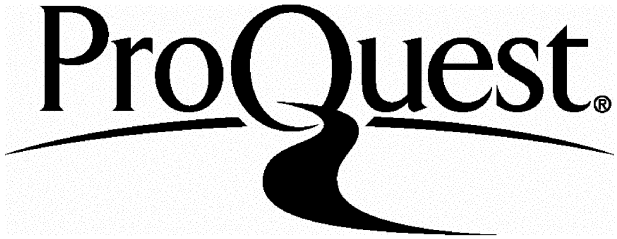

ACKNOWLEDGEMENTS

I wish to thank my supervisor Dr.J.D.Swift for suggesting the topic and for his constant advice.
I am indebted to the late Dr.R.Bolland and to Dr.T.Green of Bristol Polytechnic for their encouragement and support.
I am grateful to glassblowers Mr.P.Houlden of Bristol Polytechnic and Mr.M.Lock of the University of Bath for their help in the construction of the discharge tubes and vacuum system.

SUMMARY

Electron energy distribution functions in low pressure discharge plasmas have been investigated in helium, helium-neon and helium-nitrogen mixtures. The positive column of a discharge is examined by application of the probe analysis of Langmuir and Druyvesteyn. The second derivative of the probe current is obtained by measuring the second harmonic when an a.c. signal is superimposed on the d.c. bias applied to the probe.

The electron energy distribution curves are analysed and are generally found to be markedly non-maxwellian. The high energy tail region is examined for variations in pressure, longitudinal discharge current, location of measuring probe and for different mixture ratios. The electron densities and average electron energies are determined from the summation of areas under the distribution curves. Electron drift velocities and mobilities are calculated from an equation for the longitudinal discharge current derived from the Schottky positive column theory.

An asymmetrical double probe system is investigated and it is shown that the ratio of the reference probe area to that of the measuring probe must be 7000:1 to produce no distortion of the measurements. The necessary limit of probe radius to electron mean free path is also investigated.

The relationship between the second harmonic of the probe current ($i_{2\omega}$) and the amplitude(E) of the a.c. signal applied to the probe is investigated. A departure from the linear relationship of $i_{2\omega}$ v. E^2 is observed at higher values of E, but there are differences in behaviour for the gases nitrogen and helium. A theoretical explanation is proposed for these differences.

CONTENTS

CONTENTS (Contd.) Page:

CONTENTS (Contd.) Page:

INTRODUCTION.

The electron energy distribution function is fundamental to the understanding of most gas discharges and has been investigated both theoretically and experimentally by many workers. A literature search reveals that there are no adequate experimental techniques for directly evaluating the electron energy distribution function except in the limiting region where probes are applicable. It should be possible to use any property of a gas discharge which is dependent on electron energy to give the form of the distribution function. However, these properties relate to the distribution function and other parameters in a complex way and it makes it difficult to determine directly the distribution function.

The probe was first introduced in 1923 by Langmuir and Mott-Smith for measuring current-voltage characteristics in plasmas. Later, Druyvesteyn showed that the electron energy distribution function can be derived from the probe characteristic.

In this thesis the electron energy distribution functions in helium, helium-neon and helium-nitrogen are determined. The positive column of a low pressure discharge plasma is examined by application of the probe analysis of Langmuir and Druyvesteyn. This enables the electron energy distribution function to be obtained from an expression containing the second derivative of the probe current (with respect to the probe voltage) in the electron retarding region. A number of methods of obtaining the second derivative are available and these are reviewed in Chapter 2.

The present investigation uses a technique in which an a.c. signal is superimposed on the d.c. bias applied to the probe. The second harmonic of the probe current ($i_{2\omega}$) is detected which is proportional to the required second derivative. The probe theory and the theoretical basis of the second harmonic method are outlined in Chapter 3. The vacuum apparatus, probes and the second harmonic detecting system are described in Chapters 4 and 5.

The electron energy distribution curves obtained in the present investigation are examined with special reference to the high energy tail region. This region is examined for variations in discharge tube parameters, location of the measuring probe and for different mixture ratios. Values for average electron energy, electron density, drift velocity and mobility are derived from the distribution curves. These are compared with theoretical values and those obtained by other techniques, including non-probe techniques.

An extension of the above method for determining the electron energy distribution function is by using an asymmetrical double probe system. In this method the area of the reference probe greatly exceeds that of the measuring probe. A criterion must be found to judge whether the larger probe is sufficiently large to serve as a reference. The theoretical limits are tested in the present investigation (Section 8.6) by using a reference probe which is variable in size. It is shown that an area ratio of 7000:1 is necessary to produce no distortion of the measurements.

Another cause of distortion is having a measuring probe of too large an area. It has been shown theoretically that

the low energy part of the electron energy distribution curve is seriously affected when the ratio of the probe radius to the electron mean free path (r_p/λ_e) exceeds certain limits. This is examined in the present investigation (Section 8.7) and it is confirmed that there is considerable distortion of the low energy end for $r_p/\lambda_e \geq 0.1$.

The successful application of the Langmuir-Druyvesteyn probe analysis is dependent on a linear relationship existing between $i_{2\omega}$ and E^2 , where E is the amplitude of the a.c. signal applied to the probe. This linear relationship holds for low values of E but there is a departure at higher values. The degree of departure is examined for helium and nitrogen and the results are presented in Section 10.1. The two gases are found to behave in different ways and a theoretical explanation is proposed for these differences. This is achieved by substituting values for the Maxwellian and Druyvesteyn forms in the higher order terms of the Taylor expansion which relates the second harmonic to the second differential.

The theory of the positive column is given in Chapter 1 and its extension to binary mixtures by Dorgelo, Alting and Boers is outlined in Appendix 1. The experimental values for the average electron energies obtained in the present investigation give a reasonable agreement with theory. It is shown that the average electron energy as a function of pR is a universal curve independent of the tube diameter.

CHAPTER 1. THEORY OF THE POSITIVE COLUMN.

The homogeneous positive column consists of a region of luminosity extending from the Faraday dark space to the anode glow. It is separated from the walls by a positive ion sheath across which there is a fall in potential that suffices to maintain a net zero ambipolar current of ions and electrons between the plasma and the insulated walls. Normally the properties of the positive column do not vary axially but there are variations in the radial direction.

Other types of column are those with stationary striations and those with moving striations. With a stationary striated column the luminosity varies periodically along its length and is found to occur mainly with molecular gases in various regions of discharge current and pressure. With the moving striated column, the striations are not detectable with the eye but may be detected with a photomultiplier tube or probe in conjunction with an oscilloscope. They are found to occur generally with the rare gases and move at speeds between 10^2 and 10^3 m sec^{-1}. Like stationary striations, they occur at various regions of discharge current and pressure.

The present investigation is mainly concerned with the homogeneous positive column because wherever possible measurements were made in the absence of moving striations. For neon and some helium-neon mixtures moving striations were present for all regions of discharge current and pressure investigated. In this case measurements were made only where the amplitude of the moving striations were of small enough magnitude ($< 0.2V$) to influence only slightly the discharge properties in their path.

For helium - nitrogen mixtures no moving striations were detected but, in certain regions of pressure and discharge current, the column showed stationary striations.

The properties of the positive column are determined by radial diffusion of the electrons and the ions to the walls which are maintained by an ionisation rate depending on the field strength of the discharge. Experimentally the field strength is found to be a function of the pressure, discharge current and tube radius. In the absence of two stage ionisation the Schottky' ambipolar diffusion theory is valid.

1.1. The Schottky Theory [1.1]

The theory is only valid for a certain range of pressure, probe radius, discharge current etc. In general it can be expected to hold at pressures where the mean free path of the electrons and ions is small compared with the tube radius and the mobility law holds good.

The loss of ions and electrons is due almost entirely to ambipolar diffusion, volume recombination being neglected. In the steady state the diffusion current to the walls is given by

$$j = -D_e \nabla n_e - b_e E_r n_e \quad \text{for electrons .....(1.1)}$$

$$j = -D_+ \nabla n_+ + b_+ E_r n_+ \quad \text{for positive ions ...(1.2)}$$

where b_e and b_+ are the electronic and ionic mobilities ($b_+ \ll b_e$) n_e and n_+ the electron and positive ion densities, E_r is the radial electric field and D_e, D_+ the diffusion constants of the electrons and positive ions respectively.

In the positive column n_e and n_+ are very nearly equal and we can assume

$$n_e = n_+ = n$$

Eliminating E_r from equations (1.1) and (1.2), we obtain

$$j = -D_a . \nabla n \qquad \text{.....(1.3)}$$

where D_a is the ambipolar diffusion constant and is given by

$$D_a = \frac{D_e b_+ + D_+ b_e}{b_+ + b_e} \qquad \text{.....(1.4)}$$

The rate of creation of new electrons in unit volume must be balanced by the loss through diffusion.

Therefore for direct ionisation

$$div\, j = \nu n \qquad \text{.....(1.5)}$$

where ν is the ionisation rate per electron.

If two stage ionisation occurs the rate of ionisation will be proportional to n^2 and the above treatment is incorrect.

The magnitude of ν will depend on the ionisation probability as a function of the actual electron energy distribution 1.2,1.3 It has been shown that the electron energy distribution is independent of the distance r from the tube axis and hence ν is assumed to be independent of r .

Combining equations (1.3) and (1.5) we get

$$\nabla^2 n + \frac{\nu}{D_a} n = 0 \qquad \text{.....(1.6)}$$

which can be written as

$$\frac{\partial^2 n}{\partial r^2} + \frac{1}{r}\frac{\partial n}{\partial r} + \frac{\nu}{D_a} = 0$$

and is a Bessel equation having the solution

$$n(r) = n_0 J_0\left[\left(\frac{\nu}{D_a}\right)^{\frac{1}{2}} r\right] \qquad \text{.....(1.7)}$$

where J_o is a Bessel function of zero order and n_o is the electron density at the tube axis.

By the properties of the Bessel function

$$J_o\left[\left(\frac{\nu}{D_a}\right)^{\frac{1}{2}} r\right] = 0 \quad \text{where} \quad \left(\frac{\nu}{D_a}\right)^{\frac{1}{2}} r = 2{\cdot}405$$

Hence assuming the electron density is zero at the walls, then

$$\left(\frac{\nu}{D_a}\right)^{\frac{1}{2}} R = 2{\cdot}405 \qquad \ldots\ldots(1.8)$$

and hence

$$n(r) = n_o J_o\left(\frac{2{\cdot}405\, r}{R}\right) \qquad \ldots\ldots(1.9)$$

The resulting function is shown in Fig. 1.1. If two stage ionisation is taken into account, this makes equation (1.6) non-linear which has been solved by Spenke[1.4] and the resultant function is also shown in Fig. 1.1 for comparison. The curve resulting from two-stage ionisation drops down more quickly from the axis of the tube.

The longitudinal discharge current I_d can be expressed as

$$I_d = e\int_0^R v_d \cdot n(r)\, 2\pi r\, dr$$

$$= e\int_0^R v_d \cdot n_o \cdot J_o\left(\frac{2{\cdot}405}{R} r\right) 2\pi r\, dr$$

which gives

$$I_d = 1{\cdot}36\, e\, v_d\, n_o\, R^2 \qquad \ldots\ldots(1.10)$$

where e is the electronic charge and v_d is the electron drift velocity under the action of the field.

The Schottky theory[1.1] has been tested by various workers[1.5,1.6] who have confirmed the theoretical dependence of the electron density on distance in the radial direction from the tube axis. However, the assumption that the electron density

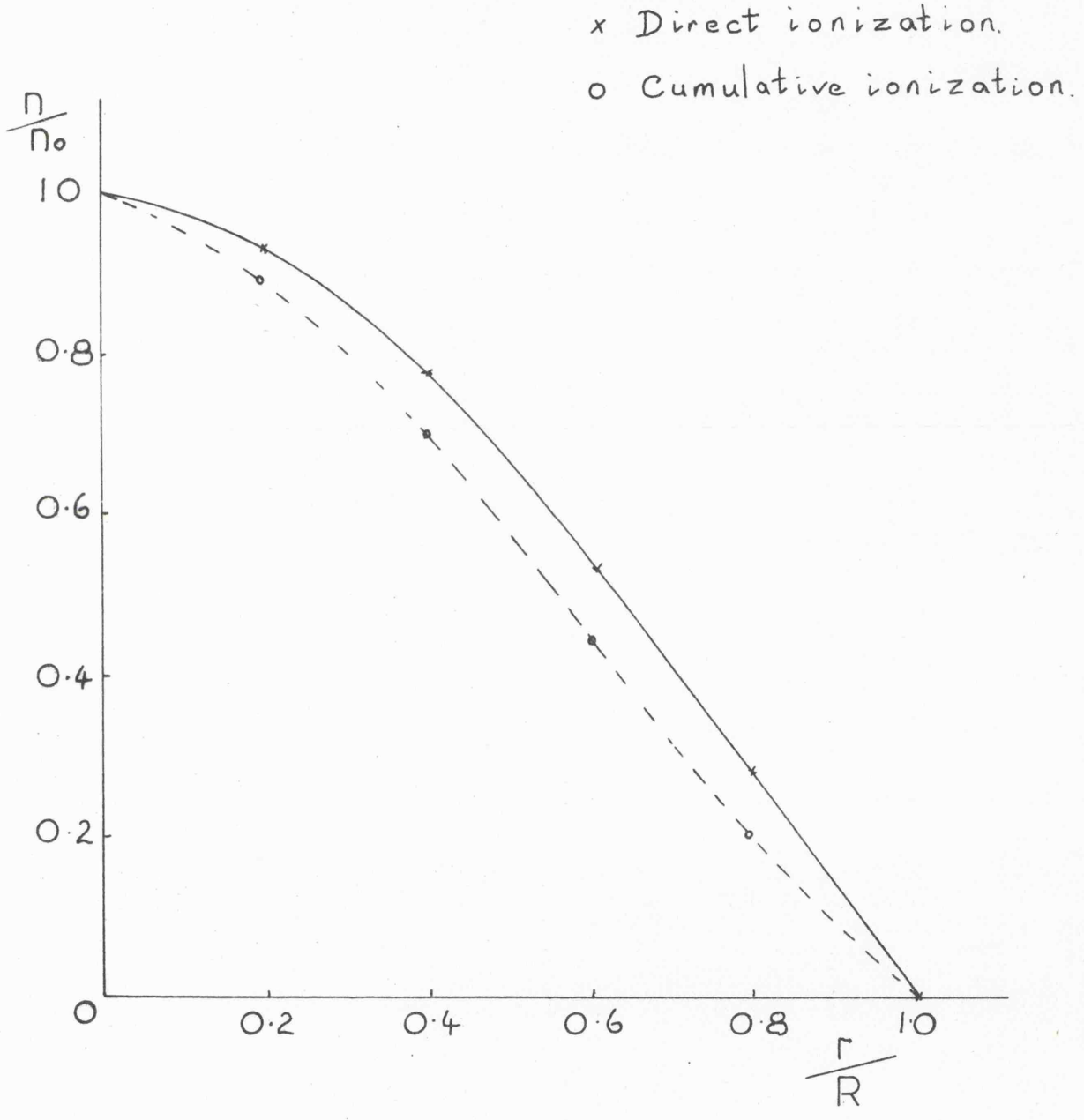

Fig. 1·1 Radial electron distribution in a positive column.

falls smoothly as the walls are approached does not hold in practice. As will be shown later, in the present investigation the experimental points lie close to the zero order Bessel function except that they decrease to a finite value at the wall. The inner surface of the walls takes up a net negative charge and a positive ion sheath forms over the surface. The thickness of this sheath is of the order of 1- 10 electronic Debye lengths.The value of the Debye length at various electron densities and temperatures is given in the Appendix.

1.2 Derivation of electron temperature [1.7]

If expressions for D_a and ν are inserted into equation (1.8) the electron temperature is obtained.

Since $D_a \approx \frac{D_e}{b_e} . b_+$ and $\frac{D_e}{b_e} = \frac{kT_e}{e}$

then $$D_a = \frac{kT_e}{e} . b_+ \qquad .....(1.11)$$

The value of ν is derived on the assumption that the number of ion pairs formed per electron (by single stage ionisation) with an energy of V, $V > V_i$ is given by

$$F(V) = a p (V - V_i) v$$

where v is the velocity of the electron, p the pressure of the gas and a is a constant. It is also assumed that the electrons have a Maxwellian distribution of energies

$$\frac{dN}{N} = \frac{2}{\sqrt{\pi}} \frac{\sqrt{eV}}{(kT_e)^{3/2}} \exp\left(\frac{-eV}{kT_e}\right) d(eV)$$

Hence the number of ion pairs formed by each electron per second

$$\nu = \int_{V_i}^{\infty} F(V) \frac{dN}{N}$$

$$= a p \frac{m}{e} \frac{2}{\sqrt{\pi}} \left(\frac{2kT_e}{m}\right)^{3/2} \exp\left(-eV_i/kT_e\right)\left[1 + \tfrac{1}{2} eV_i/kT_e\right] \qquad .....(1.12)$$

Inserting these results in equation (1.8) gives the final equation relating T_e/V_i to pR.

1.3 The Tonks and Langmuir theory.[1.8]

When the mean free path of the positive ions is greater than the tube radius, no mobility exists and the ions fall freely from the moment they are formed until they reach the tube walls. Unlike the Schottky theory, the boundary conditions are discussed in detail. It is assumed that the column does not extend to the walls but to the plasma-sheath boundary and under certain conditions the positive ion sheath thickness is appreciable. Hence the electron concentration is no longer zero, as assumed in the Schottky theory and can be calculated.

In the present investigation, the measurements were generally made outside the regime for which the free fall theory holds and the Schottky theory is expected to be more appropriate. Klarfield[1.9] and Karelina[1.10] made some measurements for which the free fall theory should apply. The comparison with results calculated using the free fall theory showed satisfactory agreement.

CHAPTER 2 PAST WORK ON THE ELECTRON ENERGY DISTRIBUTION FUNCTION

The electron energy distribution function being fundamental to the understanding of most discharges has been determined theoretically and experimentally by many workers. From the details of such disribution functions it is possible to calculate useful discharge parameters.

Gas discharge phenomena can be measured by numerous techniques but except for probes there are no adequate techniques for directly determining the electron energy distribution function. The knowledge of the electron energy distribution function is of fundamental importance in that nearly all the properties of the gas discharge can be determined from it. It is an extremely complicated procedure to determine the distribution function from individual properties of the discharge measured independently. However, these properties have been measured using non-probe techniques and in some cases attempts have been made to determine the distribution from them. Microwave techniques measure quite accurately the average electron density but only in certain special cases can they give information about the variation of electron density with position in the discharge tube. Moreover, while they yield information about electron energies and collisional frequencies averaged over the electron energy distribution, they give little or no information about the electron energy distribution itself. Probe measurements have remained the only way to get detailed information about the variation of electron density with position and about the electron energy distribution function.

2.1 Microwave Techniques.

The electron density in the discharge plasma can be measured by methods making use of the interaction of electrons with a high frequency electric field. Margenau[2.1] has shown that when electrons have a Maxwellian distribution in a gas at low pressures then the electron density is related to the imaginary part of the conductivity of the medium, provided that the electric field frequency is greater than the collisional frequency of the electrons. Early methods gave unsatisfactory results but improved with later techniques. Biondi[2.2] determined the electron density from the phase shift of the wave in the wave-guide, part of which was filled with a discharge. Another technique was to measure the change in resonant frequency of a cavity when a discharge tube is inserted. This method has given good agreement with probe measurements. Labuda and Gordon[2.3] used this technique to obtain the electron density in helium-neon mixtures. The discharge tube was placed at the centre of the cavity with its axis perpendicular to the base. The electron density was obtained from the plasma frequency which in turn was obtained from the frequency shift.

Microwave techniques can also be used for measuring the average energy of electrons. One method used by Varnerin and Brown[2.4] was to study a microwave gas discharge breakdown modified by an applied d.c. electric field. The discharge conditions are now changed because the electrons are lost both by diffusion and d.c. drift. Observation of the change in breakdown conditions permits the calculation of the ratio of electron mobility to the diffusion

coefficient. The average electron energy is calculated from this ratio. Another non-probe method for determining electron temperature is by measuring the noise produced by the discharge in the microwave region. If it is assumed that the power radiated in the frequency interval $\Delta\nu$ is $k.T_e.\Delta\nu$, [2.5] the values of T_e calculated from the power measurements agree well with those found by probes. Labuda and Gordon [2.3] used this technique for investigating the dependence of average electron energy on various discharge parameters for He-Ne mixtures. The noise power leaving the cavity due to the discharge was compared with the noise power emitted by a noise lamp using a standard noise comparison scheme.

2.2 Single and Multiple Probe Techniques.

The use of Langmuir probes to measure the electron density and the electron temperature is now well established. Langmuir probes have the advantage over other techniques in that they may be used to determine the electron energy distribution function at any point in the plasma. The single probe technique consists in placing a plane, spherical or cylindrical surface in the plasma and measuring the current drawn by the probe, when its potential is varied with respect to the plasma. One disadvantage of the single probe technique is that the current collected by the probe can be, in some cases, a large fraction of the discharge tube current. Perturbation set up by the probe can influence the parameters it is measuring, especially the electron density. A method introduced by Johnson and Malter [2.6] uses instead two probes whose potential is allowed to float. In this case the ratio of the probe current to the discharge current is very small.

In the double probe method, also suggested about the same time by Kojima and Takayama,[2.7] one probe is biased positive to collect electrons and the second is biased negative to collect an equal ion current. The second probe also acts as a reference probe. A Maxwellian electron energy distribution is assumed in the analysis of the curve. One of main disadvantages is that when the probes are of equal area only a small part of the electron characteristic is measured. However, the range of the electrons sampled can be extended by using probes of dissimilar area. Swift[2.8] has shown that if the ratio of the area of the reference probe to the measuring probe is sufficiently large then the complete distribution can be obtained.

In a method introduced by Jamanoto and Okuda[2.9] a third probe is located between the usual double probes to measure the floating potential of the plasma. The main limitation of this method is the perturbation caused by the introduction of three probes into the plasma. Another disadvantage is that the method is not applicable over the whole energy range. This disadvantage was overcome by Aisenberg[2.10] but perturbation was increased because more electron current was drawn by the probes.

2.3 Druyvesteyn Equation.[2.11]

Druyvesteyn showed that the shape of the electron distribution function may be determined from the second derivative, $\frac{d^2 i_e}{dV^2}$. Graphical differentiation of the probe characteristic is rather inaccurate and hence electronic methods have been used. The Druyvesteyn relationship is given as

$$f(V) = \frac{2}{Ae}\left(\frac{2m}{e}\right)^{\frac{1}{2}} V^{\frac{1}{2}} \frac{d^2 i_e}{dV^2}$$

where f(V) is the number of electrons per unit volume of energy V electron volts, A is the area of the probe, e the electronic charge m the electronic mass, V the potential difference between probe and plasma and i_e the electron current drawn by the probe. The complete distribution is found by measuring $\frac{d^2 i_e}{dV^2}$ and hence f(V) for each value of V.

2.4 Differentiating Networks.

Kagan et al[2.12] was able to display the second derivative directly on to an oscilloscope by applying a saw-tooth voltage waveform to the probe and using differentiating networks. This method has also been used by Lecky et al.[2.13]

Swift and Smithers[2.14] [2.15] used a differentiating circuit to record variations of $\frac{di_e}{dV}$ with V on an oscilloscope and the second differential was obtained graphically. The use of a second differentiating circuit was not found to be possible because of the high level of noise associated with the discharge under investigation.

Crawford, Garscadden and Palmer[2.16] described a double probe method by which the first derivative is measured and the second derivative obtained electronically. The principle of the method was to bias one of the two identical probes by ΔV, relative to the other, and then to sweep both probes with an additional voltage V. If the difference current is measured , then $\frac{\Delta i}{\Delta V} = \frac{di}{dV}$ so that the variation of the first derivative is obtained. The signal was then differentiated to give the second derivative directly.

2.5 a.c. probe methods.

If a small alternating voltage v is superimposed on the d.c. probe voltage V, the current becomes a function of(V+v) which can be expanded by Taylor's theorem to give the required second derivative function. Sloane and McGregor[2.17] measured the increase, i_{dc} , in the d.c. component of the probe current when an alternating potential v=E.sin t was superimposed and showed

$$i_{dc} \simeq \frac{E^2}{4} \cdot \frac{d^2 i_e}{dV^2}$$

when v was made sufficiently small. However, this technique is only suitable when the discharge is very stable.

The method was improved by amplitude modulation of the sinusoidal voltage applied to the probe. It is then possible to detect the $\frac{E^2}{4} \cdot \frac{d^2 i_e}{dV^2}$ term not as a d.c. current but as an a.c. component. Boyd and Twiddy[2.18-2.21] used this technique very successfully in their work. However, extreme care was taken to avoid accidental demodulation of the voltage applied to the probe. Friar[2.22] and Vorebeva et al[2.23] also used modulation techniques for obtaining the second derivative.

Vagner et al[2.24] taking measurements in a high frequency discharge used a three probe system consisting of a small measuring probe, a reference probe of the same size and a large counterprobe. The second derivative was determined by introducing a modulated sinusoidal voltage of small amplitude into the probe circuit. The size of the counterprobe was chosen so that the whole electron part of the characteristic, up to the space potential could be taken with the measuring probe.

An a.c. component of the probe current can be detected as the second harmonic when a small sinusoidal signal of the form $v = E.\sin\omega t$ is superimposed on the d.c. probe voltage. This component at twice the frequency of the applied signal can be shown to be related to the second derivative by an equation of the form

$$i_{2\omega} \approx \frac{E^2}{4} \frac{d^2 i_e}{dV^2}$$

where v is again kept small. This is the basis of the technique used in the present investigation. It has been used successfully in nitrogen by Thomas[2.25] and by Kilvington, Swift and Jones[2.26] and in helium by Luijedijk and Van Eck.[2.27] The latter experimenters compared a second harmonic method , based on one given by Branner et al,[2.28] with an intermodulation method and a high frequency modulation method. The high frequency modulation method was similar to that used by Malyshev and Fedorov.[2.29]

The three methods were compared in turn under the same tube conditions. They found that the second harmonic method and the intermodulation method agreed within 1%. However,the high frequency modulation method gave a difference of 10 to 25% in the maximum of the second derivative curve, when compared with the other methods.

Friar[2.22] compared his intermodulation system with the second harmonic method and showed the results were the same within the experimental error.

2.6 Techniques used with moving striations.

It can be shown that the techniques normally used to measure the electron energy distribution are not applicable in the presence

of moving striations, especially when there are large amplitude fluctuations of the plasma potential. Drouet [2.30] modified the double probe technique of Crawford et al [2.16] to examine the plasma potential variations in moving striations. A sampling technique was added to display on an oscilloscope the first derivative of the probe current as a function of the applied potential for different positions in a striation.

A technique for measuring the electron energy distribution function over the length of a moving striation is given by Rayment and Twiddy [2.31-2.33]. A small sinusoidal signal was superimposed on the probe bias for a small part of each striation period and the first derivative of the probe current with respect to the probe potential was found. This was differentiated to give the second derivative and hence the electron energy distribution function was obtained. The probe characteristic along a striation was determined by varying the delay time of the signal pulse relative to the beginning of the striation. Sicha et al [2.34] used a similar technique but differs from that proposed by Rayment and Twiddy in that it enables the direct measurement of the second derivative. The circuit included a gate which was triggered at the frequency of the ionisation waves and allowed measurement of the probe current during a small part of the ionisation wave period. The voltage pulse required to open the gate is provided by a pulse generator which is triggered by a signal from the output of a photomultiplier.

Various other techniques have also been used. Kagan et al [2.35-2.36] used a method whereby a sinusoidal signal of frequency very much greater than the striation frequency is introduced

into the probe circuit. By varying the probe current they were able to obtain a set of values of the second derivative and hence the electron energy distribution at each point of the striation. Oreshak et al[2.37] found the second derivative by double electronic differentiation. Using two photomultiplier tubes, one directly opposite the measuring probe and another which could be displaced parallel to the tube axis, they were able to measure the second derivative at any point of the moving striation. The moveable photomultiplier tube was used to trigger the oscilloscope displaying the second derivative. The second one fed its signal to another oscilloscope giving a profile of the striation and a bright spot indicated the point on the striation at which the second derivative was being measured.

CHAPTER 3 THEORY OF PROBE TECHNIQUES .

The collection of charged particles by a probe is related to the properties of the plasma in which it is immersed and hence it has found wide applications in diagnostic techniques. However, taking measurements with a probe has its limitations and it is only useful within a certain regime of discharge conditions. The current reaching the probe is dependent on the particle density near the probe, the electric field produced by the probe and various collisional processes. Certain conditions must be fulfilled before the information obtained by the probe can be treated unambiguously. Firstly, the probe must be small compared with the mean free path, otherwise the theory must be modified. Secondly the sheath- a layer of ions formed on the surface of the probe- must be small compared with the probe. Finally, plasma oscillations must be absent.

In spite of the problems that exist, the method has the advantage over other diagnostic techniques in that it can make local measurements. Almost all other techniques, such as spectroscopy or microwave propagation, give information averaged across the plasma.

3.1. Probe Theory of Langmuir and Mott-Smith.[3.1]

Langmuir and Mott-Smith investigated the theory of collectors in gaseous discharges. They described the action of planar, cylindrical and spherical collectors immersed in a plasma when brought to a suitable potential. The probe becomes surrounded by a sheath of positive ions or electrons depending on its potential with respect to the plasma. If the gas pressure is low enough then the number of collisions in the sheath is negligibly small. The current collected by the probe can then be calculated

in terms of the radius of the probe and the drop in potential across the sheath.

A plot of probe current against V_p, the probe voltage with respect to an arbitrary reference point is shown in Fig. 3.1. At the space potential, V_S, the probe is at the same potential as the plasma. Since no potential difference then exists, the charge particles move towards the probe at thermal velocities and is predominantly electron current. If the probe is made positive with respect to the plasma the electrons are accelerated to the probe, this is called the accelerating region of the characteristic. At potentials below V_S, that is with the probe negative with respect to the plasma, the electrons are beginning to be repelled and the ions accelerated. The electron current falls as V_p decreases in this region, which is called the retarding field region of the probe. If the electron distribution was Maxwellian the plot of probe current against probe voltage would be expodential in this region. At V_F, the floating potential, the probe is sufficiently negative so that an equal number of electrons and positive ions are collected by the probe, so there is no net current. An insulated probe inserted in the plasma would attain this potential.

If the probe is made strongly negative, all the electrons are repelled and ions are attracted. A sheath of ions forms on the surface of the probe and can sometimes be observed as a dark zone separating it from the plasma. The current to the probe, consisting entirely of positive ions, is limited by this space charge.

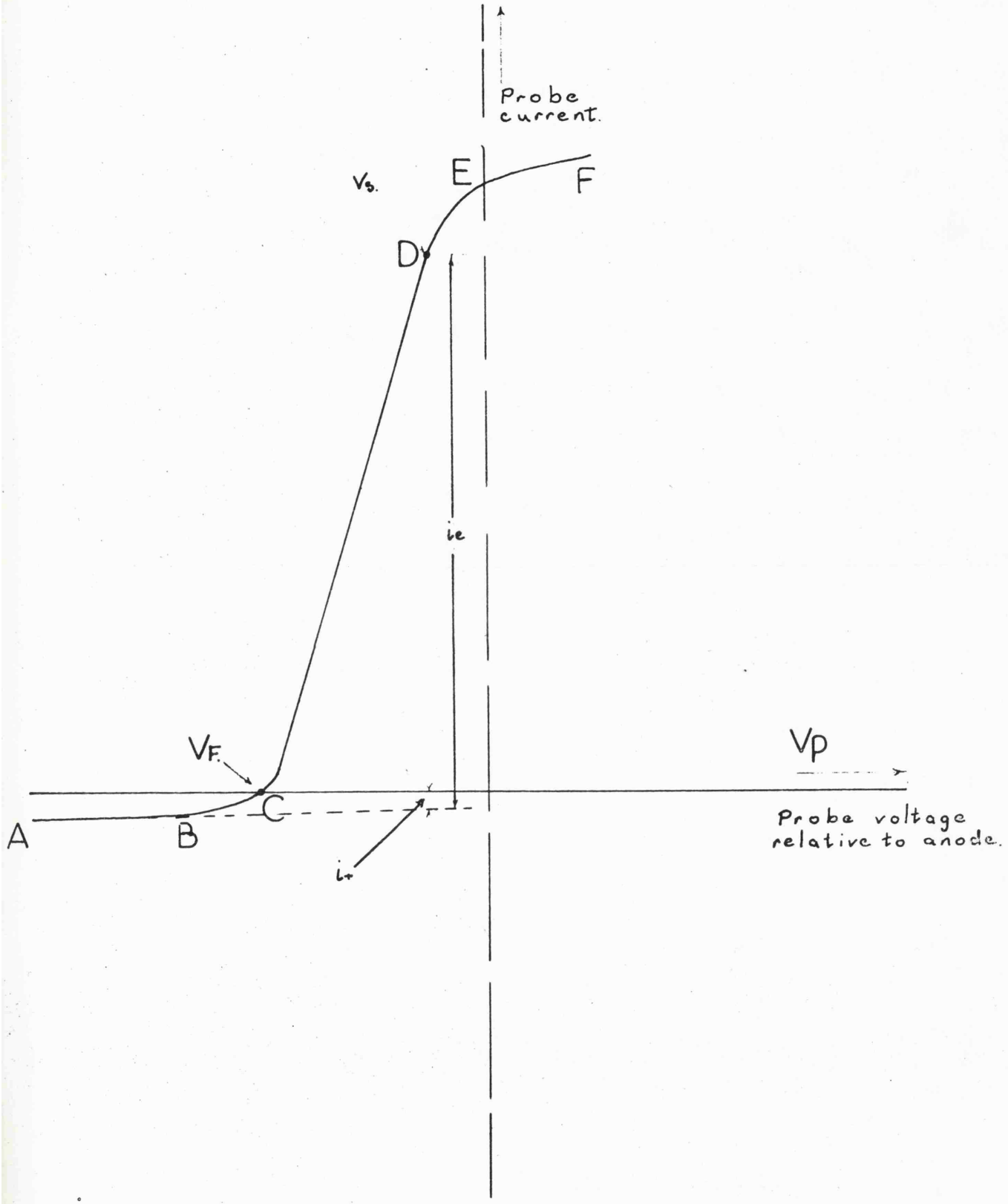

Fig. 3·1 General form of probe characteristic

The current density conforms to the Child - Langmuir equation and is given by

$$j_+ = \frac{\sqrt{2}}{9\pi}\sqrt{\frac{e}{m_+}}\frac{V^{\frac{3}{2}}}{x^2} \qquad \ldots\ldots(3.1)$$

where x is the thickness of the sheath, V the potential across it and m_+ the mass of the ions. The thickness x is an important quantity whose relation to the mean free path, λ_e, determines the limit of application of the method.

Assuming the electrons in the surrounding plasma move in all directions and have a Maxwellian distribution of velocities. Then, if the probe is made less negative, some of these electrons can reach the probe surface against the retarding potential across the sheath. Furthermore, if the probe were a perfect reflector, all the electrons would rebound and the distribution would be undisturbed. Boltzmann's relation can be applied to determine the electron density n_{e_p} at the probe surface relative to the density n_{e_s} at the plasma boundary of the sheath edge.

Thus
$$n_{e_p} = n_{e_s}\exp\left(\frac{-eV}{kT_e}\right) \qquad \ldots\ldots(3.2)$$

where V is the potential of the probe relative to the plasma and T_e is the electron temperature. Then the electron current density to the probe is

$$j_{e_p} = j_{e_s}\exp\left(\frac{-eV}{kT_e}\right) \qquad \ldots\ldots(3.3)$$

where j_{e_s} is the random plasma electron density given by

$$j_{e_s} = \tfrac{1}{4} n_{e_s} e \bar{v} \qquad \ldots\ldots(3.4)$$

where $\bar{v}$ is the mean electron velocity.

Taking the logarithm of each side in equation (3.3) we have

$$\log j_{ep} = \log j_{es} - \frac{eV}{kT_e} \qquad \ldots\ldots(3.5)$$

from which, multiplying by the probe area, we get

$$\log i_{ep} = \log i_{es} - \frac{eV}{kT_e} \qquad \ldots\ldots(3.6)$$

Therefore, the logarithm of the electron current to the probe is a linear function of the probe voltage relative to the plasma, provided the voltage is retarding the electrons. A Maxwellian distribution function is assumed. The electron temperature may be obtained from the slope.

The electron current i_e and the probe - space potential difference V are not actually measured. The measured current, i, is equal to $i_e - i_+$ and i_+ is obtained from the part AB of the characteristic curve in Fig 3.1. extrapolated to give the value at the space potential. The potential V is not actually obtained because in making the measurement one of the electrodes (anode) in the plasma is used as a reference, so that the probe characteristic is shifted on the voltage scale.

3.2. The Langmuir-Druyvesteyn Method of Analysis.[3.2]

In the Langmuir-Druyvesteyn method of analysis it is not assumed that the distribution of velocities amongst the electrons is Maxwellian as in the Langmuir and Mott-Smith theory but only that it is isotropic.

Suppose that the electrons in the plasma have

a velocity distribution $f(v)dv$, that is the number per unit volume in the range $v - v+dv$.

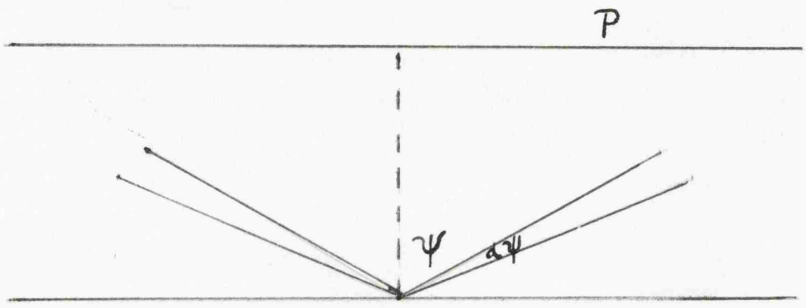

The fraction of these electrons travelling towards a plane probe in a direction making angles $\psi - \psi+d\psi$ to the normal is given by

$$\frac{2\pi \sin\psi\, d\psi}{4\pi} = \frac{\sin\psi\, d\psi}{2} \qquad \ldots\ldots\ldots(3.7)$$

If A is the area of the probe sheath , the number of electrons in the given velocity and direction ranges which cross the sheath per second is

$$A\, v \cos\psi . f(v) . dv . \frac{\sin\psi}{2} . d\psi \qquad \ldots\ldots\ldots(3.8)$$

Consider electrons of given velocity v, it is only when the angle of motion is less than a certain value will they be able to overcome the retarding potential and reach the probe.

If V is the retarding potential and θ the critical angle of the electrons to reach the probe, that is $\psi \leq \theta$ then

$$\tfrac{1}{2} m v^2 \cos^2\theta = eV \qquad \ldots\ldots\ldots(3.9)$$

Thus it follows that the electron current to the probe is given by

$$i_e = \frac{Ae}{2} \int_{\left(\frac{2eV}{m}\right)^{\frac{1}{2}}}^{\infty} v.f(v)\,dv \int_{0}^{\Theta} \sin\psi.\cos\psi.d\psi \qquad \ldots\ldots(3.10)$$

when $v < \left(\frac{2eV}{m}\right)^{\frac{1}{2}}$ even electrons travelling at right angles will be unable to reach the probe, so that

$$i_e = \frac{Ae}{4} \int_{\left(\frac{2eV}{m}\right)^{\frac{1}{2}}}^{\infty} v(1-\cos^2\Theta) f(v)\,dv \qquad \ldots\ldots(3.11)$$

Replacing $\cos^2\Theta = \frac{2eV}{mv^2}$ from equation (3.9)

then

$$i_e = \frac{Ae}{4} \int_{\left(\frac{2eV}{m}\right)^{\frac{1}{2}}}^{\infty} v\left[1 - \frac{2eV}{mv^2}\right] f(v)\,dv \qquad \ldots\ldots(3.12)$$

Differentiating twice with respect to V

$$\frac{d^2 i_e}{dV^2} = \frac{e^2 A}{4m} \frac{1}{V} f\left(\frac{2eV}{m}\right)^{\frac{1}{2}}$$

rearranging

$$f(v) = V.\frac{d^2 i_e}{dV^2}\left(\frac{4m}{e^2 A}\right) \qquad \ldots\ldots(3.13)$$

where A is the area of the probe, $V = V_s - V_p$ and i_e is the total electron current to the probe.

In terms of energy expressed in volts the equation becomes

$$f(V) = \frac{2}{Ae}\left(\frac{2m}{e}\right)^{\frac{1}{2}} V^{\frac{1}{2}} \frac{d^2 i_e}{dV^2} \qquad \ldots\ldots(3.14)$$

Hence the distribution function of electron energies can be found from equation (3.14). It was shown by Druyvesteyn[3.2] that this equation is applicable to planar, cylindrical and spherical probes. This was confirmed by Kagan[3.3] who generalised the theory to apply to any non-concave probe. Therefore, if the observed curve of i_e against V is twice differentiated with respect to V and multiplied by $\frac{2}{Ae}\left(\frac{2m}{e}\right)^{\frac{1}{2}} V^{\frac{1}{2}}$ the quantity $f(V)$ is obtained. This gives the form of the distribution law. In differentiating the observed relation, it is not necessary to differentiate the actual potential V, since V differs from the applied potential V_p by a constant term.

As discussed in Section 2.5, $\frac{d^2 i_e}{dV^2}$ can be found in several ways some of the most accurate being electronic techniques, since graphical differentiation is both laborious and imprecise.

3.3 Theoretical basis of the present technique.

Landale[3.4], in his analysis of triode valve rectification, has shown that on the application of a sinusoidal voltage, $v = E\sin\omega t$ to a simple grid rectifier the current produced contained new harmonic terms and also a steady current.

He showed, by expanding using Taylor's theorem, that when an a.c. potential, $E\sin\omega t$, was superimposed on the grid voltage, the current produced was given by the equation

$$i = f(V) + v\,f'(V) + \frac{v^2}{2!} f''(V) + \frac{v^3}{3!} f'''(V) + \ldots \qquad \ldots\ldots (3.15)$$

where $f'(V), f''(V), f'''(V)$ .... are the first, second, third differentials with respect to voltage.

Substituting $v = E\sin\omega t$ in equation (3.15) one gets

$$i = f(V) + \frac{E^2}{4} f''(V) + \frac{E^4}{64} f^{IV}(V)$$
$$+ \left[E f'(V) + \frac{E^3}{8} f'''(V)\right] \sin\omega t$$
$$- \left[\frac{E^2}{4} f''(V) + \frac{E^4}{48} f^{IV}(V)\right] \cos 2\omega t$$
$$- \frac{E^3}{24} f'''(V) \sin 3\omega t + \frac{E^4}{192} f^{IV}(V) \cos 4\omega t$$
.....(3.16)

This equation for the current showed that new harmonic terms are produced by the rectifier and also a steady current whose value is

$$f(V) + \frac{E^2}{4} f''(V) + \frac{E^4}{64} f^{IV}(V)$$
.....(3.17)

The term $f(V)$ is due to the bias voltage alone and not to the superimposed sinusoidal voltage. Hence the increase in the d.c. component is given by

$$i_{d.c.} = \frac{E^2}{4} f''(V) + \frac{E^4}{64} f^{IV}(V)$$
.....(3.18)

For any given value of E the d.c. component will therefore depend on V the bias voltage.

When v is sufficiently small equation(3.16) may be approximated to give

$$i = f(V) + \frac{E^2}{4} f''(V) + E f'(V) \sin\omega t$$
$$- \frac{E^2}{4} f''(V) \cos 2\omega t - \frac{E^3}{24} \sin 3\omega t$$
$$+ \frac{E^4}{192} \cos 4\omega t + \ldots$$
.....(3.19)

3.5 Branner, Friar and Medicus have shown that the same theory is applicable to a biased probe with a superimposed sinusoidal signal.

If E is small

$$i_{d.c.} = i_{2\omega} = \frac{1}{4} E^2 f''(V) = \frac{E^2}{4} \frac{d^2 i_e}{dV^2} \qquad \ldots\ldots(3.20)$$

Hence $\frac{d^2 i_e}{dV^2}$ can be determined either by measurement of $i_{d.c.}$ as shown by Sloane and McGregor[3.6] or $i_{2\omega}$ as in the present investigation.

CHAPTER 4 DESCRIPTION OF APPARATUS.

4.1 The Vacuum System

The vacuum system shown in Fig. 4.1. was a circulating type based on one originally devised by Tolansky.[4.1] If the pressure in the system is low enough then the diffusion pump D_1 still functions when the circulating part of the system is isolated from the rotary pump by closing valve V_3. As a result of this the gas in the system circulates through the traps T_4 to T_1 and a high degree of purity can be obtained. It is essential to employ a diffusion pump whose upper limiting backing pressure exceeds the maximum pressure of the circulating gas, otherwise circulation ceases. Oil diffusion pumps generally require a fairly low backing pressure and are not suitable in a system of this type, so a mercury diffusion pump was used. The range of pressures covered in the investigations varied from 0.05 to 0.3 torr and the critical backing pressure of diffusion pump D_1 was 0.8 torr enabling it to function efficiently.The advantages of such a system are firstly, any condensible impurities evolved during the investigation were removed during the circulation of the gas. Secondly, the pressure remained reasonably constant during a run, whereas with a static system there were variations in pressure.

The system was constructed from glass except for stainless steel bakeable valves, V_1 to V_4 manufactured by Vacuum Generators, Type CR25. These were used because valves with elastometer sealing components give rise to organic contamination which cannot be tolerated in the system. They also enabled the entire system to be baked to achieve the lowest attainable pressure.The CR25 bakeable valve produces a vacuum seal by establishing a high interfacial pressure between a gold plated copper pad driven against a stainless

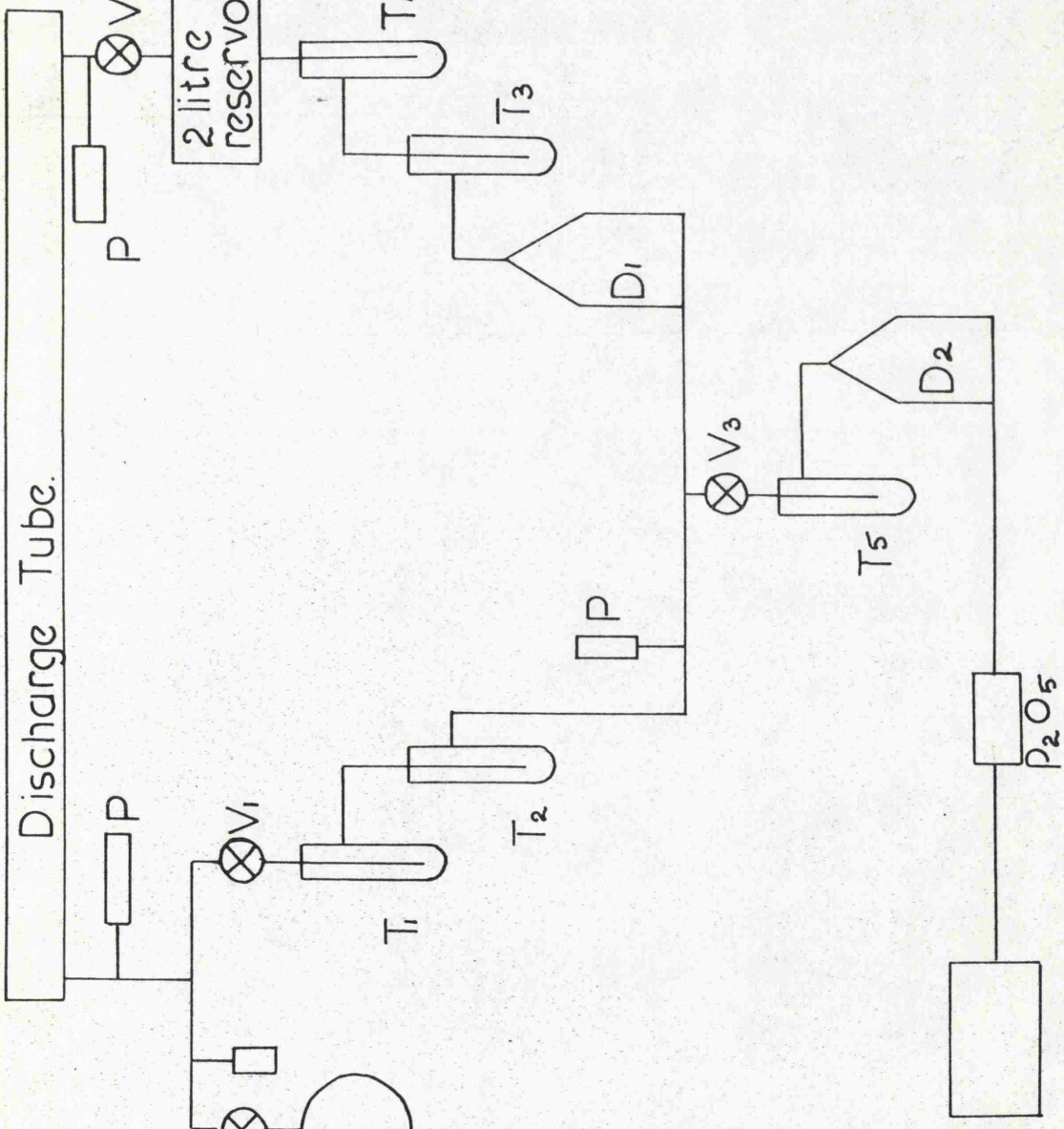

Fig. 4.1. The Vacuum System.

steel knife edge. The valves are bakeable in an open or closed position to 400°C but it was found in practice inadvisable to bake above 300°C in the closed position. At higher temperatures a bond is formed between the pad and the knife edge of the valve which could result in a small part of the pad sticking to the knife and leaving a crater in the pad. Also, when baking in the closed position the temperature rise was limited to less than 200° C per hour. This was to prevent differential thermal expansion which could produce deformations of the copper pad and cause leakage on subsequent valve closures. Finally, great care was taken not to allow the pressure to rise above 10^{-4} torr during bakeout, to prevent oxidation of the internal parts of the valves.

Evacuation procedure.

The system was evacuated using the rotary pump alone to a pressure of about 10^{-2} torr. All the traps T_1 - T_5 were then filled with liquid nitrogen to prevent the diffusion of mercury throughout the entire system. It was not considered advisable to fill the traps before this because the water vapour in the system may be condensed rather than pumped away. The rotary pump itself was protected by a dish of phosphorous pentoxide which collected most of the moisture appearing at the pump inlet. The diffusion pumps D_1 and D_2 were then switched on and without leaks a pressure of 2×10^{-6} torr was reached.

The entire system was then heated to about 300° C using covered thermal tapes on the glass and heaters on the supporting brackets of the isolation valves. Higher temperature bakeout was thought unnecessary because clean stainless steel

and glass have outgassing rates of less than 1×10^{-12} torr.l.s^{-1} after a vacuum bakeout at 250° C.[4.2] The system was heated at this temperature for several hours and an ultimate of 2×10^{-7} torr was attained. This was reduced further to less than 10^{-7} torr by outgassing the metal parts of the discharge tube and by outgassing the ionisation gauge. The anode was outgassed using an induction heater and the filaments were run for several hours at maximum operating current. After heating the system and outgassing the metal parts the valves V_1 and V_2 were not opened with the traps unfilled to reduce the possibility of mercury entering the discharge tube.

Admission and Circulation of the gas.

Following the evacuation of the system the valve V_3 was isolated bringing the circulating part of the system into operation With V_4 closed, an iron slug enclosed in a glass envelope was used to break the seal on the grade-X bottle. The valve V_4 was then opened very slowly to bring the system to the required pressure. A policy of frequent renewal of the grade - X bottle was adopted to further reduce the possibility of contamination. The system was flushed out several times with the gas to dilute the impurities present, Finally, the system was filled to about 0.3 torr and the discharge run at 400 mA for 30 minutes or so. This current was as high as any used during a run so that the discharge temperature didn't rise above that obtained in this way. With all the precautions described above axial field measurements showed that the drift of electric field strength with time was negligible.

The reservoir attached to the discharge tube reduced the effect of clean-up of the gas and the pressure remained constant within 1% during the runs. Thermocouples were attached to various parts of the discharge tube wall and were found to reach equilibrium in less than 30 minutes at 400 mA discharge current and in shorter periods for lower currents.Hence a period of 30 minutes was allowed after striking the discharge before any measurements were made.

Calibration of the gauge.

The gas pressure in the system was measured using a L.K.B. Autovac gauge, which is a pirani-type gauge. The useful measuring range of this instrument starts at 70 torr and goes down to 10^{-3} torr. This range is split into two parts with an adjustable automatic range switching device usually set at 0.1 torr. The range of pressure used in the investigation was from 0.05 torr to 0.3 torr and so it was essential to calibrate both parts of the range. This was done for He, Ne, N_2 , He-Ne and He-N_2 mixtures using an auxiliary vacuum system. The gauge was periodically recalibrated for He, Ne and N_2 to provide a check on drift in the calibration.

Each gauge was calibrated using the following procedure. The cable to the gauge tube was plugged into the first jack position on the instrument but left disconnected from the tube. The tube holder was short-circuited and a resistor corresponding to the jack position 1 was adjusted until a Wheatstone bridge,which which was connected to the test contacts at the rear of the instrument , read the resistance on the gauge tube to be used. The short circuit was removed and the gauge tube inserted into the holder. The instrument was then warmed up for 15 minutes and with

the gauge tube at atmospheric pressure, the meter was adjusted to 100 torr. The gauge tube was pumped down to 10^{-4} torr and the meter set to zero. Atmospheric pressure was again applied and the meter adjusted to 100 torr. After these adjustments the gauge tube was ready for use. The manufacturers provided calibration charts for He, Ne and N_2 but as a safeguard the instrument was also calibrated against a McLeod for these gases and for the mixtures.

The McLeod gauge used was an Edwards High sensitivity gauge HS1A , modified to read from 0 - 200 microns by replacing the closed capillary with one twice the diameter. The error introduced by changing the capillary can be calculated and is less than 0.1%. The accuracy of the McLeod gauge was determined prior to calibration by checking the capillary depression , this being the main source of error. First the gauge was evacuated until it read sticky gauge, that is the lowest possible reading. The mercury was then raised and starting from zero level, the differences in the mercury level were measured between the closed end capillary and the main tube, and between the open end capillary and the main tube. These differences denoted by Δh_1 and Δh_2 respectively were plotted as a function of h, as shown in Fig.4.2. The difference $|\Delta h_1 - \Delta h_2|$ is the actual error which has to be taken into account and was in all cases less than 0.6%. The manufacturers calibration curves and those obtained by calibrating against a McLeod gauge for He,Ne,N_2 , He-Ne and He-N_2 mixtures are shown in Figures 4.3 (a) and (b).

4.2 Details of gases used.

The gases used in the investigation were obtained from B.O.C. Special Gases Division and were spectroscopically pure. The actual

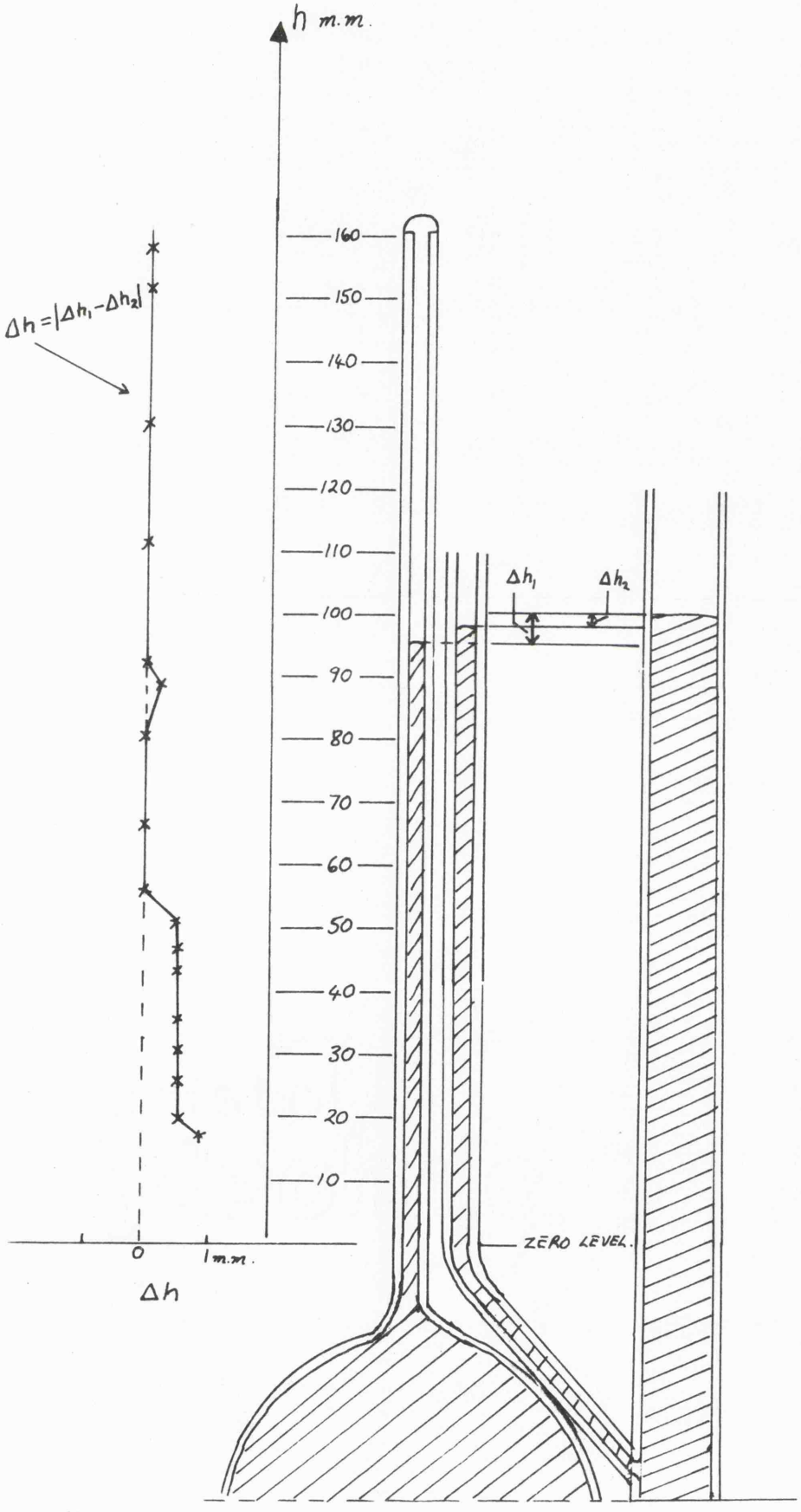

Fig. 4.2 Capillary depression Δh as a function of the height h of the mercury level.

Fig. 4·3 Calibration of L.K.B. (Pirani) Gauge.

(a) For helium, neon and helium–neon mixtures.

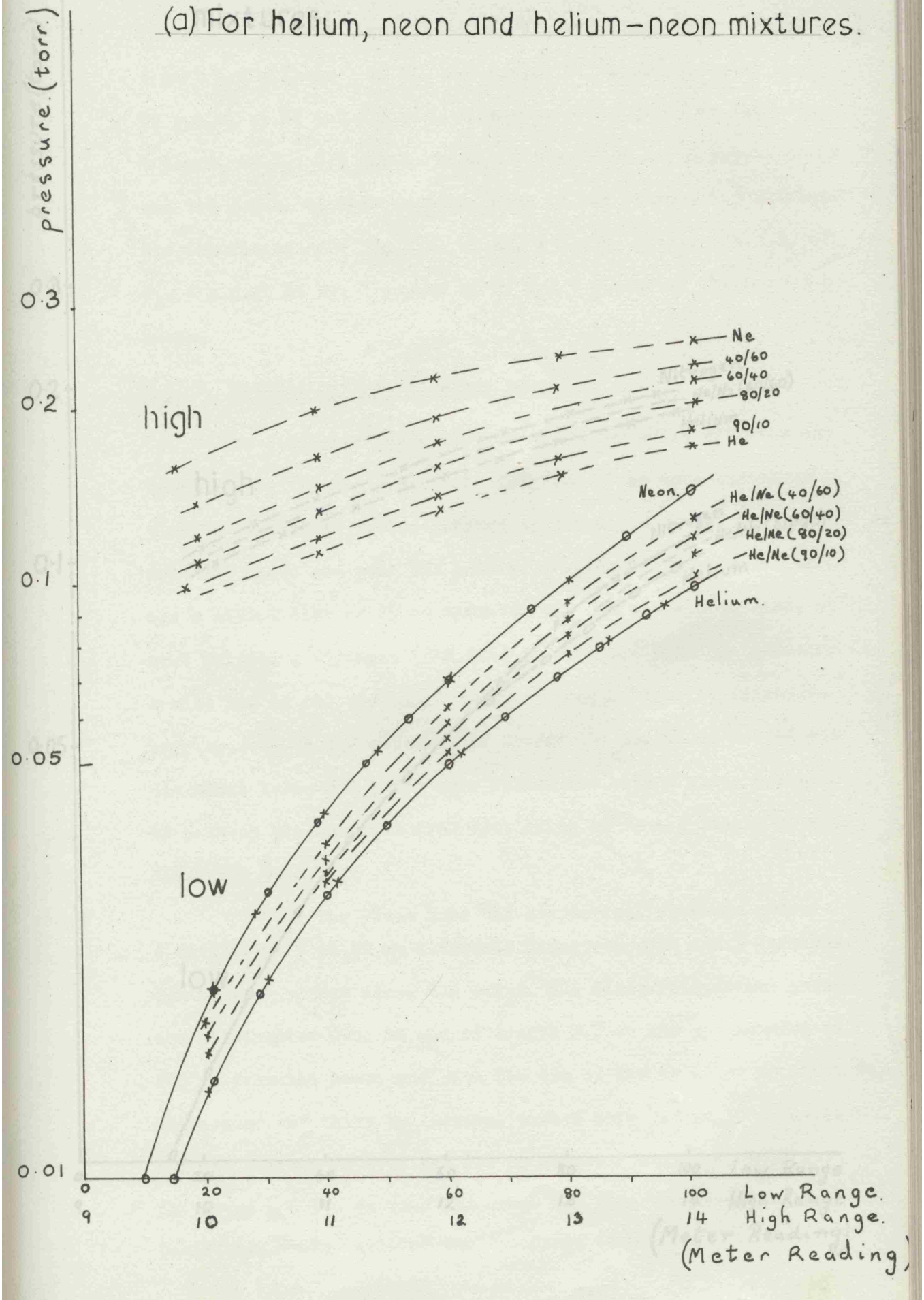

Fig. 4.3 (b) Calibration of L.K.B. (PIRANI) Gauge for helium, nitrogen and helium–nitrogen mixtures.

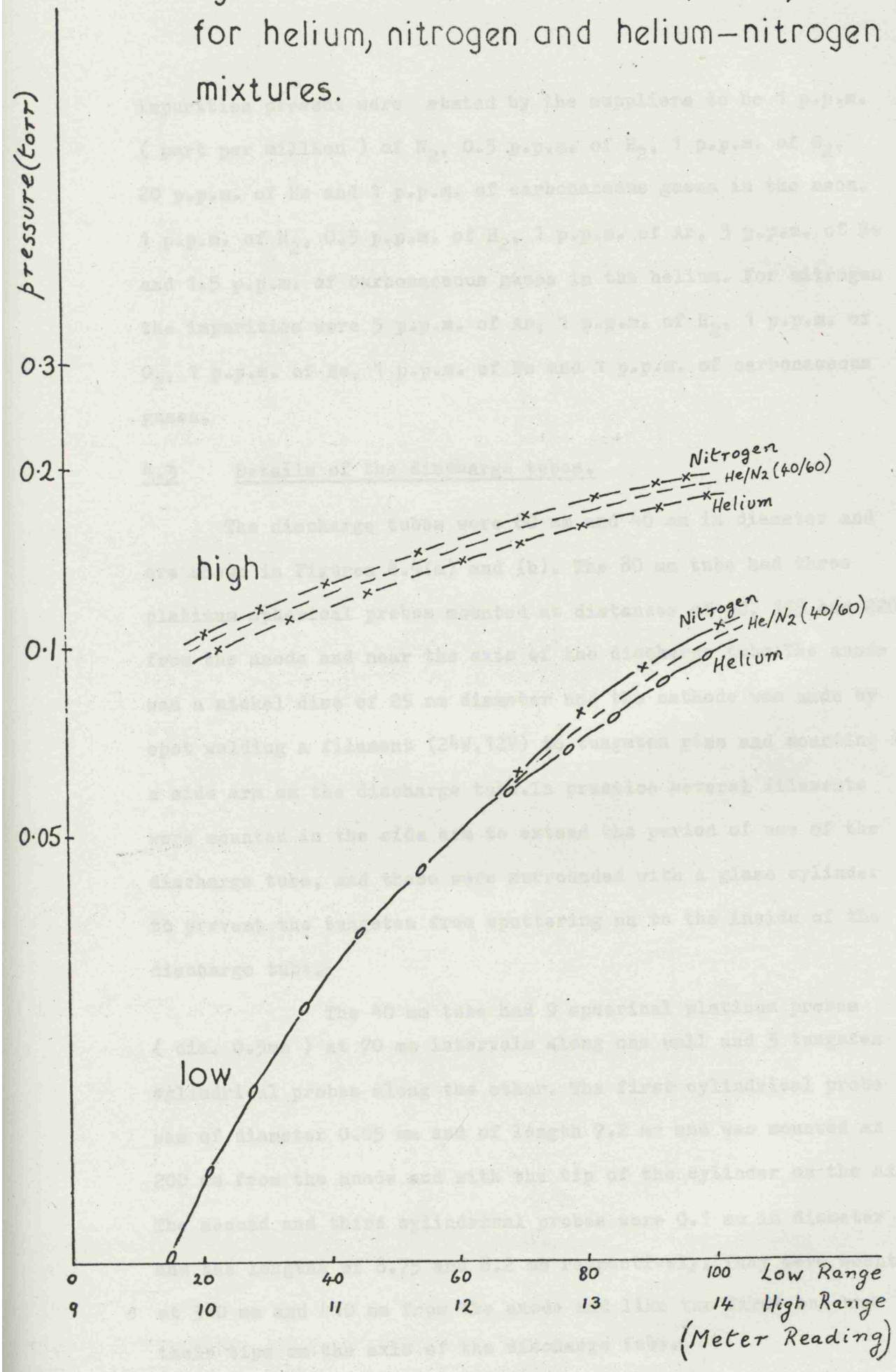

impurities present were stated by the suppliers to be 1 p.p.m. (part per million) of N_2, 0.5 p.p.m. of H_2, 1 p.p.m. of O_2, 20 p.p.m. of He and 1 p.p.m. of carbonaceous gases in the neon. 1 p.p.m. of N_2, 0.5 p.p.m. of H_2, 1 p.p.m. of Ar, 3 p.p.m. of Ne and 1.5 p.p.m. of carbonaceous gases in the helium. For nitrogen the impurities were 5 p.p.m. of Ar, 1 p.p.m. of H_2, 1 p.p.m. of O_2, 1 p.p.m. of He, 1 p.p.m. of Ne and 1 p.p.m. of carbonaceous gases.

4.3 Details of the discharge tubes.

The discharge tubes were 80 mm and 40 mm in diameter and are shown in Figures 4.4(a) and (b). The 80 mm tube had three platinum spherical probes mounted at distances of 90, 155 and 220 mm from the anode and near the axis of the discharge tube.The anode was a nickel disc of 25 mm diameter and the cathode was made by spot welding a filament (24W,12V) to tungsten pins and mounting in a side arm on the discharge tube.In practice several filaments were mounted in the side arm to extend the period of use of the discharge tube, and these were surrounded with a glass cylinder to prevent the tungsten from sputtering on to the inside of the discharge tube.

The 40 mm tube had 9 spherical platinum probes (dia. 0.5mm) at 70 mm intervals along one wall and 3 tungsten cylindrical probes along the other. The first cylindrical probe was of diameter 0.05 mm and of length 7.2 mm and was mounted at 200 mm from the anode and with the tip of the cylinder on the axis. The second and third cylindrical probes were 0.1 mm in diameter and had lengths of 8.75 and 8.2 mm respectively. They were mounted at 340 mm and 410 mm from the anode and like the first one had their tips on the axis of the discharge tube.

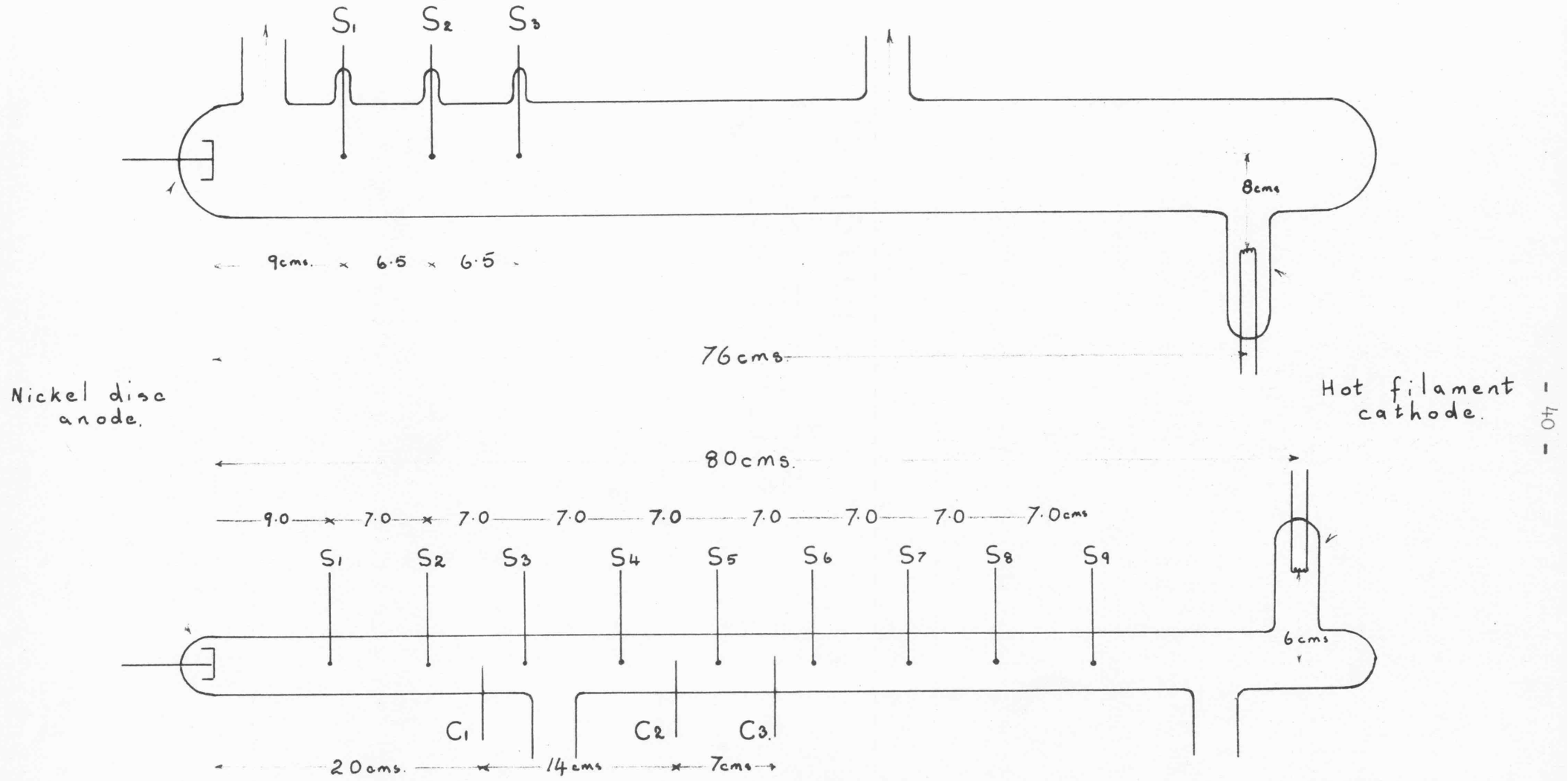

Fig. 4·4. Schematic representation of the discharge tubes.

(a) 8 cm. diameter tube. S_1 - S_3 spherical probes.

(b) 4 cm. diameter tube. S_1 - S_9 spherical probes. C_1 - C_3 cylindrical probes.

A third discharge tube was constructed which contained a moveable probe for radial measurements and had a series of counterprobes for investigating the influence of the reference electrode on probe characteristics. A diagram of the discharge tube is shown in Fig.4.4(c The radial probe was constructed to have complete movement across the tube. It was moved and held in position by a strong magnet which controlled an iron slug (in a glass envelope) attached to the probe. The probe was connected to the external tungsten pin by means of a flexible conducting wire. The tube also had three other fixed probes positioned as shown in the diagram.

The three counterprobes were made of platinum and were positioned at the centre of the tube. They were outgassed by the radiated heat from a tungsten filament in a silica envelope, which was placed near the counterprobes. They were fixed 6 mm apart and had surface areas of 2560 mm^2, 1620 mm^2 and 1280 mm^2. When connected together they had a maximum surface area of approximately 10^4 times the surface area of the measuring probe.

4.4 Details of the probes.

The accuracy of the results obtained in the investigation depends essentially on the design of the probes used in making the measurements As discussed in section 3.2 the Druyvesteyn theory holds for probes of any non-concave shape, however, this is only valid when the distribution is isotropic. It has been shown by Boyd and Twiddy[4.3] that whenever the isotropic nature of the energy distribution is in doubt it is necessary to use a spherical probe. Furthermore, Rayment and Twiddy[4.4] showed that in a low pressure positive column the electron energy distribution is anisotropic.For these reasons spherical probes have been used as a primary means of determining the electron energy

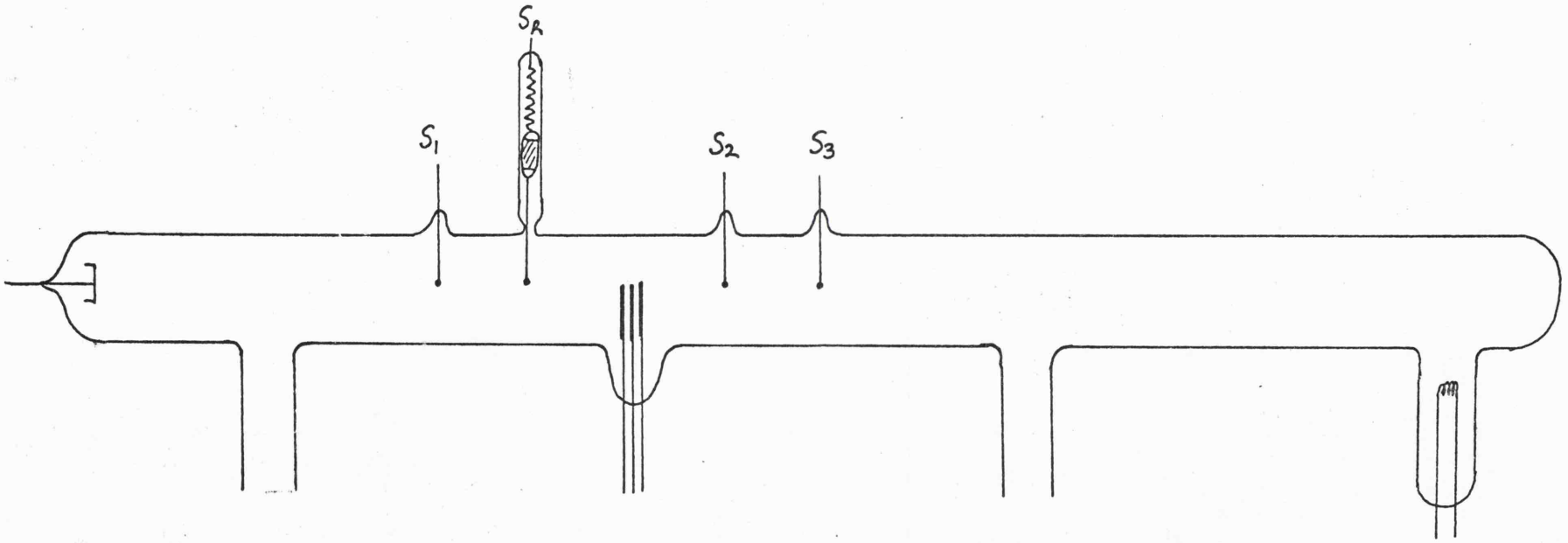

S_{1-3} spherical probes.
S_R radial spherical probe.
C_{1-3} counterprobes.

Fig 4.4(c) Schematic representation of discharge tube containing moveable probe and counterprobes.

distributions in the positive column, although cylindrical probes were added to the 40 mm discharge tube for comparitive purposes.

The size of the probe is important because it produces a disturbance in the discharge plasma. The probe theory requires that the mean free paths of the plasma particles are large compared with the probe diameter. If this is not true it has been shown by Waymouth[4.5] that the plasma density and potential in the vicinity of the probe may differ from those of the undisturbed plasma. Furthermore, Case[4.6] has shown that the collisionless probe theory only holds when the electron mean free path is very much greater than the probe diameter, otherwise the probe theory needs modification. In addition the probe can disturb the discharge plasma by drawing an electron current which is not negligible compared with the drift current. This problem was considered by Swift[4.7] who showed that in the case of probe measurements in helium, neon and nitrogen, the error involved in determining the electron energy distribution at energies greater than $\frac{1}{2}\overline{V}$, where $\overline{V}$ is the average electron energy, is less than 25% provided that the product of probe radius(a) and gas pressure(p) was less than 0.3 mm.torr for helium, 0.8 mm.torr for neon and 0.15 mm.torr for nitrogen.Clearly, therefore, the radius of the probe must be kept small and in the present investigation the ap product was at all times low enough to satisfy the foregoing limits.

Another problem which arose in the construction of the spherical probe was that it was necessary to shield most of the lead-in wire with a glass sleeveto prevent the collection of electrons

on the wire. Immediately adjacent to the spherical probe there was an area of exposed wire, the stem, which if too long could bring about a distortion of the electron energy distribution. However, if it was made too short the glass insulating sleeve itself will set up a disturbance distorting the parameters measured by the probe. An estimation of the disturbance caused by the insulating sleeve can be calculated using an equation derived by Waymouth[4.5] and is negligible when the mean free path of the electrons is very large compared with the radius(effective) of the insulating sleeve.The effect of the insulating sleeve on spherical Langmuir probe characteristics has been investigated by Richards et al[4.8] who constructed a probe in which the length of the stem could be varied.They found that at short stem lengths the probe underestimates the electron density. In the present investigation the ratio of the surface area of the sphere to that of the exposed wire was such as to minimise the effect of the disturbance and shielding caused by the glass sleeve covering the supporting wire. Also, the size of the glass sleeve was such as to minimise the capacitive effect first discussed by Olson and Medicus.[4.9]

The surface of the probes were examined periodically to check whether their dimensions had been changed to any extent. During the course of a series of runs the surface of the probe is being bombarded by the particles in the discharge plasma and it may be partly evaporated away. Checking was therefore necessary to prevent any error in the analysis of the data obtained. This becane particularly important after cleaning the probes by electron bombardment. The probes were also examined for any evidence

of sputtering on the glass insulating sleeve because electrical contact between this and the probe would cause an underestimation of the effective collecting area.

In an investigation of this nature it is essential that the contact potential of the probe surface remains constant with time and likewise the electrode(anode) used to return the probe current should have constant contact potential with the plasma. Hence, to prevent any changes in work function of the surfaces the anode was cleaned regularly by induction heating and the probe was kept free of contaminants by flashing red hot by electron bombardment before each run. A check on any changes in contact potential during a run was made by returning the probe to an earlier potential and measuring again the value of the second differential. In all cases the change in value was less than 1% and this was indicative of a stable contact potential over the long term.

The probes used in the investigation are shown in Figures 4.5(a),(b) and (c). The spherical probes were made by melting the end of 0.1 mm diameter wire (platinum) in an oxygen - coal gas flame. By using this method it was found that smooth bright spheres were formed as the wire melts and runs back on itself. By trial and error the size of the spheres were made all very nearly equal in diameter,0.5 mm, and after examination and measurement using a travelling microscope were assembled and joined to the discharge tube. The exposed wire near the sphere was also measured to ensure that it was within the limits discussed earlier.

The radial probe was constructed as shown in Figure 4.5(c). It had complete movement across the discharge tube and was held in position by a magnet which attracted an iron slug

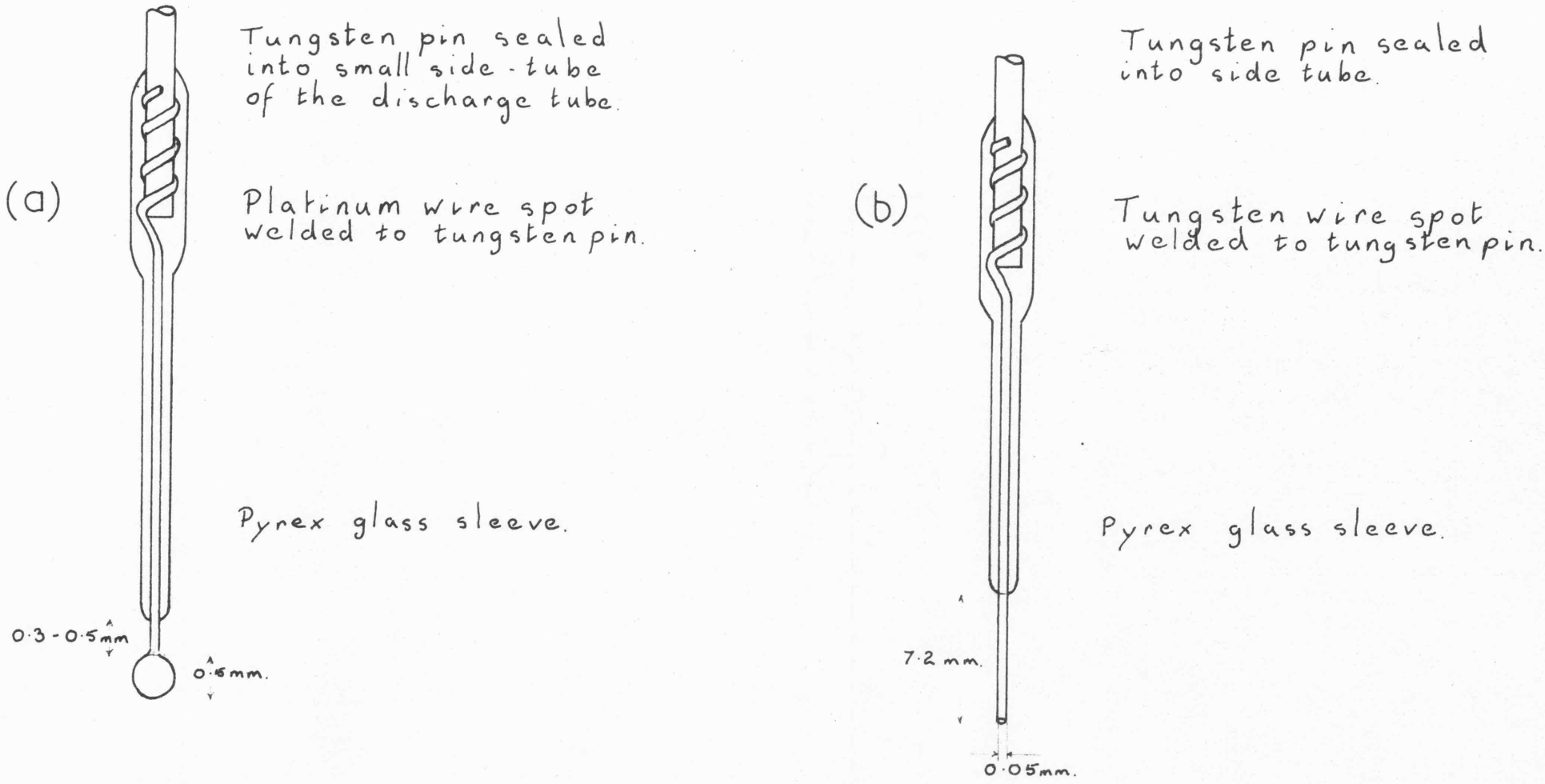

Fig. 4·5. Schematic representation of the construction of
(a) the spherical probe (platinum)
(b) the cylindrical probe (tungsten)

Fig. 4.5(c)

The radial probe.

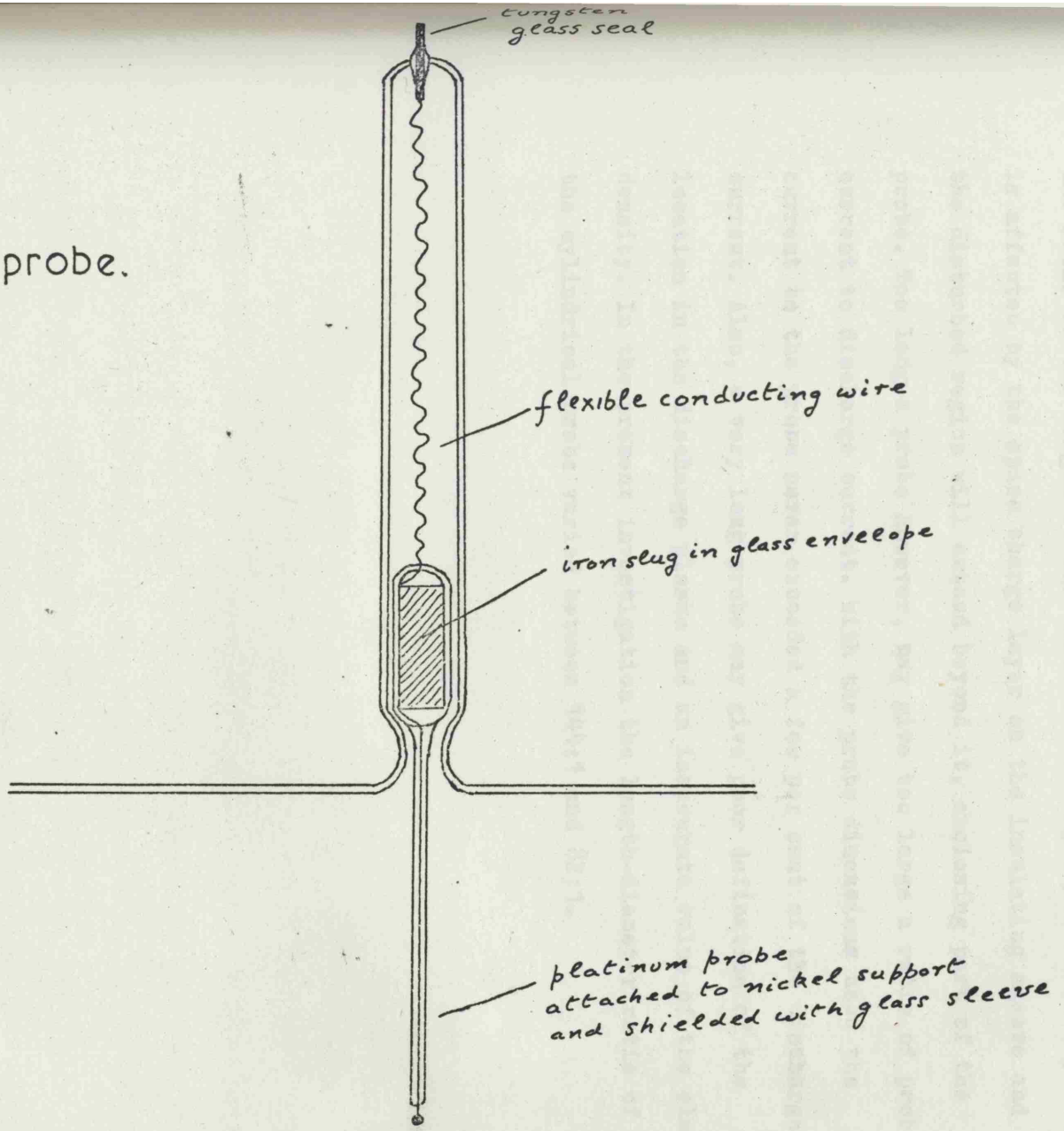

in a glass envelope attached to the probe.

The cylindrical probe dimensions were chosen so that the ratio of the length to the diameter was high. Too short a probe is affected by the space charge layer on the insulating sleeve and the disturbed region will extend beyond it, enclosing part of the probe. Too long a probe however, may give too large a ratio of probe current to discharge current. With the probe dimensions used the current to the probe never exceeded a few per cent of the discharge current. Also, a very long probe may give poor defination of the location in the discharge plasma and an inaccurate value of the electron density. In the present investigation the length-diameter ratio of the cylindrical probe varied between 144:1 and 82:1.

CHAPTER 5 THE ELECTRONIC EQUIPMENT AND METHOD OF CALIBRATION.

5.1 The probe circuitry.

To measure the second differential of the probe current a small pure sinusoidal signal is superimposed on to the d.c. bias applied to the probe and a voltage, proportional to the a.c. component of the probe current, is produced across a resistance R in series with the probe. A simplified diagram indicating the general arrangement is shown in Figure 5.1. The second harmonic of the a.c. current to the probe , which as shown in section 3.3 is related to the second differential, is selected by a filter. This is amplified by a narrow band amplifier and detected by a phase sensitive detector, giving a reading proportional to the second harmonic.

The method of introducing the sinusoidal signal and the technique used for detecting the second harmonic component of the current in the Langmuir probe circuit will now be described.

5.2 Method of introduction of sinusoidal signal.

The main limitation of introducing the sinusoidal signal into the probe circuit is the danger of forming an earth loop. The method used in the present investigation was by introducing the sinusoidal signal via a transformer and was first successfully used by Malyshev and Federov[5.1] and later by other workers.

The signal generator used was a low distortion oscillator supplied by Radford Electronics Ltd. The generator had an output impedance of 600Ω. Apart from its low distortion it was also attractive in that it had high inherent frequency stability. The distortion produced by the oscillator was approximately 0.005% at the frequency used and with the 600Ω attenuator in the circuit.

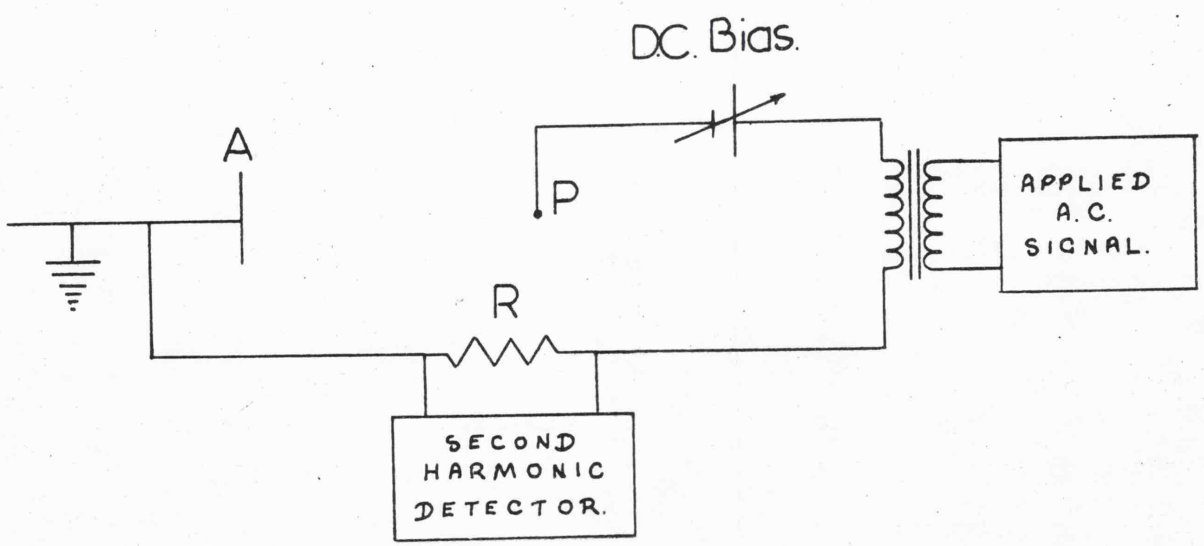

Fig. 5.1. A simplified diagram of the probe circuitry

This was checked by using a distortion measuring set. The frequency stability after a warm up of 30 minutes was better than one part in 10^4. This was checked originally by using an Advance TC5 frequency counter and during the investigation by observing the variation in output of the phase sensitive detector at a particular setting.

5.3 Isolation and amplification of the S.H. component.

The a.c. probe current measured by R contains many harmonics of the applied signal, but the predominant one is the first harmonic. It is essential to filter out this harmonic to prevent the swamping of the second harmonic which is to be detected. A twin T-type filter was used to eliminate the first harmonic and is shown diagrammatically in Figure 5.2. The component values were checked and are shown. The transmission characteristics of the filter is shown in Figure 5.3. An Advance TC5 counter was used for the frequency measurements. The transmission characteristics of the filter show zero transmission at 496 Hz whereas the actual transmission was 1 mV for a 10.0V input, that is 80 dB attenuation. The filter output was also measured at twice the frequency, 992 Hz, that is at the frequency of the second harmonic to be detected. It was measured as 1.9V giving an attenuation of 15 dB , which is not too excessive.

Having filtered out the first harmonic, the second harmonic is amplified by a tuned amplifier which has a sufficiently narrow bandwidth to remove higher harmonics. The higher harmonics are very small compared with the first and second. The tuned amplifier used should have a high signal-to-noise ratio and the one shown in the Mullard's Reference Manual[5.2] was built. The amplifier

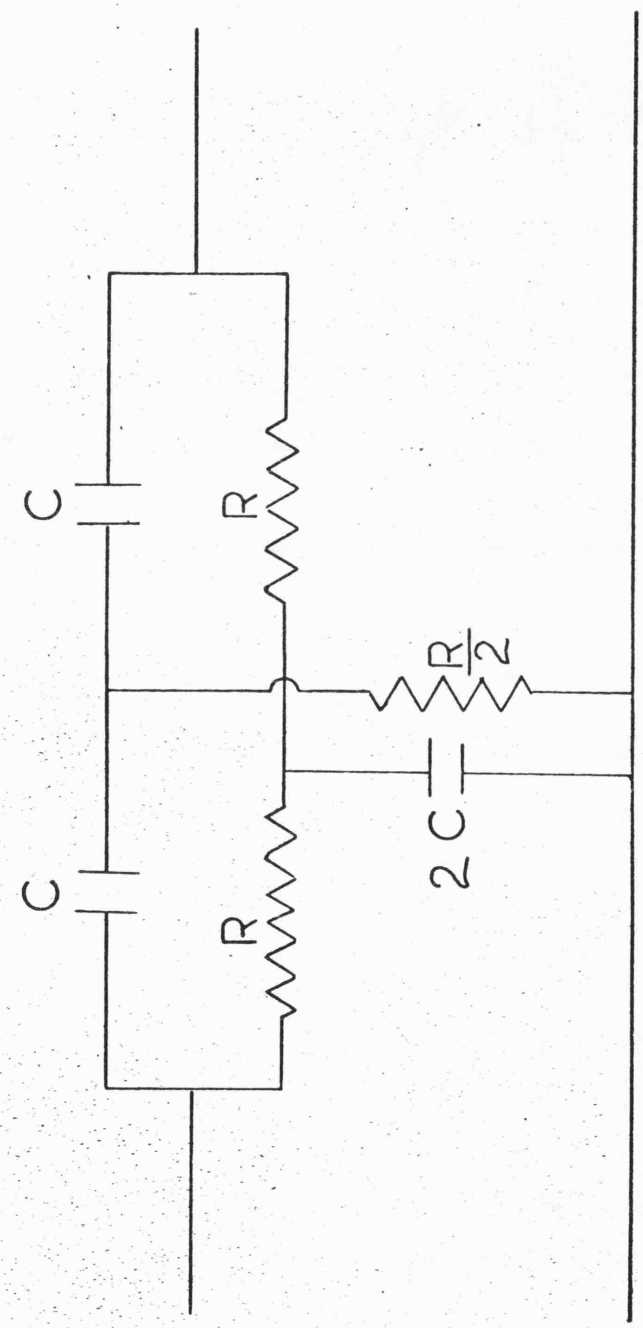

Fig.5.2 Parallel twin T-type filter.

Fig. 5.3 Transmission characteristics for twin–T type filter. (Input - 10 Volts)

Zero transmission when

$$\omega = \frac{1}{CR}$$

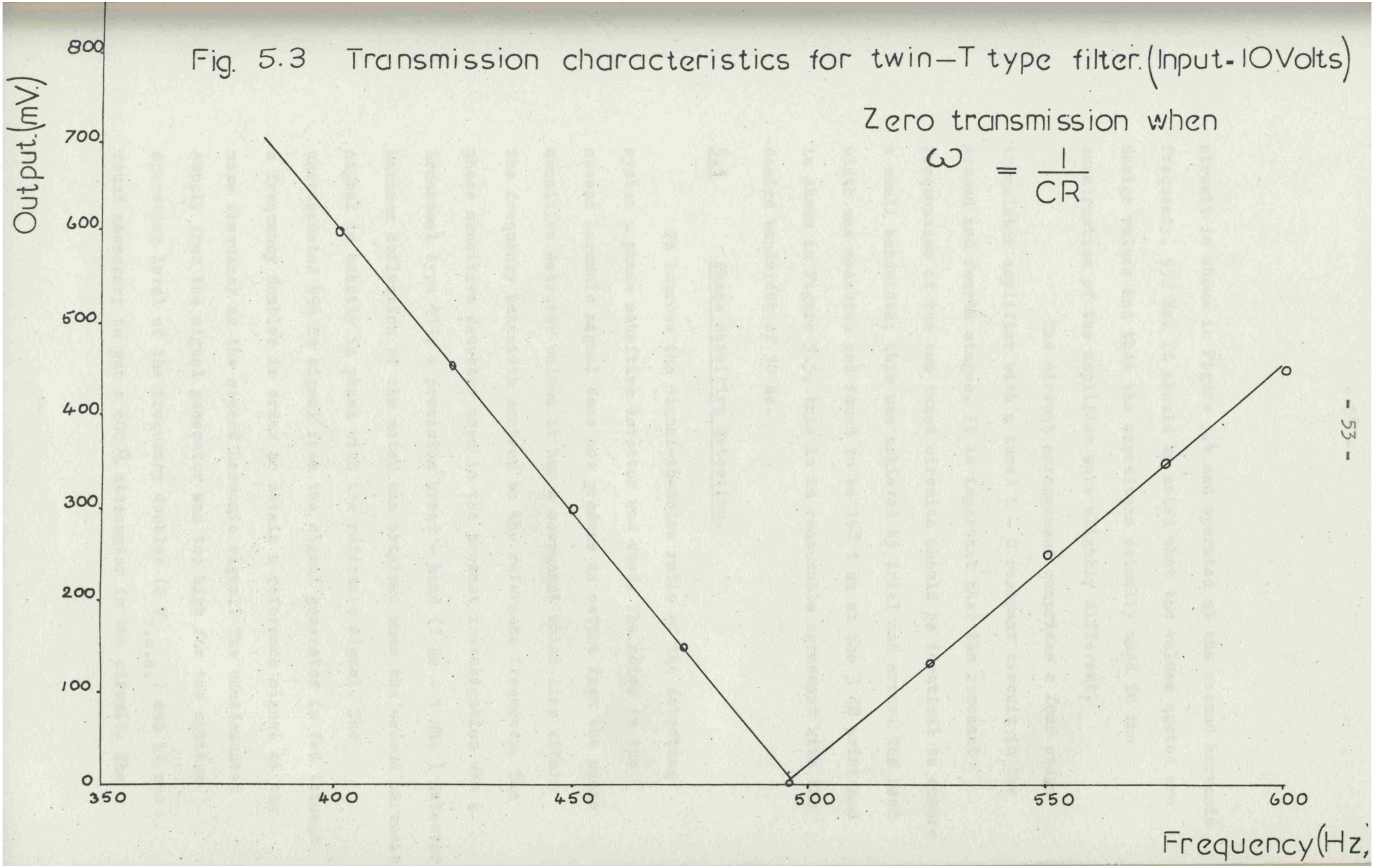

circuit is shown in Figure 5.4 and operated at the second harmonic frequency, 992 Hz. It should be noted that the values quoted are design values and that the capacitors actually used in the construction of the amplifier were slightly different.

The circuit arrangement comprises a four stage transistor amplifier with a tuned L - C resonant circuit in the second and fourth stages. It is important that the resonant frequencies of the two tuned circuits should be identical to ensure a small bandwidth; this was achieved by trial and error. The band width was measured and found to be 16 ± 1 Hz at the 3 dB point and is shown in Figure 5.5, this is in reasonable agreement with the design bandwidth of 10 Hz.

5.4 Phase sensitive detection.

To improve the signal-to-noise ratio of the detecting system a phase sensitive detector was used. The noise in the second harmonic signal does not produce an output from the phase sensitive detector unless it has a component which lies within the frequency bandwidth centred on the reference frequency. The phase sensitive detector used in the present investigation was a Brookdeal type 411, a precision broad - band (1 Hz - 1 MHz) detector. Maximum deflection of the meter was obtained when the second harmonic signal is exactly in phase with the reference signal. The unattenuated 496 Hz signal from the signal generator is fed through a frequency doubler in order to obtain a reference signal at the same frequency as the second harmonic signal. The unattenuated supply from the signal generator was too high for the optimum operating level of the frequency doubler (2 $V_{r.m.s.}$) and it was found necessary to put a 600 Ω attenuator in the circuit. The

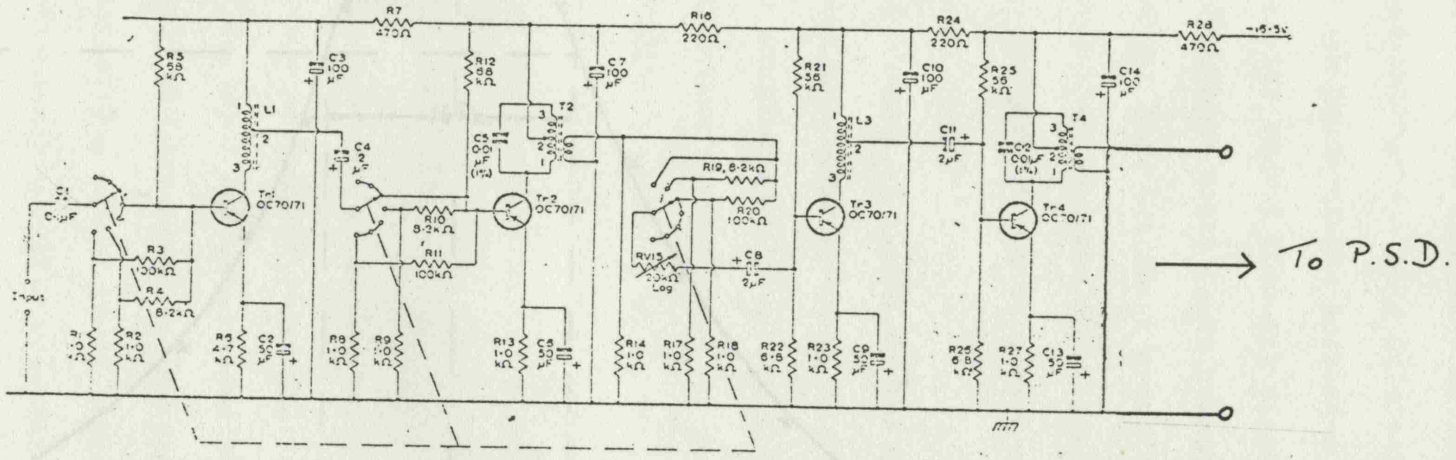

L1 and L3 are Ferroxcube LA1 pot cores: 3680 turns of 45 s.w.g. Lewmex type F wire, tapped at 726 turns: primary inductance 5H. T2 is Ferroxcube LA13 pot core: *primary* 1312 turns of 38 s.w.g. Lewmex type F wire tapped at 175 turns: primary inductance 2·54H ± 0·5% at 1000c/s for small signals: undamped Q ≥ 150; *secondary* 25 turns of same wire. T4 is Ferroxcube LA1 pot core: *primary* 2620 turns of 44 s.w.g. Lewmex type F wire tapped at 605 turns: primary inductance 2·54H ± 5% at 1000c/s for small signals: *secondary* 150 turns of same wire.

Fig. 5.4 992 Hz tuned amplifier.

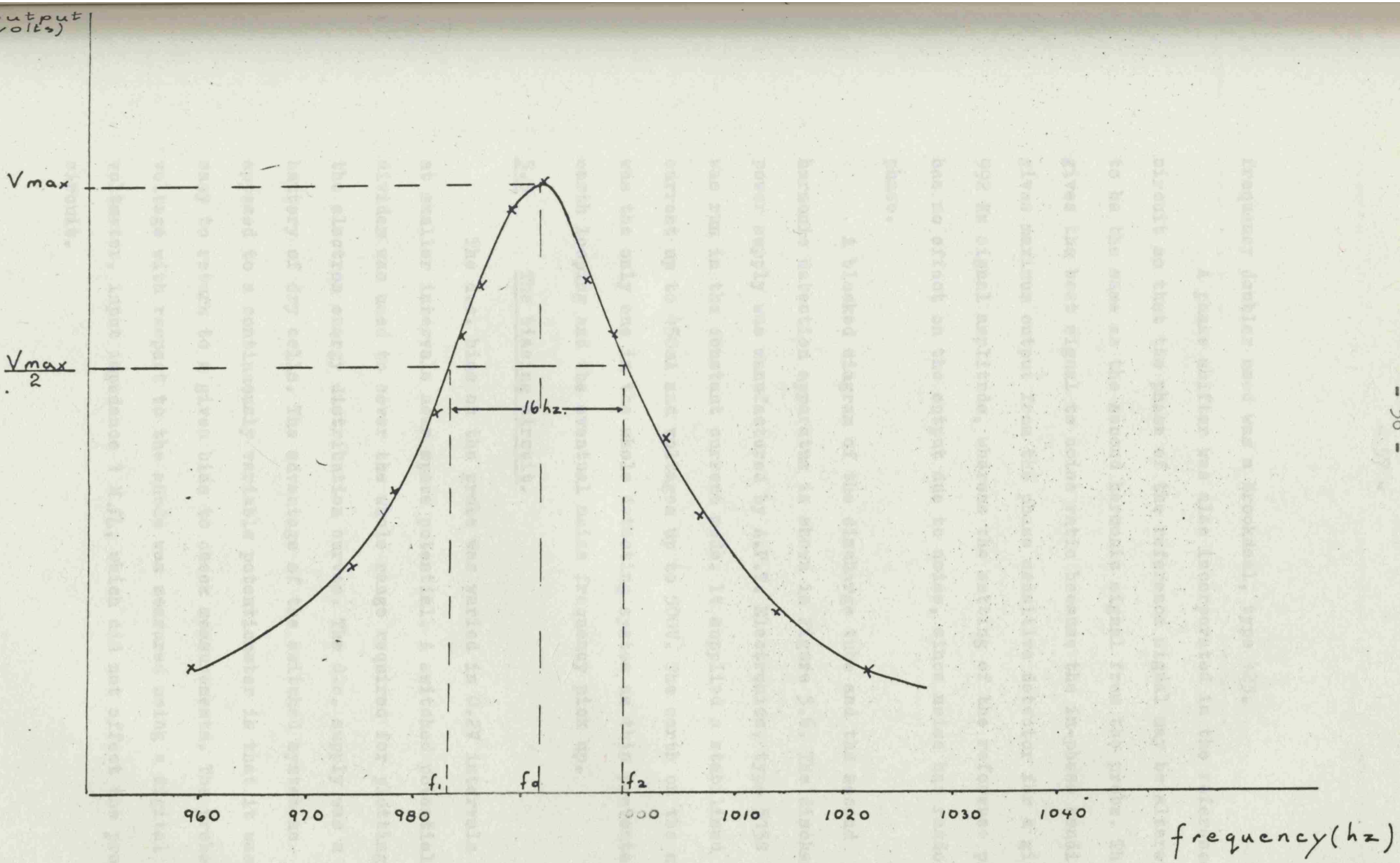

Fig 5.5 Bandwidth of 992 hz. tuned amplifier.

frequency doubler used was a Brookdeal, type 423.

A phase shifter was also incorporated in the reference circuit so that the phase of the reference signal may be altered to be the same as the second harmonic signal from the probe. This gives the best signal to noise ratio because the in-phase condition gives maximum output from the phase sensitive detector for a given 992 Hz signal amplitude, whereas the setting of the reference phase has no effect on the output due to noise, since noise has random phase.

A blocked diagram of the discharge tube and the second harmonic detection apparatus is shown in Figure 5.6. The discharge power supply was manufactured by A.P.T. Electronics, type 515S and was run in the constant current mode. It supplied a stabilised current up to 450mA and voltages up to 500V. The earth on the anode was the only one in the whole detecting system as this prevented earth looping and the eventual mains frequency pick up.

5.5 The biasing circuit.

The d.c. bias on the probe was varied in 0.2V intervals and at smaller intervals near space potential. A switched potential divider was used to cover the whole range required for plotting the electron energy distribution curves. The d.c. supply was a battery of dry cells. The advantage of the switched system as apposed to a continuously variable potentiometer is that it was easy to return to a given bias to check measurements. The probe voltage with respect to the anode was measured using a digital voltmeter, input impedance 1 MΩ, which did not affect the probe circuit.

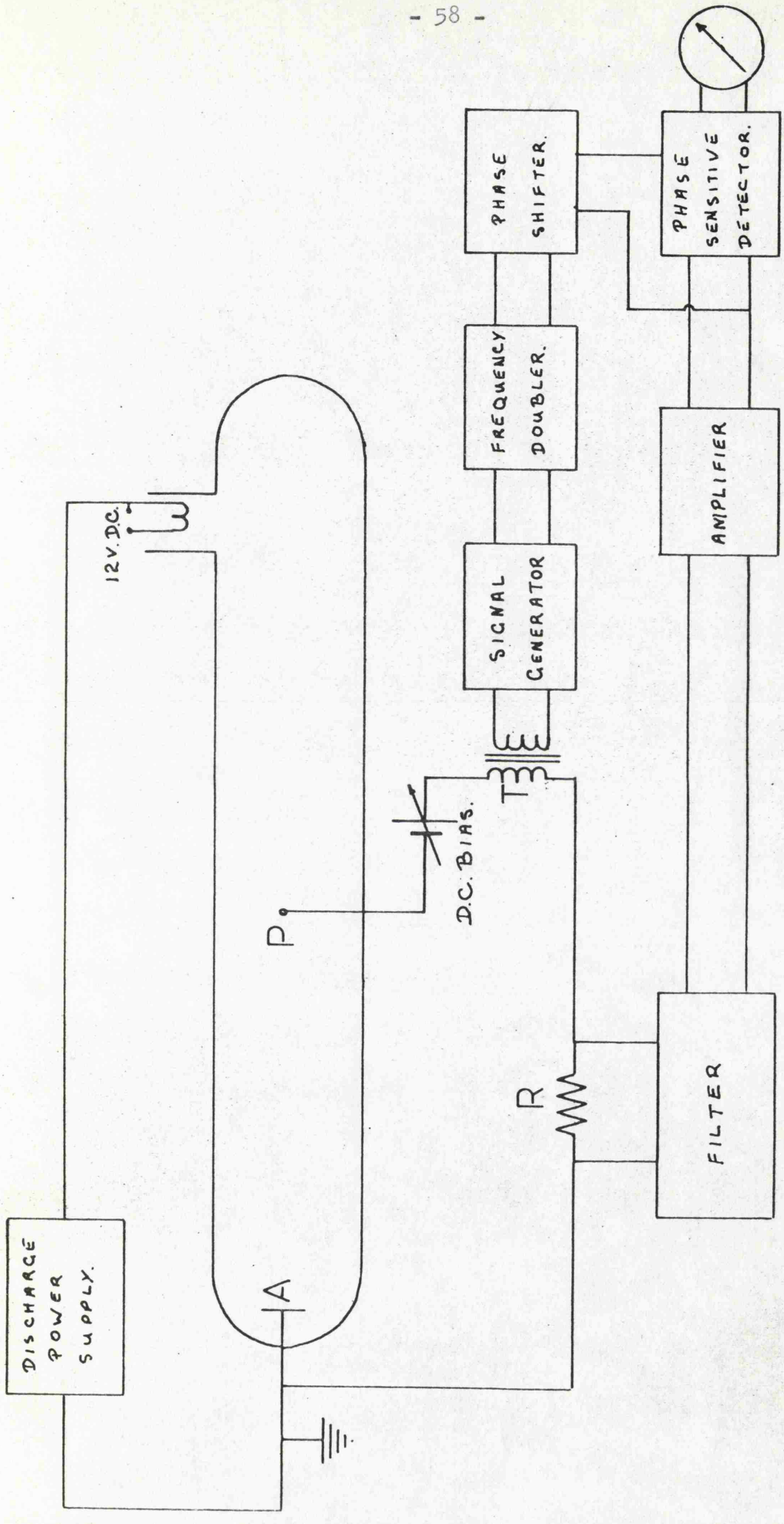

Fig. 5.6 Blocked diagram of second harmonic detection apparatus.

5.6 Calibration of the detecting system and check of linearity.

A signal, calibrated using a Tetronik oscilloscope, was applied to the amplifier - phase sensitive detector system and the galvanometer deflection noted. The calibrated signal, at twice the frequency (992 Hz) of that applied to the probe, was fed from the 600 Ω output of the signal generator through a variable 600 Ω attenuator. An input signal to the detecting system of 1.3×10^{-4} V gave a galvanometer deflection of 100 units.

Hence the current corresponding to 1 unit of galvanometer deflection = $\frac{1.3 \times 10^{-4}}{100} \times \frac{1}{600}$ amps

$$= 2.16 \times 10^{-9} \text{ A} = k$$

This was the calibration constant, k , used throughout the investigation. This was checked systematically for variation with time but was found to remain unchanged.

It has been shown earlier that the second harmonic signal detected in the present investigation is related to the second differential of the probe current by the equation

$$i_{2\omega} = \frac{E^2}{4} \frac{d^2 i_e}{dV^2}$$

The dependence on E^2 is a useful check on the correct functioning of the detecting system. It is seen from Figure 5.7 that the output from the detecting system varies linearly with E^2 for all values up to 0.1 $(\text{volts})^2$, that is for $E < 0.3$ volts. In the present investigation the E used was always within this upper limit. For the high energy tail of the distribution curve higher values of the amplitude were used, because it has been shown by Kilvington et al[5.3] that in this region increasing E has little effect on the linearity.

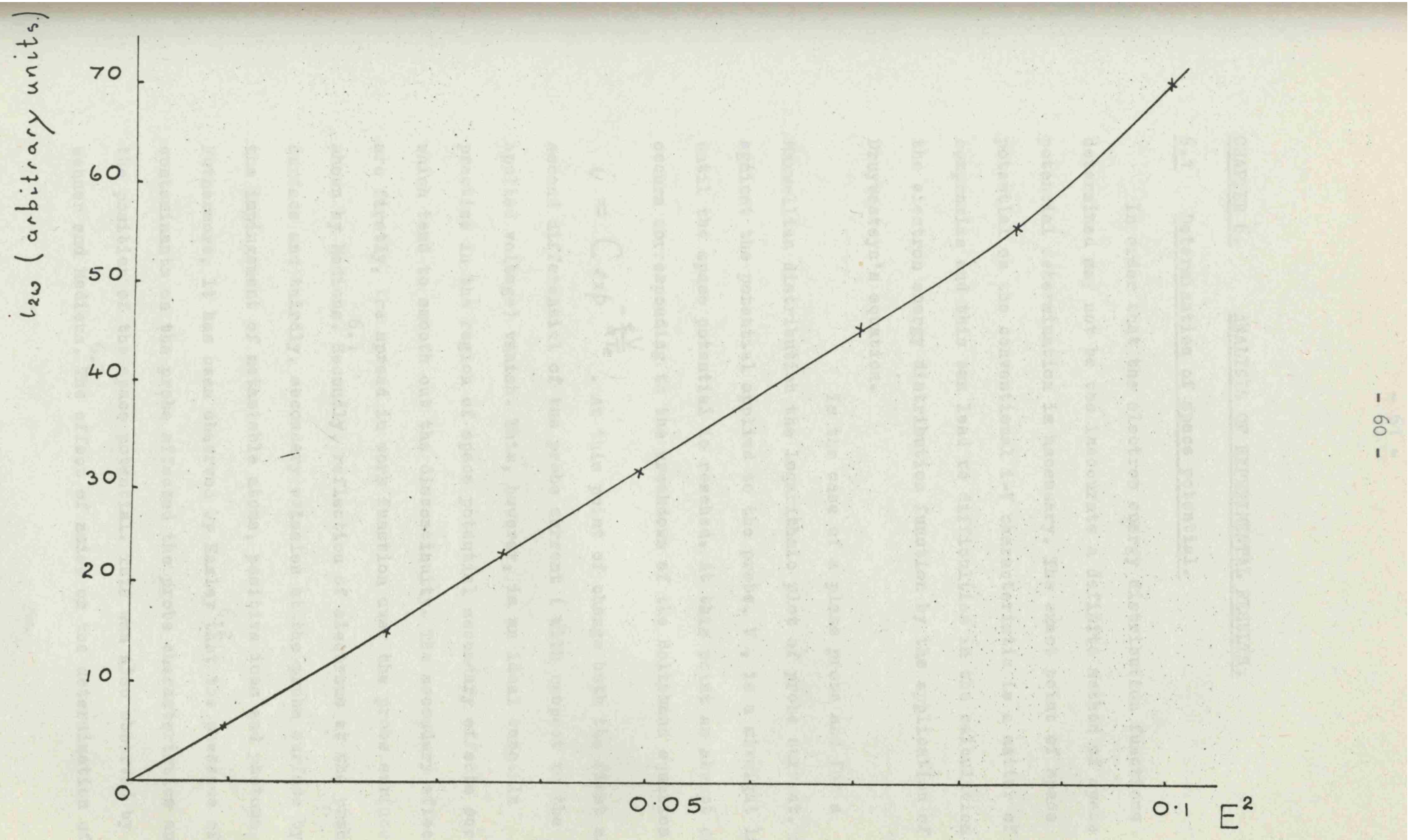

Fig. 5.7 The variation of $i_{2\omega}$ with E^2.

CHAPTER 6. ANALYSIS OF EXPERIMENTAL RESULTS.

6.1 Determination of space potential.

In order that the electron energy distribution functions determined may not be too inaccurate a definite method of space potential determination is necessary. The exact point of space potential on the conventional i-V characteristic is a matter of compromise and this can lead to difficulties in the calculation of the electron energy distribution function by the application of Druyvesteyn's equation.

In the case of a plane probe and for a Maxwellian distribution the logarithmic plot of probe current, i , against the potential applied to the probe, V , is a straight line until the space potential is reached. At this point an abrupt change occurs corresponding to the breakdown of the Boltzmann equation $i = C\,exp^{-\frac{eV}{kT_e}}$. At this point of change both the first and second differential of the probe current (with respect to the applied voltage) vanish. This, however, is an ideal case. In practice in the region of space potential secondary effects occur which tend to smooth out the discontinuity. The secondary effects are firstly, the spread in work function over the probe surface as shown by Medicus.[6.1] Secondly, reflection of electrons at the probe surface and thirdly, secondary emission at the probe surface by the impingement of metastable atoms, positive ions and photons. Futhermore, it has been observed by Easley[6.2] that the presence of contaminants on the probe affected the probe characteristics and the position of the space potential. This was also observed by Wehner and Medicus.[6.3] The effect of noise on the determination of

space potential has been discussed by Garscadden and Emeleus.[6.4] They observed that for noisy discharges the apparent space potential break on the semi-log plot in the presence of oscillations is several volts negative to that in their absence. In the present investigation measurements were taken whenever possible in the absence of oscillations, but for neon and some helium-neon mixtures oscillations were present at all pressures and discharge currents investigated.

The effect of electron drain from the plasma has been discussed earlier in Section 4.4. In the present investigation the ap (a is the probe radius, p the gas pressure) values used were well below the limit at which this disturbance occurs and hence minimal distortion of the electron energy distribution function was expected from this effect.

As a result of these secondary effects instead of the derivatives decreasing rapidly to zero as for the ideal case, they now decrease at different voltages and there is a spread of voltage between the top and bottom of the second derivative curve as shown in Figure 6.1. Consequently, the position of the space potential becomes a matter of compromise.

Various methods of determining the space potential have been given. Some take the break-away point of the semi-log plot which will probably be lower than the actual space potential because of secondary effects. This error is not significant provided the characteristics are only being used for comparitive purposes such as the variation of average electron energy or electron density with various discharge tube parameters.

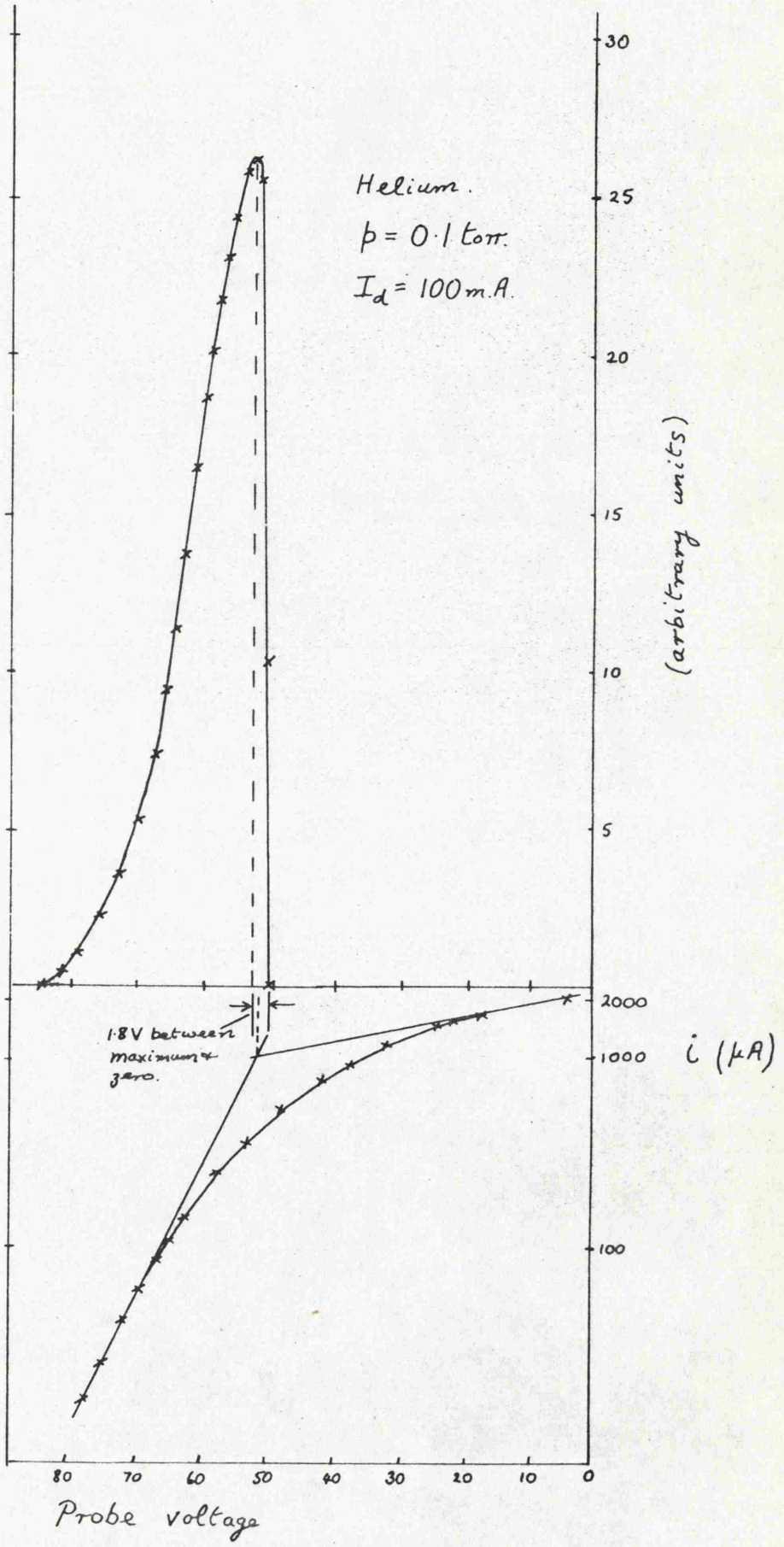

Fig. 6.1 A second derivative curve and semi-log plot.

However, it is important that the point where the space potential occurs should be accurately defined and determined. The graphical method of the double differentiation of the conventional i-V plot is not sufficiently accurate and hence some other method must be used. In the present investigation this point was taken as where the second derivative, obtained using the second harmonic method, reduced rapidly to zero.

The space potential must be accurately defined because it is used as the zero of the electron energy distribution function. Druyvesteyn[6.5] suggested defining the space potential as the intersection of the tangents to the semi-log plot at the bend of the curve. However, definition here is poor because it depends on the slope of the semi-log plot in the retarding region and on the slope in the accelerating region which is not clearly defined. In the present investigation the point at which the tangents intersected was not found to coincide with the zero cross of the second derivative. A second derivative curve and a semi-logarithmic plot are shown in Figure 6.1 for a helium positive column at 0.1 torr pressure and 100 mA discharge current. As can be seen from the figure the intersection of the tangents of the Langmuir plot lies between the maximum and zero cross of the second derivative curve.

Zaitsev[6.6] found that the intersection of the tangents to the conventional i-V curve coincided with the maximum probe noise. As the presence of a space charge sheath causes a suppression of the noise it is expected that the noise will be maximum when the probe is at space potential, since sheaths are absent at this point.

Recently, Milenin[6.7] showed that in helium and neon the noise maximum coincided with the zero cross of the second derivative curve. He also showed that it coincided with the maximum of the first derivative The first derivative has a more pronounced variation in going through the space potential than the current itself.The second derivative is even more sensitive and reverses sign at a probe potential near the space potential. Luijendijk and Van Eck[6.8] indicate unambiguously that the bend in the probe characteristic corresponds to the space potential because the second derivative is zero there. Furthermore, Hemsworth and Twiddy[6.9] have shown that the intersecting tangent on the Langmuir plot and the zero cross of the second derivative curve coincide within one volt.

Consequently, in the present investigation the zero cross of the second derivative curve is taken as defining space potential and is used as the origin of the electron energy distribution function.

6.2 Examination of the distribution functions for Maxwellian or Druyvesteyn forms.

A general equation for the form of the distribution curve can be given as

$$f(V) = A V^{a} \exp\left(-k V^{b}\right)$$

where a=0.5, b=1 for the Maxwellian and a=0.5, b=2 for the Druyvesteyn form.

The equation can be written as

$$\log_e \frac{f(V)}{V^{a}} = \log_e A - k V^{b}$$

and hence a graph of $\log_e \frac{f(V)}{V^{a}}$ plotted against V^{b} should yield a

straight line provided the right values of a and b are chosen. The values of a and b were derived by trial and error. An example of this approach is shown in Figure 6.2 for helium at 0.15 torr pressure and 100mA discharge current. An equation which appears to fit the low energy end of the distribution is

$$f(V) = A V^{4} \exp(-k V^{\frac{1}{2}})$$

This corresponds to the slow electrons and is a confirmation of the empirical equation deduced by Swift[6.10] working with nitrogen who found a similar equation fitted the greater part of the distribution curve at a pressure where only the slow electron swarm is present. In Figure 6.3 the experimental values are plotted with $a=\frac{1}{2}, b=1$ corresponding to a Maxwellian and $a=\frac{1}{2}$, $b=2$ corresponding to a Druyvesteyn form. As can be seen from the figure the experimental values lie closer to a Druyvesteyn form than the Maxwellian. It is apparent therefore that the high energy tail corresponds to the Druyvesteyn form of distribution , whereas the low energy part of the distribution curve seems to satisfy the empirical equation derived.

The deviations from linearity when $\log \frac{f(V)}{V^{\frac{1}{2}}}$ is plotted against V is a clear indication of the breakdown of the Maxwellian distribution and it is concluded therefore that neither the low energy part nor the high energy tail corresponds to the Maxwellian form of distribution.

To confirm the above conclusions the Maxwellian and Druyvesteyn distribution functions for the same average electron energy are plotted for comparison with the observe distribution curve. This is shown in Figure 6.4 for helium at 0.15 torr pressure and 100mA discharge current. It is seen that there is

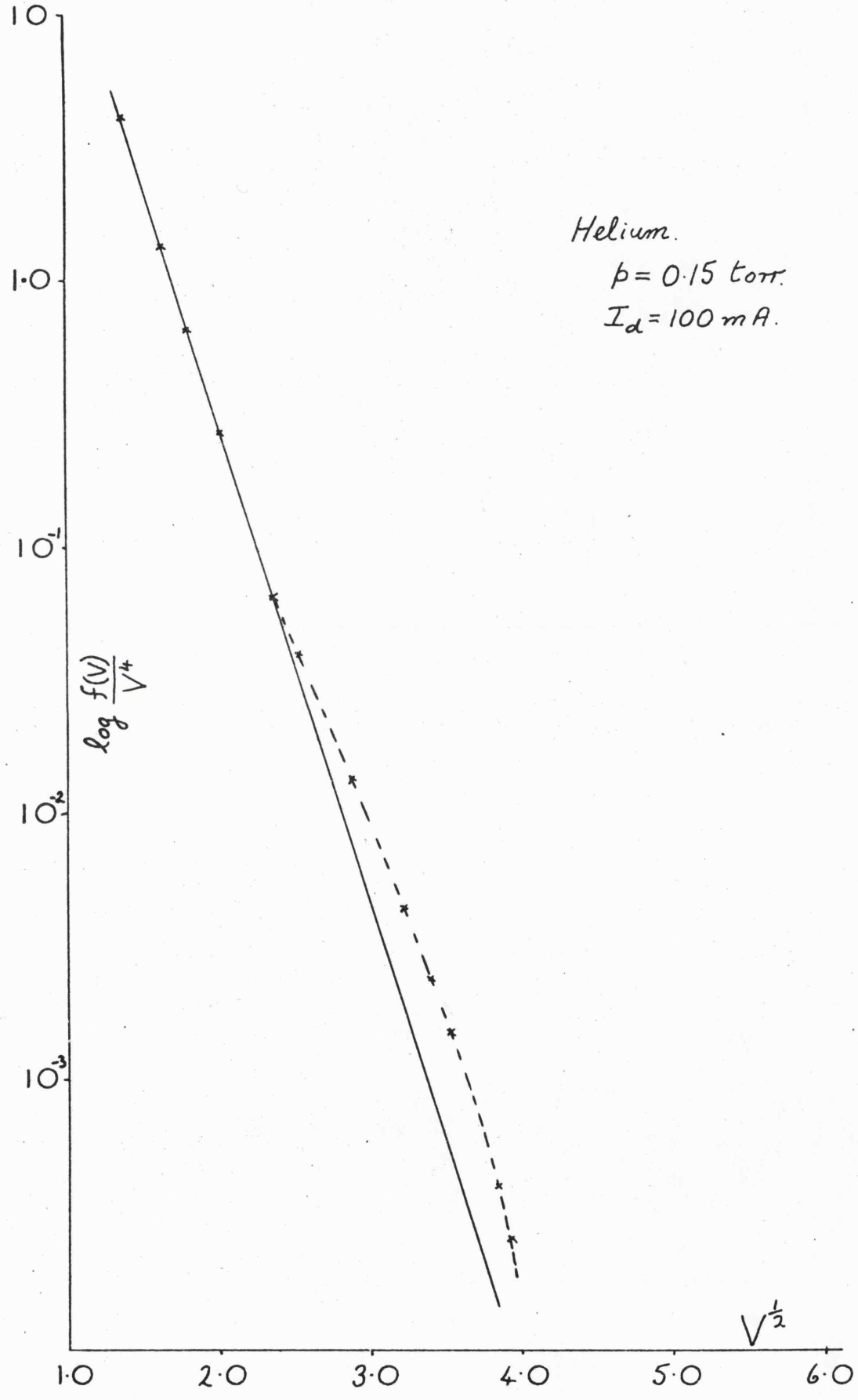

Fig. 6.2 Semi logarithmic analysis of experimental results.

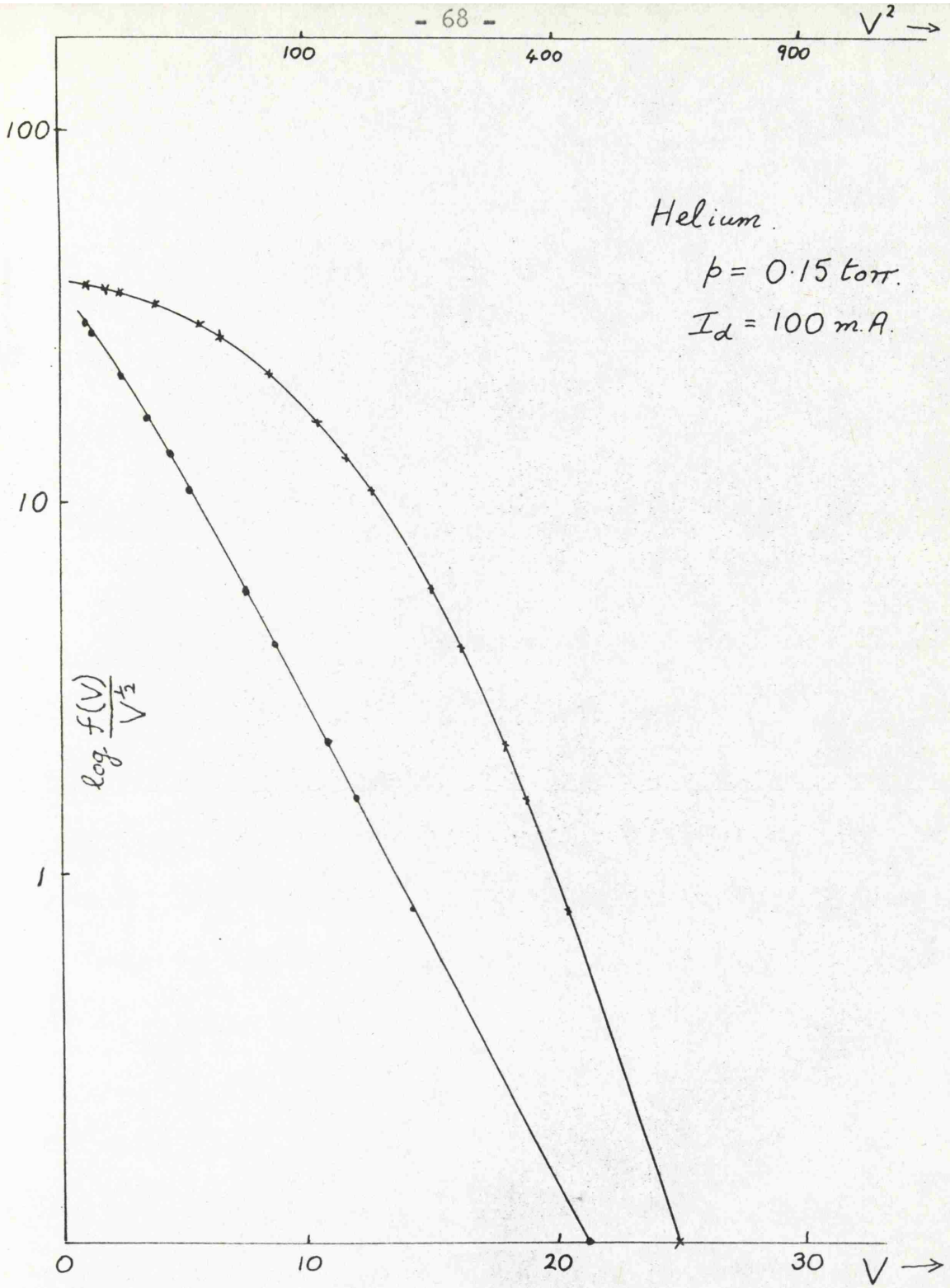

Fig. 6.3 Semi logarithmic analysis of experimental results to test for Maxwellian and Druyvesteyn distribution.

Fig. 6.4 Comparison of experimental distribution curve with the Maxwellian and Druyvesteyn functions.

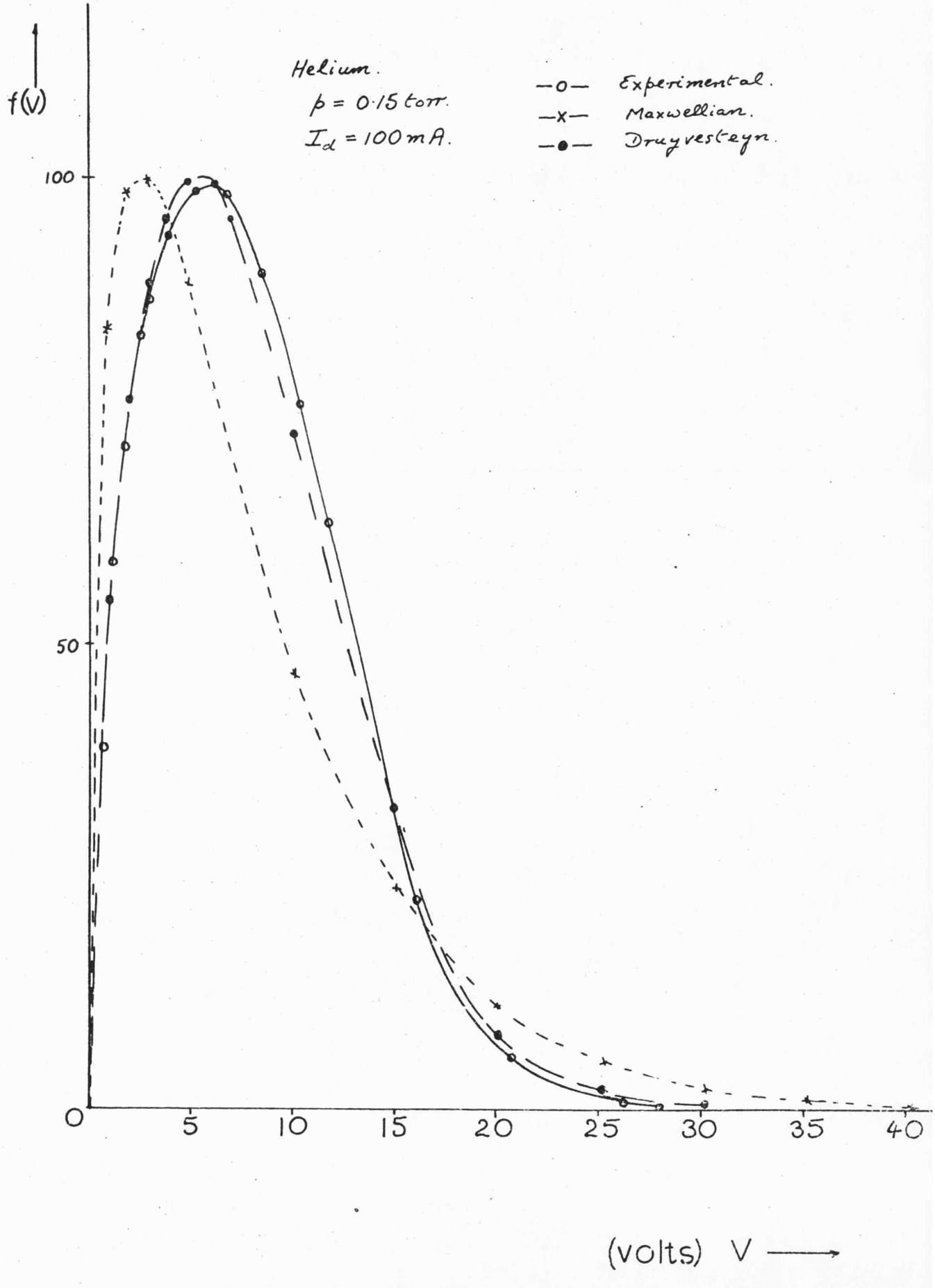

a strong difference between the experimental curve and the Maxwellian in that the high energy tail is much more rapidly attenuated. However, there appears to be a similarity with the Druyvesteyn curve.

Further comparisons between the experimental distribution curves and theoretical forms for various tube parameters and mixture ratios will be given later. These will be discussed in Chapter 8.

6.3 Electron density from $\bar{v}$ and i_p.

The electron density, n_e, can be obtained from the equation

$$j_p = \frac{e\, n_e}{4} \cdot \bar{v}$$

where j_p is the current density to the probe at space potential and $\bar{v}$ is the mean electron velocity given by

$$\bar{v} = \frac{\int_0^\infty v \cdot f(V) \cdot dV}{\int_0^\infty f(V) \cdot dV} = \left(\frac{2e}{m}\right)^{\frac{1}{2}} \left[\frac{\int_0^\infty V \cdot \frac{d^2 i_e}{dV^2} \cdot dV}{\int_0^\infty V^{\frac{1}{2}} \frac{d^2 i_e}{dV^2} \cdot dV}\right]$$

$$= \left(\frac{2e}{m}\right)^{\frac{1}{2}} \cdot \frac{I_2}{I_1}$$

where e is the electronic charge and m the electronic mass. The ratio in the squared brackets $\frac{I_2}{I_1}$ was obtained from the second harmonic readings measured at various values of V, where $V = V_p - V_s$ (V_p is the probe voltage with respect to the anode as reference and V_s is the space potential). The second harmonic readings were multiplied by V and $V^{\frac{1}{2}}$ respectively and plotted against V. The integrals were obtained using the trapezium rule for integration.

This is illustrated by referring to Figure 6.5. The area under the curve from A to B is the sum of all the trapeziums

$$T_1 + T_2 + T_3 + \ldots\ldots\ldots T_n = I$$

where $T_1 = \frac{1}{2}(y_1 + y_2) \times (x_2 - x_1)$

Similarly T_2 to T_n can be found and then summated.

Hence $$I_1 = \sum_{1}^{n-1} \frac{1}{2} \left(\left[V^{\frac{1}{2}} \frac{d^2 i_e}{dV^2} \right]_{n+1} + \left[V^{\frac{1}{2}} \frac{d^2 i_e}{dV^2} \right]_n \right) \times \left(V_{n+1} - V_n \right)$$

and $$I_2 = \sum_{1}^{n-1} \frac{1}{2} \left(\left[V \frac{d^2 i_e}{dV^2} \right]_{n+1} + \left[V \frac{d^2 i_e}{dV^2} \right]_n \right) \times \left(V_{n+1} - V_n \right)$$

and therefore

$$j_p = \frac{e . n_e}{4} \left(\frac{2e}{m} \right)^{\frac{1}{2}} \frac{I_2}{I_1}$$

or $$i_p = \frac{e . n_e . A}{4} \left(\frac{2e}{m} \right)^{\frac{1}{2}} \frac{I_2}{I_1}$$

where is the current to the probe at space potential and A is the area of the probe.

The value of the ratio $\frac{I_2}{I_1}$ was calculated by feeding the data of the detecting system output and the measured probe potential (V_p) into a Computer ICL 1902A, which was programmed using the Fortran system for evaluating this ratio.

The above equation can be reduced to

$$n_e = \frac{i_p}{1.8 \times 10^{-14} \times \frac{I_2}{I_1}}$$ for a spherical probe of diameter 0.5mm

where i_p is the probe current in amperes and n_e is the number of electrons per cubic metre.

Fig. 6.5 Illustration of trapezium rule for finding the area under the electron energy distribution curve.

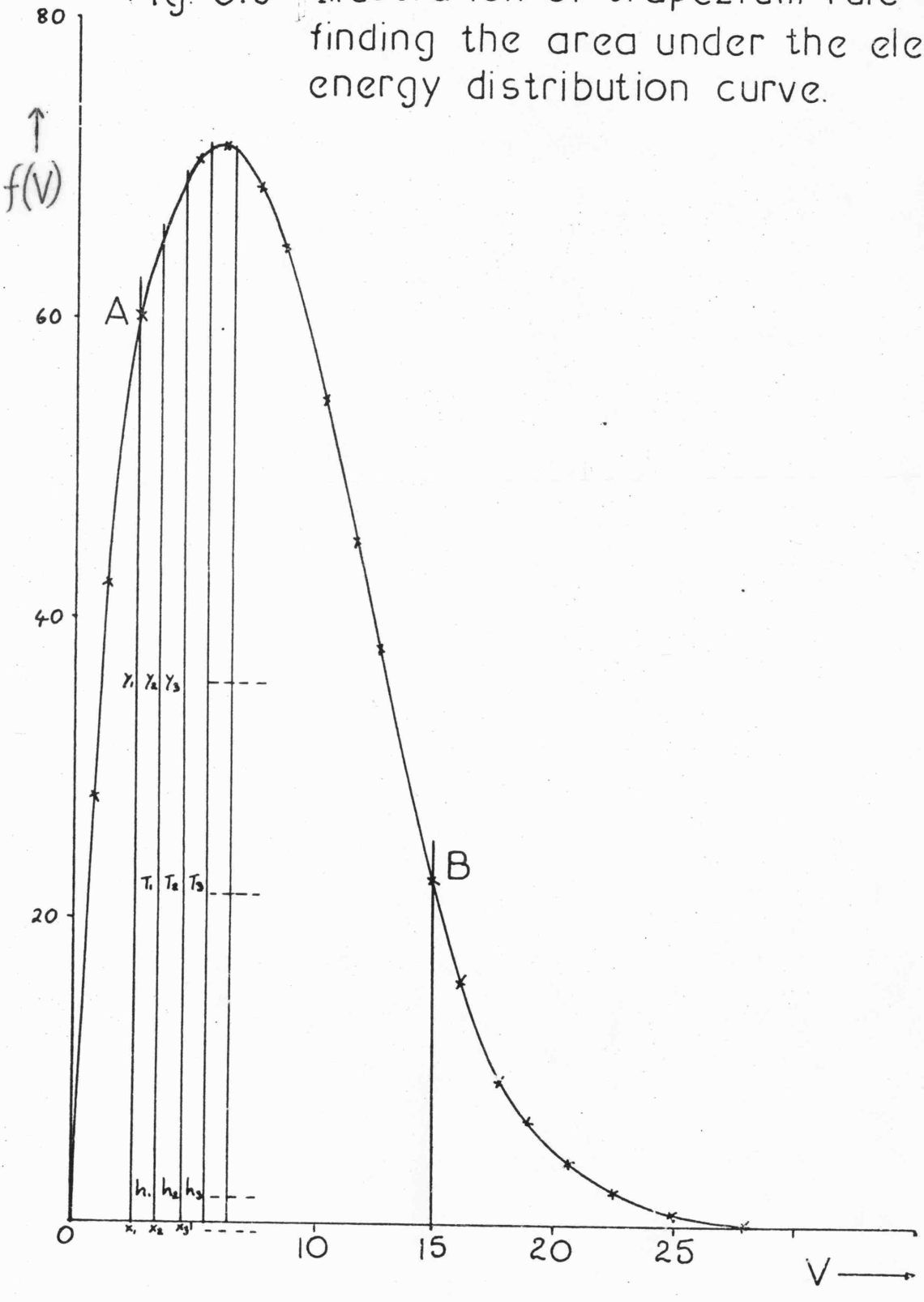

6.4 Electron density from the calibration of the detecting system.

As described in Section 5.6 the detecting system was calibrated electronically by feeding in a small sinusoidal signal. A calibration constant, k , corresponding to the current producing unit galvanometer deflection was calculated. Hence the second harmonic current $i_{2\omega}$ detected is related to the galvanometer deflection (S) by an equation

$$i_{2\omega} = kS$$

From Druyvesteyn's equation

$$f(V) = \frac{2}{Ae}\left(\frac{2m}{e}\right)^{\frac{1}{2}} V^{\frac{1}{2}} \frac{d^2 i_e}{dV^2}$$

and as shown in Section 3.3

$$i_{2\omega} = \frac{E^2}{4} \cdot \frac{d^2 i_e}{dV^2}$$

where E is the amplitude of the sinusoidal signal applied to the probe.

Hence

$$f(V) = \frac{2}{Ae}\left(\frac{2m}{e}\right)^{\frac{1}{2}} V^{\frac{1}{2}} \frac{4}{E^2} \cdot k \cdot S$$

which can be written as

$$f(V) = \frac{bk}{E^2} \cdot V^{\frac{1}{2}} S \qquad \text{where} \quad b = \frac{8}{Ae}\left(\frac{2m}{e}\right)^{\frac{1}{2}}$$

Therefore

$$n_e = \int_0^\infty f(V)\,dV = \int_0^\infty \frac{bk}{E^2} V^{\frac{1}{2}} S \cdot dV$$

$$= \frac{bk}{E^2}\int_0^\infty V^{\frac{1}{2}} S \cdot dV = \frac{bk}{E^2} \times \text{area under the distribution curve.}$$

The area under the distribution curve was again evaluated by the application of the trapezium rule for integration.

6.5 Determination of the average electron energy.

The average electron energy in the positive column was determined from an expression of the form

$$\bar{V} = \frac{1}{n_e} \int_0^\infty V \cdot f(V)\, dV$$

$$= \frac{\int_0^\infty V^{3/2} \frac{d^2 i_e}{dV^2} \cdot dV}{\int_0^\infty V^{1/2} \frac{d^2 i_e}{dV^2} \cdot dV}$$

As described in Section 6.3 the integrals were obtained using the trapezium rule for integration, so we can write

$$\bar{V} = \frac{I_3}{I_1}$$

where I_1 is as shown in Section 6.3 and I_3 is given by

$$I_3 = \sum_1^{n-1} \frac{1}{2} \left[\left(V^{3/2} \frac{d^2 i_e}{dV^2} \right)_{n+1} + \left(V^{3/2} \frac{d^2 i_e}{dV^2} \right)_n \right] \times \left[V_{n+1} - V_n \right]$$

again the Computer ICL 1902 A was programmed to evaluate I_1 and I_3 from the data of the detecting system output and the measured probe potential.

The values of the average electron energies obtained for various discharge tube parameters will be discussed in the next chapter.

6.6 Measurement of the axial field intensity.

The axial field intensity (E) was obtained by measuring for a number of probes distributed along the tube, in rapid succession, the potential with respect to the reference probe employed for the distribution function measurements. In the present investigation the anode was used as the reference probe. By dividing the voltage differences by the distances between the probes, the field intensity was obtained. A digital voltmeter with a high input impedance(1MΩ)

was used for measuring the voltages and a travelling microscope for measuring the distances between the probes. Measured values of E/N in the positive column for helium and helium-neon mixtures are shown in Figure 6.6. These were obtained in the 40mm diameter tube at 100mA discharge current. The measured values of E/N for helium-nitrogen mixtures are shown in Figure 6.7. These were obtained in the 80mm diameter tube at 100 mA discharge current.

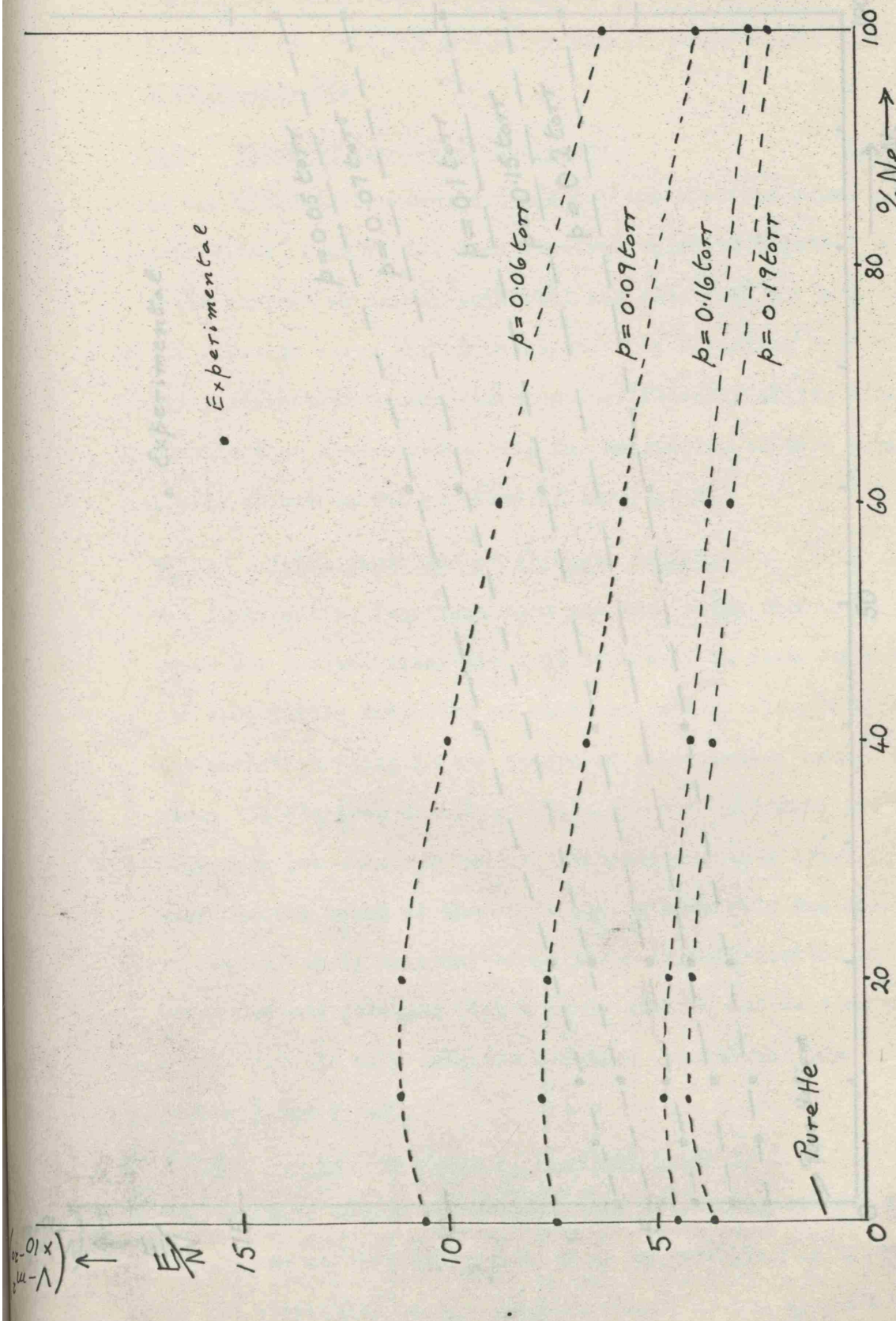

Fig. 6.6 $\frac{E}{N}$ for helium–neon mixtures.

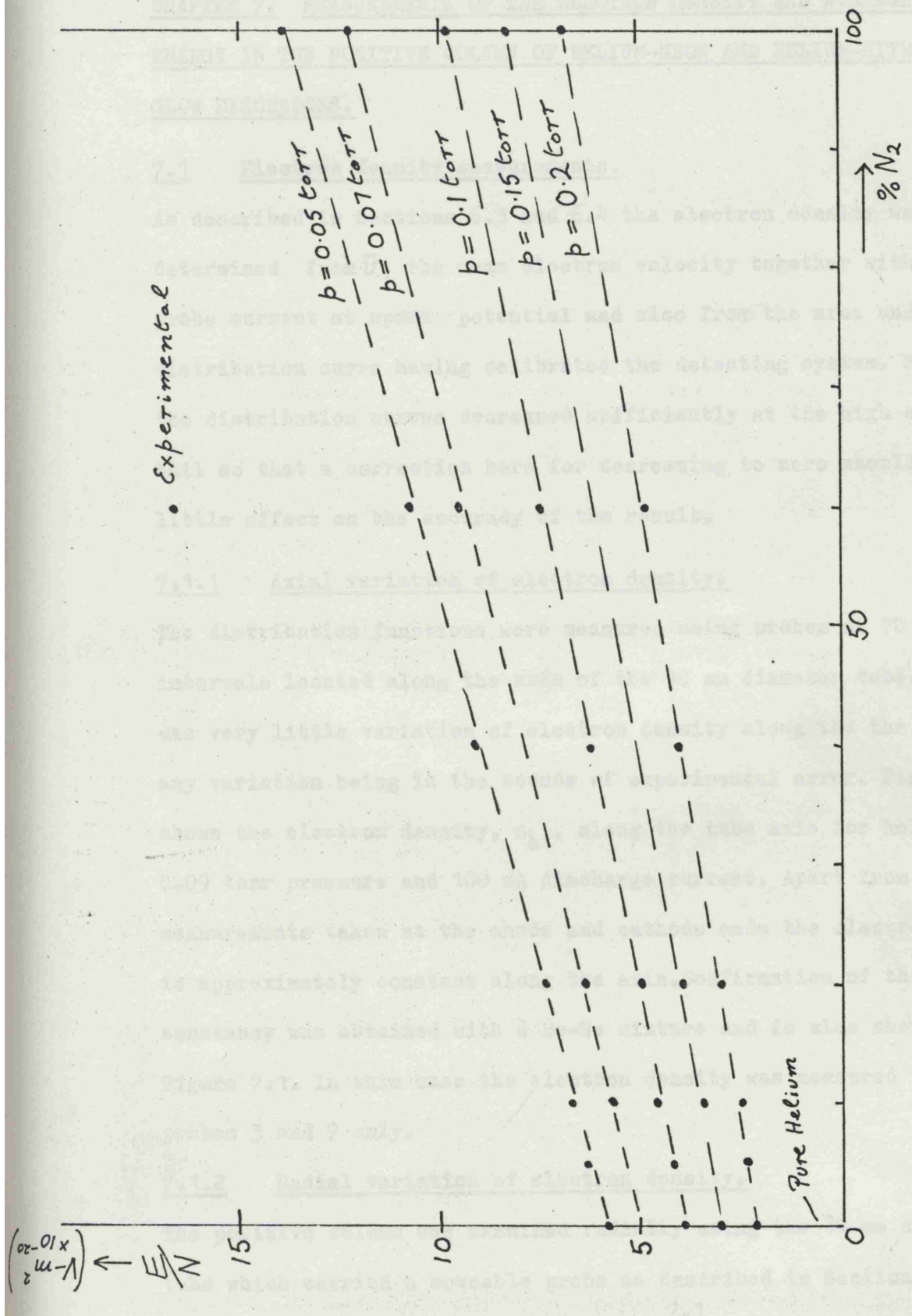

Fig 6.7 $\frac{E}{N}$ for helium–nitrogen mixtures.

CHAPTER 7. MEASUREMENTS OF THE ELECTRON DENSITY AND AVERAGE ELECTRON ENERGY IN THE POSITIVE COLUMN OF HELIUM-NEON AND HELIUM-NITROGEN GLOW DISCHARGES.

7.1 Electron density measurements.

As described in Sections 6.3 and 6.4 the electron density was determined from $\bar{v}$, the mean electron velocity together with the probe current at space potential and also from the area under the distribution curve having calibrated the detecting system. Most of the distribution curves decreased sufficiently at the high energy tail so that a correction here for decreasing to zero should have little effect on the accuracy of the result.

7.1.1 Axial variation of electron density.

The distribution functions were measured using probes at 70 mm intervals located along the axis of the 40 mm diameter tube. There was very little variation of electron density along the the tube axis, any variation being in the bounds of experimental error. Figure 7.1 shows the electron density, n_e, along the tube axis for helium at 0.09 torr pressure and 100 mA discharge current. Apart from the measurements taken at the anode and cathode ends the electron density is approximately constant along the axis. Confirmation of this constancy was obtained with a He-Ne mixture and is also shown in Figure 7.1. In this case the electron density was measured between probes 3 and 7 only.

7.1.2 Radial variation of electron density.

The positive column was examined radially using the 80 mm diameter tube which carried a moveable probe as described in Section 4.3. In the derivation of the Schottky theory[7.1] it was assumed that the

Fig 7.1 Variation of electron concentration with location of probe along the axis of the 4 cm. tube.

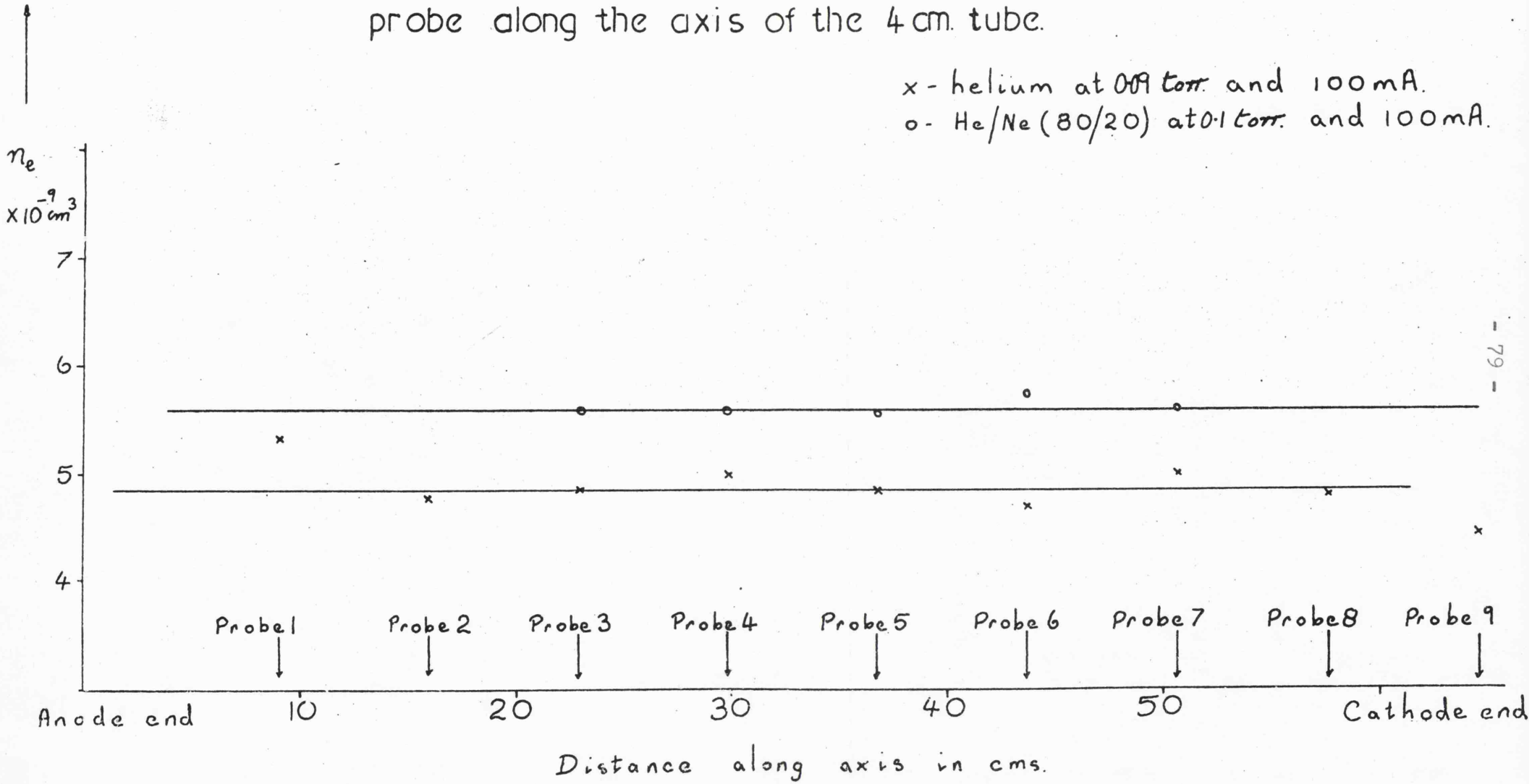

ionisation was a single stage process and the theory predicts there is a falling off of electron density from axis to wall which obeys a Bessel function of zero order, $n(r) = n_0 J_0\left(2.4\frac{r}{R}\right)$ where n_0 is the electron density at the axis. In the case of two-stage ionisation the rate of production of electrons will depend on n^2 instead of n. This will produce a steeper decrease in electron density from axis to wall than that arising from single stage ionisation.

In the present investigation the gas mixtures were investigated to test for single-stage or two-stage ionisation. The positive column was investigated at the axis and at small intervals up to the wall. A typical experimental plot is shown in Figure 7.2 and shows that the points lie close to the zero Bessel function predicted by the Schottky theory,[7.1] except that they decrease to a finite value at the wall. In the case of He- N_2 (95/5) mixture shown the value of the density at the wall was about 6% of that at the axis. The Spenke curve[7.2] for cumulative ionisation is also shown and gives a much sharper drop to zero than that obtained in the present investigation. The results confirm that for the range of pressure and discharge currents investigated only single stage ionisation occurs. The variation radially of the shape of the distribution curve and the average electron energy will be discussed later.

7.2 Variation of electron density with pressure and discharge current.

The variation of electron density with pressure at constant discharge current is shown in Table 7.1 for helium. The electron density was determined mainly by using the (calibration of the detecting system) method, but some results are shown where n_e was obtained using $\overline{v}$ and

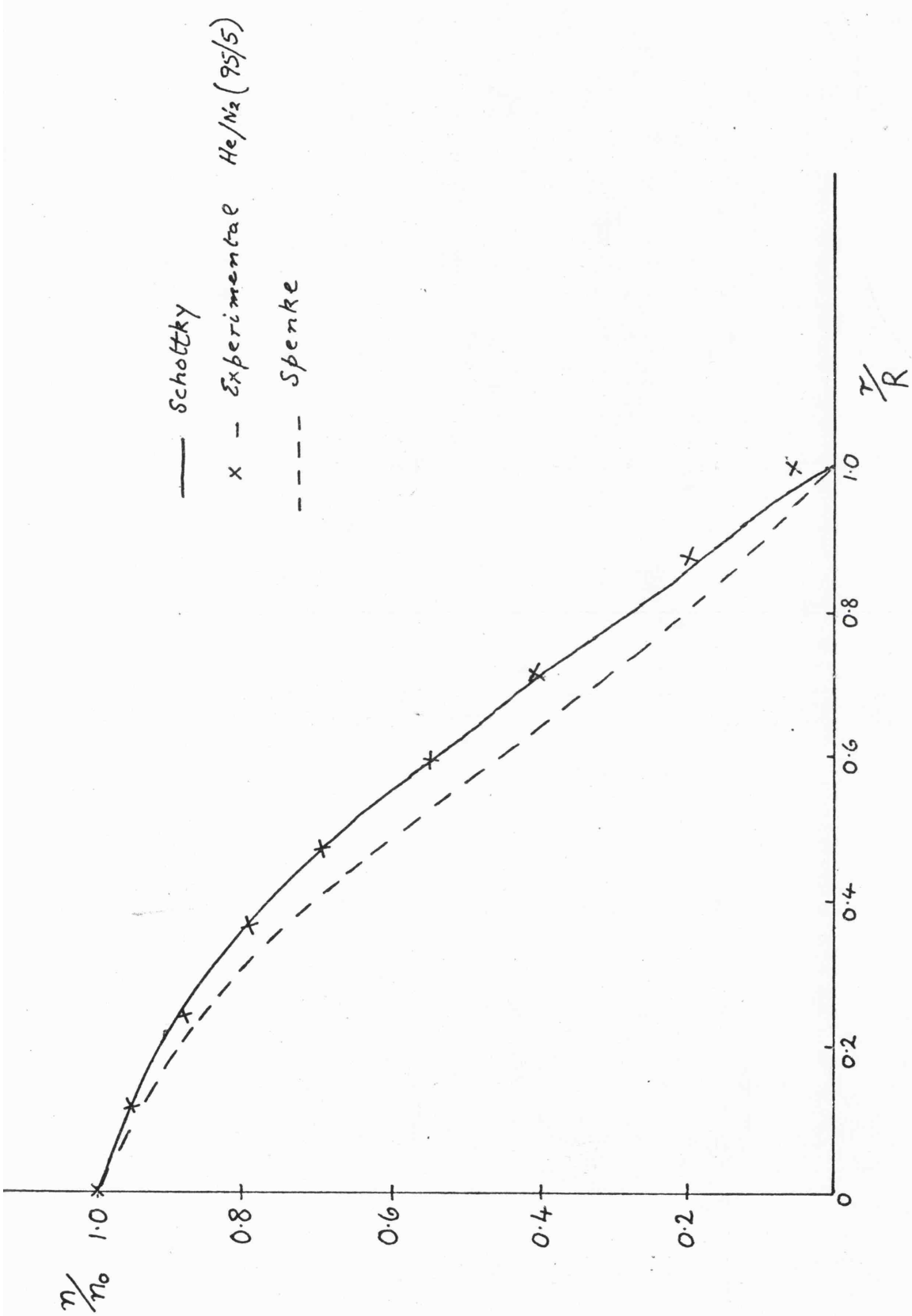

Fig. 7.2 Radial distribution of electron density in the positive column.

TABLE 7.1 ELECTRON DENSITY FOR HELIUM.

p_o pressure, torr at 0°C	I_d Discharge current mA	n_e(A) Electron density $m^{-3}x10^{-15}$	n_e(B) $m^{-3}x10^{-15}$
0.06	100	3.5	3.3
0.07	"	4.3	4.6
0.085	20	1.0	–
"	40	1.8	–
"	60	2.7	–
"	80	3.7	–
"	100	4.6	–
"	120	5.6	–
"	140	6.4	–
"	160	7.3	–
"	180	8.2	–
"	200	8.9	–
0.09	100	4.7	4.5
0.10	"	5.3	5.6
0.13	"	6.1	–
0.15	"	6.4	6.0
0.18	"	6.3	6.5

n_e(A) Calibrated using electronic method (Section 6.4)

n_e(B) From $\bar{v}$ and current to probe, i_p, at space potential.

the current to the probe at space potential. Tables 7.2 and 7.3 show the electron densities obtained for various He-Ne and He-N_2 mixtures at constant discharge current and their dependence on pressure. The results for He-Ne were obtained using a 40 mm diameter discharge tube, those for He-N_2 in a 80 mm diameter discharge tube. There was a good agreement between the two methods of obtaining the electron density but some error will occur in the second method because of the difficulty of locating the space potential.

The variation with discharge current is shown in Figure 7.3 for helium-neon and helium-nitrogen mixtures. As can be seen from the figure the electron density was proportional to the discharge current over the range 20-200 mA which is expected if only single-stage ionisation occurs. At high pressures a non-linear dependence was detected showing the start of two-stage ionisation. In this case collisions are frequent enough to give a high probability that an excited atom will collide during its life-time giving it sufficient energy to ionise the atom.

7.3 Drift velocity determinations.

The electron drift velocity in helium has been measured by Townsend and Bailey[7.3], Nielsen[7.4], Bowe[7.5], Hornbeck[7.6] and others at low values of E/N and by Phelps[7.7], Pack and Frost[7.8], Takayama and Anderson[7.9] at higher values. In Neon Bowe[7.5], Nielsen[7.4], Pack and Phelps[7.10] have measured values at low E/N and Takayama[7.8], Anderson[7.9], Sugawara and Chen[7.11] have extended measurements to higher values. In the present investigation the relationship between drift velocity v_D and E/N was determined from the simultaneous

TABLE 7.2 ELECTRON DENSITY FOR HELIUM-NEON MIXTURES.

He-Ne ratio	p_o pressure, torr at 0°C	I_d Discharge Current mA	$n_e(A)$ electron density $m^{-3} \times 10^{-15}$
90-10	0.07	50	2.4
	"	100	4.9
	"	150	7.1
	"	200	9.6
	0.09	100	5.5
	0.11	"	6.1
	0.12	"	6.4
	0.14	"	6.6
	0.16	"	6.7
80-20	0.03	100	1.8
	0.045	"	2.7
	0.075	"	4.6
	0.1	"	5.6
	0.14	"	6.2
60-40	0.035	100	2.6
	0.09	"	5.3
	0.11	"	5.7
	0.16	"	6.6
	0.18	"	7.0
	0.20	"	7.1

TABLE 7.3 ELECTRON DENSITY FOR HELIUM-NITROGEN MIXTURES.

(80 mm diameter tube)

$He-N_2$ ratio	p_o pressure, torr at 0°C	I_d discharge current, mA	$n_e(A)$ electron density $m^{-3} \times 10^{-15}$
He	0.05	100	1.3
	0.08	"	1.7
	0.10	"	2.3
	0.15	"	2.7
	0.20	"	3.6
$He-N_2$ 95/5	0.05	100	1.5
	0.10	"	2.1
	0.15	"	2.8
$He-N_2$ 90/10	0.075	100	1.7
	0.10	"	2.2
	0.18	"	2.9
	0.20	"	3.2
$He-N_2$ 80/20	0.08	100	1.6
	0.16	"	2.8
	0.22	"	3.8
$He-N_2$ 60/40	0.05	100	1.4
	0.08	"	1.7
	0.10	"	2.0
	0.15	"	2.6
	0.20	"	3.0
$He-N_2$ 40/60	0.06	100	1.6
	0.10	"	2.0
	0.15	"	2.3
	0.20	"	2.9
N_2	0.05	100	1.6
	0.10	"	2.9
	0.15	"	2.8
	0.20	"	3.0

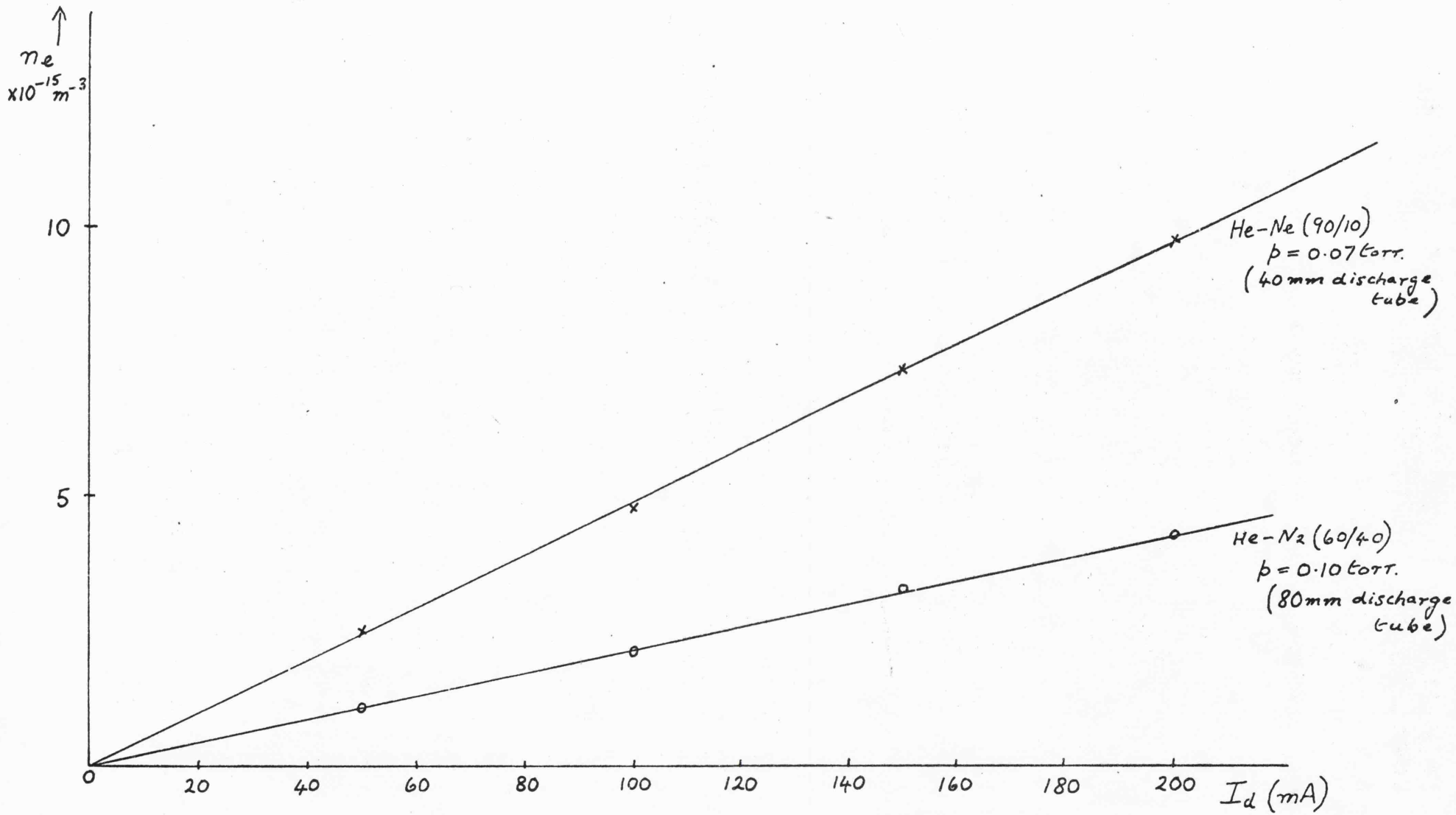

Fig 7.3 Variation of electron density with discharge current.

measurements of the pressure p, the electric field E and the electron density at a particular discharge current I_d. The drift velocity was calculated from the electron density by the application of the equation

$$I_d = 1{\cdot}36\, n_e . e . v_D . R^2$$

which was derived in Section 1.1 from the Schottky theory[7.1] for the positive column. It assumes a radial distribution based on a Bessel function of zero order with the electron density, n_e, being maximum at the axis of the tube and zero at the walls.

Table 7.4 shows the variation of the electron drift velocity with He-Ne ratio at fixed E/N values. Also shown are the values obtained by Phelps, Pack and Frost[7.7] for pure helium. Table 7.5 shows the values obtained in the present investigation for He-N_2 mixtures.

The differences of the observed data for drift velocities in the present investigation with those of Phelps et al[7.7] may be accounted for by the dissimilar techniques and slight unforseen differences in the purity of the helium gas. The discharge investigated by Phelps et al was contained in a 13 mm diameter Vylor tube about 300 mm long and was operated at a pressure between 0.25 and 3 torr and at a discharge current of 1 to 10 mA. A non-probe technique was used. The electron density was calculated from a measurement of the frequency shift of a rectangular resonant cavity surrounding a section of the discharge tube. As in the present investigation a correction was made for the radial variation of the electron density. The microwave measurements yielded an average

TABLE 7.4 DRIFT VELOCITY OF ELECTRONS IN HELIUM-NEON MIXTURES.

E/N ($V\text{-}m^2 \times 10^{-19}$)	0.51	0.65	0.77	0.87	0.97
Drift Velocity, V_D ($m\ s^{-1} \times 10^{-5}$)					
He, Phelps et al.	1.5	2.0	2.6	2.5	2.8
He, Present investigation	1.9	2.2	2.5	2.7	3.2
He-Ne, 90/10	1.7	1.9	2.1	2.3	–
He-Ne, 80/20	1.8	2.1	2.5	–	–
He-Ne, 60/40	2.0	2.2	–	–	–

TABLE 7.5(a) DRIFT VELOCITY OF ELECTRONS IN HELIUM-NITROGEN MIXTURES.

E/N ($V\text{-}m^2 \times 10^{-19}$)	0.2	0.3	0.4	0.45	0.5	0.6
Drift Velocity, V_D ($m\ s^{-1} \times 10^{-5}$)						
He, Phelps et al.	0.6	0.8	1.2	-	1.3	1.8
He, Present investigation	0.9	1.2	1.4	-	1.9	2.4
$He\text{-}N_2$, 95/5	-	1.15	1.5	-	-	2.1
$He\text{-}N_2$, 90/10	1.0	1.1	-	1.45	-	1.9
$He\text{-}N_2$, 80/20	0.85	-	-	-	-	2.0

TABLE 7.5(b) Drift velocity of electrons in $He\text{-}N_2$ mixtures(cont.)

E/N ($V\text{-}m^2 \times 10^{-19}$)	0.4	0.5	0.6	0.7	0.75	0.85	0.9	1.0	1.4
V_D ($ms^{-1} \times 10^{-5}$)									
$He\text{-}N_2$, 60/40	1.1	1.25	1.6	-	1.8	-	2.3	-	-
$He\text{-}N_2$, 40/60	-	1.1	1.4	-	1.6	-	---	2.0	-
N_2, Present investigation	-	-	-	1.05	-	1.15	-	1.1	2.0
N_2, Anderson	-	-	-	0.9	-	1.0	-	1.2	1.8

of the electron density in terms of the measured shift of the resonant frequency produced by the electrons.

In the derivation of the Schottky equation, section 1.1, it was assumed that the electron density decreased to zero at the walls at all pressures. Sugawara and Chen [7.11] found that for neon at 1 torr the radial distribution fitted well with the Schottky theory and the electron density was found to be zero at the walls. However, at lower pressures the radial distribution deviated from the Schottky theory, not decreasing to zero at the walls and being generally a broader distribution showing a departure from the ambipolar diffusion theory. Verweig [7.12] working with argon-mercury mixtures found that the ratio α of the average density $\bar{n}$ over the cross-section and the density at the axis, n_e varied over the range of measurements (0.01 to 3 torr) from α = 0.39 to 0.56. By ignoring this variation a large error can be introduced. The Schottky theory gives α = 0.43 which can be calculated by comparing the Schottky equation for the longitudinal discharge current with

$$I_d = \pi R^2 \bar{n} e v_D$$

This latter equation assumes the electron density is uniform over the cross-section of the tube.

In the present investigation with He-Ne and He-N_2 mixtures it was found that the radial profile of variation of the electron density closely followed that predicted by the Schottky theory but did not fall to zero at the walls, being of the order of 6-10% of that at the axis.

In the present investigation it is assumed that the electron velocity reaches an equilibrium value in the distance between the cathode and the probe. This assumption holds if the 'characteristic time' of the electron is smaller than the drift time between the cathode and the measuring probe. An order of magnitude of the 'characteristic time' may be obtained from $\frac{\lambda_e}{\bar{v}} \cdot \frac{1}{K}$, where $\frac{\lambda_e}{\bar{v}}$ is the time between collisions and K is the average fraction of energy lost per collision. The drift time between the cathode and the measuring probe can be shown to be an order of magnitude greater than the 'characteristic time.' Hence the assumption of an equilibrium value being attained is fulfilled.

7.4 Mobility measurements in He-Ne and He-N_2 mixtures.

The Schottky equation for the longitudinal discharge current can be written as

$$I_d = 1{\cdot}36\, n_e . e . b' . E/p \cdot R^2$$

where b' is defined as the mobility constant given by

$$b' = \frac{v_d}{E/p}$$

Hence by measuring the electron density, n_e, at the axis, the field strength E and the longitudinal discharge current I_d at gas pressure p, it is possible to calculate b'. These values are given in Tables 7.6, 7.7 and 7.8 for helium, helium-neon and helium-nitrogen respectively.

The measurement of the mobility constants for helium are compared with those obtained by Kinderdijk and Van Eck [7.13] in Figure 7.4. Also shown are those calculated from the drift velocity

TABLE 7.6 MOBILITY MEASUREMENTS IN HELIUM.

E/N ($V\text{-}m^2 \times 10^{-19}$)	v_D , $ms^{-1} \times 10^{-5}$	b' , $m^2\ torr\ V^{-1}s^{-1} \times 10^{-2}$
0.36	1.8	1.38
0.41	1.8	1.20
0.50	1.9	1.06
0.65	2.2	0.96
0.77	2.5	0.92
0.87	2.7	0.87
0.94	3.2	0.94

TABLE 7.7 MOBILITY MEASUREMENTS IN He-Ne MIXTURES.

He-Ne ratio	E/N ($V\text{-}m^2 \times 10^{-19}$)	v_D ($ms^{-1} \times 10^{-5}$)	b' ($m^2 torr.V^{-1}s^{-1} \times 10^{-2}$)
90-10	0.45	1.7	1.06
	0.50	1.7	0.94
	0.60	1.8	0.86
	0.65	1.9	0.83
	0.77	2.1	0.78
	0.87	2.3	0.74
80-20	0.39	1.8	1.29
	0.50	1.8	1.00
	0.65	2.1	0.91
	0.77	2.5	0.93
	1.30	4.2	0.91
	1.55	6.5	1.16
60-40	0.33	1.6	1.33
	0.39	1.8	1.29
	0.50	2.0	1.11
	0.65	2.2	0.96
	1.25	4.4	0.98

TABLE 7.8 MOBILITY MEASUREMENTS IN $He-N_2$ MIXTURES.

$He-N_2$ ratio	E/N ($V-m^2 \times 10^{-19}$)	v_D ($ms^{-1} \times 10^{-5}$)	b' ($m^2 torr.V^{-1}s^{-1} \times 10^{-2}$)
95-5	0.60	2.10	1.00
	0.40	1.50	1.04
	0.30	1.15	1.06
90-10	0.60	1.90	0.91
	0.45	1.45	0.90
	0.30	1.10	1.02
	0.20	1.00	1.38
80-20	0.60	2.00	0.95
	0.20	0.85	1.18
60-40	0.90	2.30	0.71
	0.75	1.80	0.66
	0.60	1.60	0.76
	0.50	1.25	0.70
	0.40	1.10	0.76
40-60	1.00	2.00	0.57
	0.75	1.60	0.60
	0.60	1.40	0.67
	0.50	1.10	0.61

Fig. 7.4 Comparison of mobility measurements in helium.

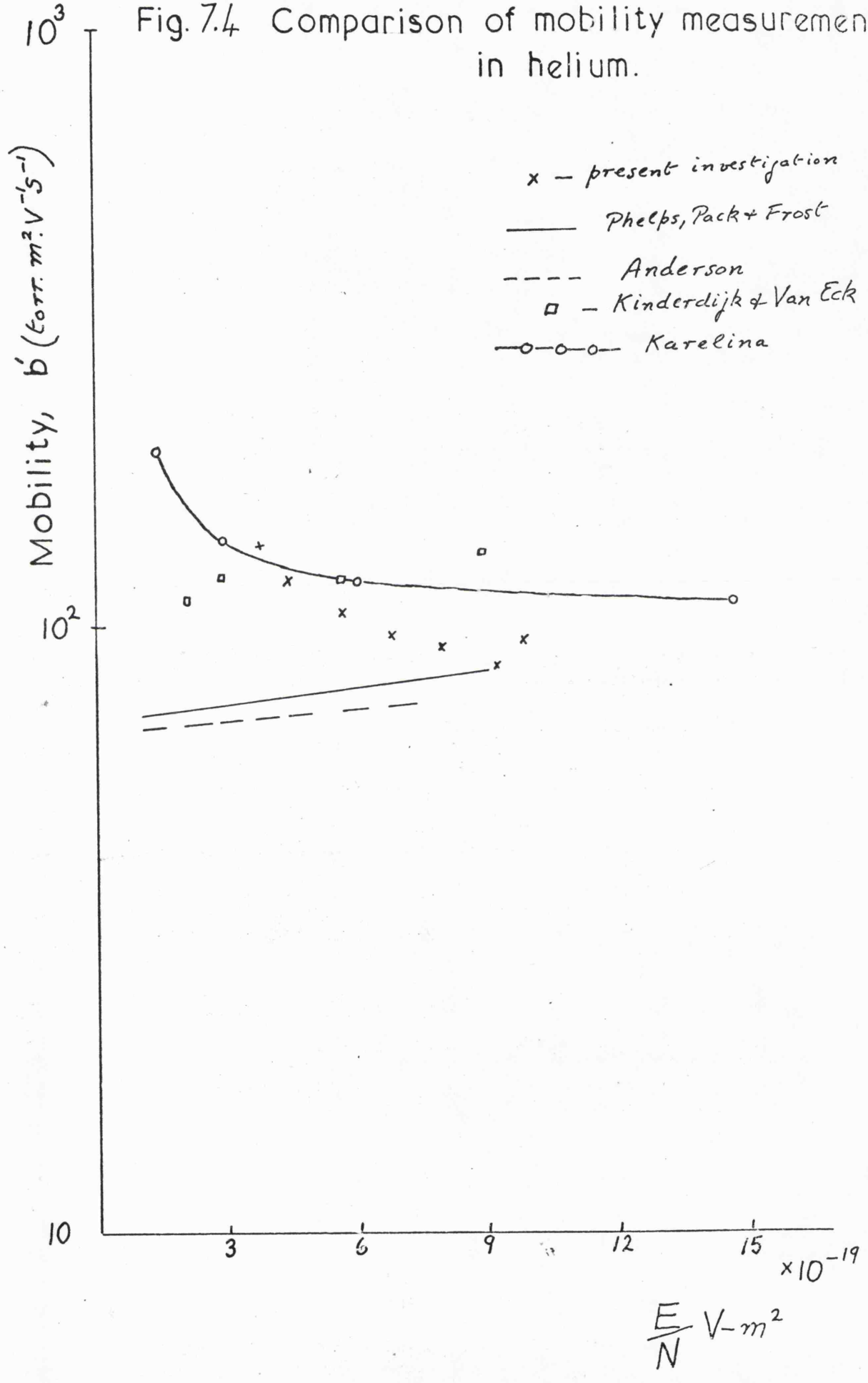

measurements of Anderson[7.9] and Phelps et al[7.7] and from the electron density measurements of Karelina.[7.14]

The measurements taken by Kinderdijk and Van Eck[7.13] and by Karelina[7.14] were obtained using probe techniques. As can be seen from Fig. 7.4 there is a close correlation between the results obtained in the present investigation with those obtained by probe techniques However, these are generally higher than those obtained by other methods. Anderson and Phelps et al used microwave techniques for their measurements, basing their calculations of the drift velocity on the equation for the longitudinal current given by the Schottky theory. One of the disadvantages of microwave techniques is that they have poor space resolution and give an average value of the electron density across the discharge tube. Furthermore, for the investigations using microwave techniques, low discharge currents (1-10mA) were generally used. In rare gases E/p decreases with increasing discharge current and could account for the differences in measurements between microwave and probe techniques, the latter using higher discharge currents. Also, there may be some differences in the purity of the helium used. Also the mobilities in the present investigation were calculated using the Schottky theory for the positive column which assumes a Bessel type decrease in the electron density from axis to wall, falling to zero at the wall. Radial investigations have shown that in all cases there was a finite value for the electron density at the wall.

The mobility values calculated for He-Ne mixtures are shown in Figure 7.5. These are compared with Phelps et al[7.7] and Anderson[7.9] for helium and with Takayama[7.8] and Anderson for neon.

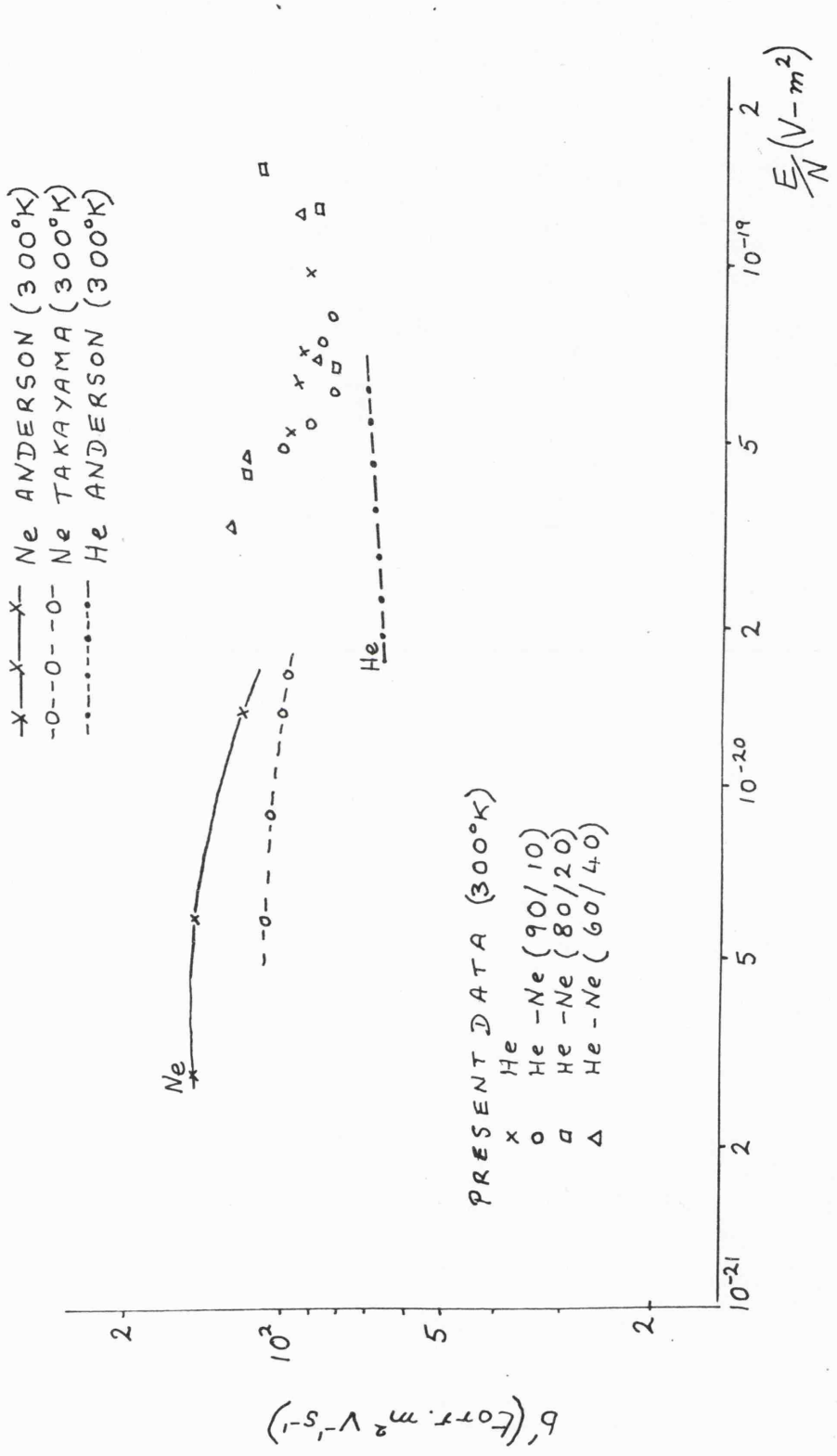

Fig. 7.5 Electron mobilities in helium and helium–neon mixtures as a function of E/N.

The values for He-N_2 mixtures are compared with those obtained for helium and for nitrogen by Anderson[7.9] using microwave techniques. These are shown in Figure 7.6.

7.5 Variation of average electron energy with discharge tube parameters

The electron temperature or the average electron energy $\bar{V}$ has been measured in the positive column by a number of investigators for helium. In the present investigation the average electron energy may be found from the electron energy distribution function using

$$\bar{V} = \frac{\int_0^\infty V f(V) dV}{\int_0^\infty f(V) dV}$$

The relationship between T_e and $\bar{V}$ is given by

$$\bar{V} = \frac{3}{2} \frac{KT_e}{e} \quad \text{, that is } T_e = 7740\bar{V} \text{ in volts}$$

This relationship between the average electron energy and the electron temperature can only exist if the electron energy distribution is Maxwellian and in the present investigations, very few distributions remotely resembled the Maxwellian forms. If the form of the distribution is not exactly known, the relationship still holds approximately provided there is no radical departure from the Maxwellian form.

In the present investigations it was found that the average electron energy was independent of the longitudinal discharge current at low pressures which is consistent with the electron density being a linear function as shown in Section 7.2. However, at higher pressures a slight fall in average energy was noted which indicated the onset of two-stage ionisation. Some typical values at reduced pressure for helium, He-Ne and He-N_2 mixtures are shown in Table 7.9.

The variation with pressure is shown in Figure 7.7 where the average electron energy for helium and helium-neon mixtures

Fig. 7.6 Electron mobilities in helium–nitrogen mixtures as a function of E/N.

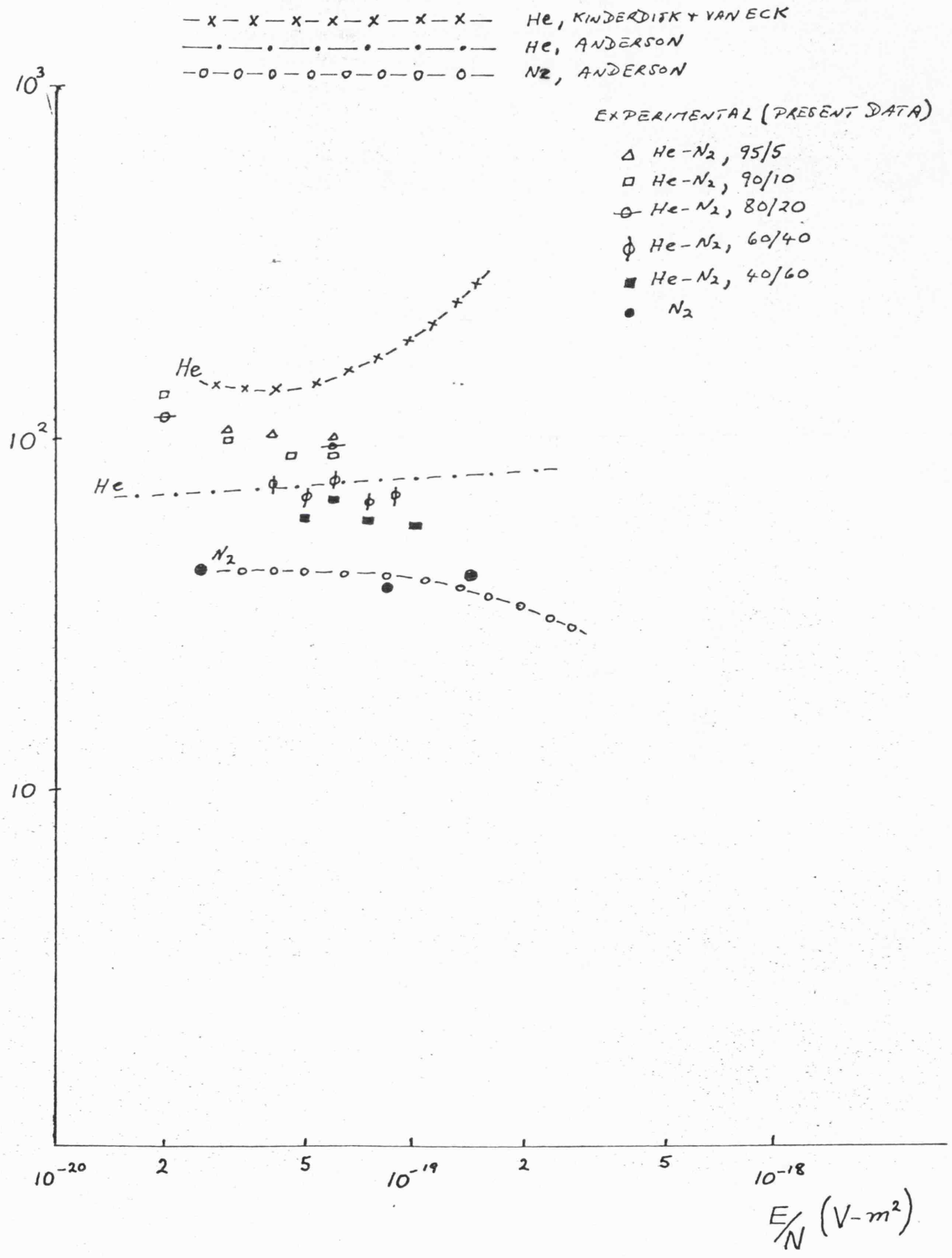

TABLE 7.9 Variation of $\bar{V}$ with the discharge current.

Gas	Pressure (torr)	Discharge Current. (mA)	Average electron energy. (eV)
Helium	0.1	60	9.6
"	"	100	9.9
"	"	160	10.1
"	"	180	10.0
He-Ne 90-10	0.1	50	9.6
"	"	100	9.8
"	"	150	10.0
"	"	200	10.1
He-Ne 80-20	0.13	50	8.6
"	"	100	9.1
"	"	150	9.2
"	"	200	8.7
He-Ne 60-40	0.12	100	8.8
"	"	150	8.7
"	"	200	9.2
$He-N_2$ 60-40	0.06	100	6.8
"	"	200	6.8
"	"	300	7.1

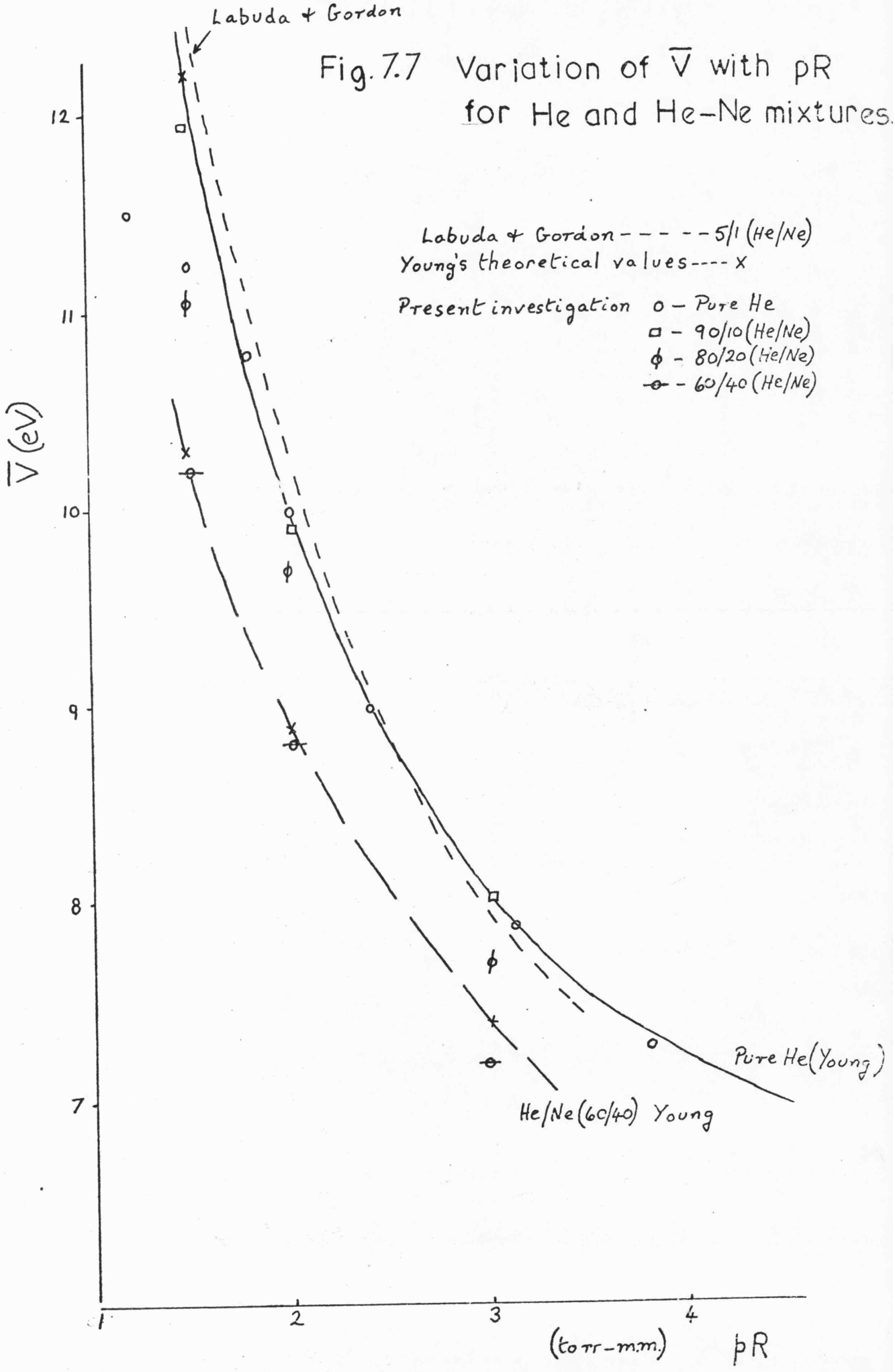

Fig. 7.7 Variation of $\bar{V}$ with pR for He and He–Ne mixtures.

has been plotted against pR, where R is the radius of the discharge tube. As can be seen the average electron energy is a function of pR at constant discharge current.

The diffusion theory of Schottky has been extended by Dorgelo, Alting and Boers[7.15] to give theoretical values of the electron temperature in the positive column in mixtures of atomic gases.The theory was further developed by Young[7.16] to give a relationship between the electron temperature and pR for binary mixtures. The theoretical values for helium and helium-neon mixtures are shown in Figure 7.7. Also plotted are the microwave measurements of Lubuda and Gordon[7.17] for a 5:1 helium-neon mixture which were taken in four tubes of different diameters.They showed that the average electron energy as a function of pR should be a universal curve independent of the tube diameter. This follows from the Schottky theory where ambipolar diffusion is taken as being the predominant loss mechanism and cumulative ionisation is absent.The average electron energy is a function of pR, n_e, the mixture ratio and the gas temperature,T_g. The dependence of V on n_e has been shown to be negligible in the present investigation especially at low pR values. The gas temperature is nearly constant and hence a constant pR should give a constant average electron energy.

The variation of $\bar{V}$ radially was examined in the positive column of a He-N_2 (95/5) mixture. The value of $\bar{V}$ was found to be constant over the radius except for a small fall in value at the wall. The values obtained are shown in Table 7.10 for He-N_2 (95/5) mixture at 0.1 torr pressure and 100 mA discharge current.

TABLE 7.10

VARIATION OF $\bar{V}$ WITH RADIAL LOCATION OF PROBE. ($He-N_2$ 95/5)

Distance from tube wall (mm)	$\bar{V}$ (eV)
38	6.3
30	6.3
20	6.2
10	5.9

The variation of average electron energy with mixture ratio was examined in He-Ne and He-N_2 mixtures. For He-Ne the mixture ratios examined were 90/10, 80/20, 60/40 and 40/60. Some difficulty was found in obtaining readings for the 40/60 mixture because moving striations were present at most pressures and most discharge currents. However, those readings obtained in the presence of moving striations are shown with error bars denoting the resultant spread in the electron energy values.

Values of the average electron energies for various helium-neon ratios were calculated by Young [7.16] from a modified form of the equation derived by Dorgelo et al [7.15] for binary mixtures. Their theory for binary mixtures was an extension of the Schottky theory [7.1] and is given in detail in the Appendix.

The experimental values obtained in the present investigation at various pR values are shown in Figure 7.8 for the 40 and 80 mm diameter tubes. Also shown are the theoretical values of Young. As can be seen the experimental values give a reasonable agreement with theory. Total agreement is not expected because the theory of the positive column is based on the assumptions of a Maxwellian electron energy distribution and single stage ionisation. In Figure 7.7 it is seen that at values of pR $<$ 1.5 torr.mm, there is a divergence of the experimental values from the theoretical curve. This is to be expected because below this value we are entering a regime outside that of the Schottky theory ($\lambda_e \geqslant$ R) and where the Langmuir-Tonks theory [7.18] is more appropriate. Also at values of pR $>$ 4.0 torr.mm a divergence was noted which can be explained by the collisionless probe theory beginning to break down and a start of cumulative ionisation.

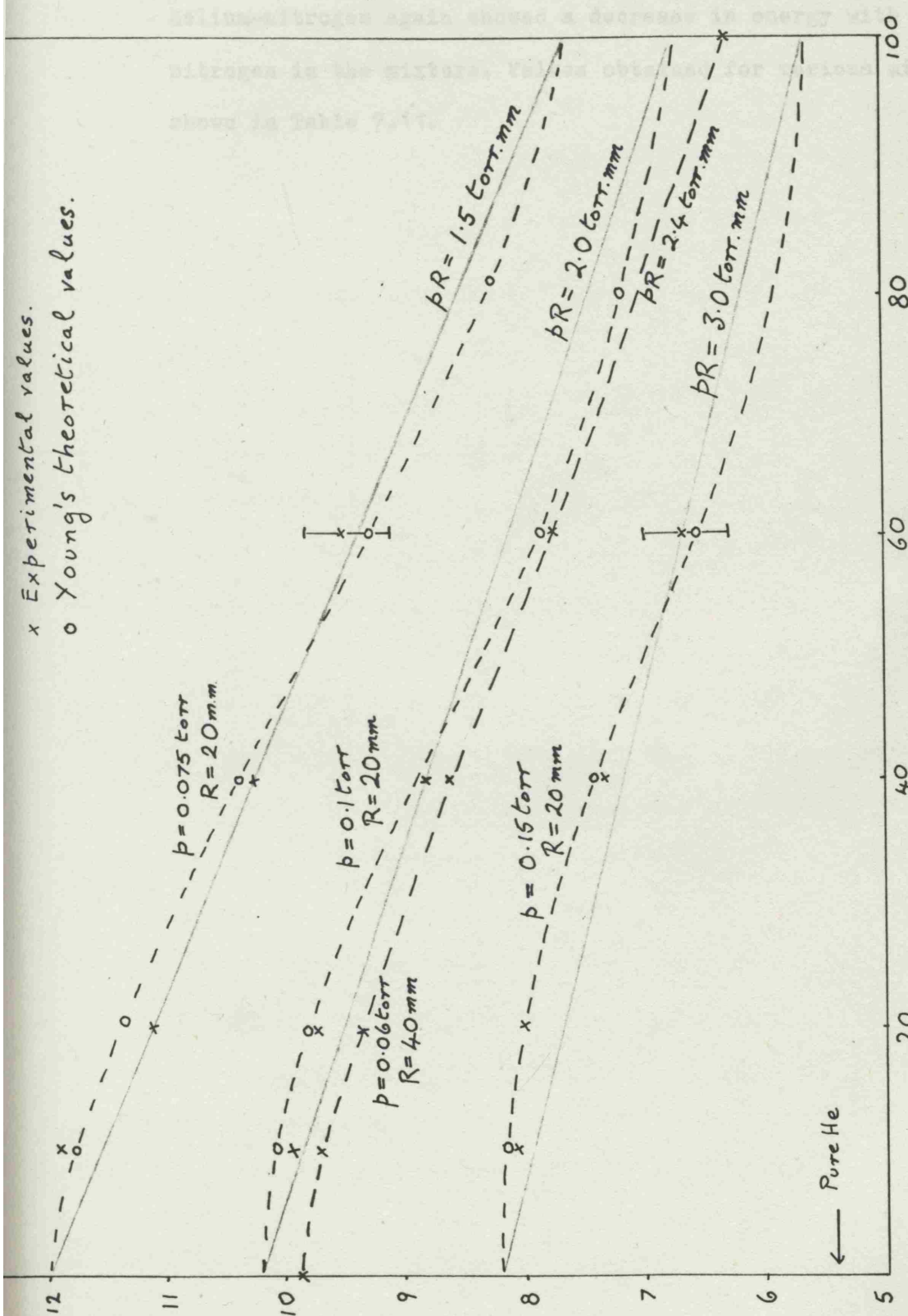

Fig. 7.8 $\bar{V}$ for helium–neon mixtures at various pR values.

The variation of average electron energy with mixture ratio in helium-nitrogen again showed a decrease in energy with increase of nitrogen in the mixture. Values obtained for various mixtures are shown in Table 7.11.

TABLE 7.11

VARIATION OF $\overline{V}$ WITH MIXTURE RATIO FOR $He-N_2$ MIXTURES. (80mm dia. tube)

(eV)

Pressure (torr)	He	$He-N_2$ 95/5	$He-N_2$ 90/10	$He-N_2$ 80/20	$He-N_2$ 60/40	$He-N_2$ 40/60	N_2
0.06	8.5	7.4			6.8	5.9	4.2
0.10	7.5	7.4	7.8	5.2	4.9	4.5	3.0
0.15	6.9		5.6				
0.20	6.4		5,0				

CHAPTER 8. EXAMINATION OF THE HIGH ENERGY TAIL OF THE ELECTRON ENERGY DISTRIBUTION FUNCTIONS.

The electron energy distribution function is a significant characteristic of the positive column. Unless this function is known it is difficult to determine accurately the average electron energy of the electrons and their density. For a long time it was thought that the electron energy distribution in the positive column was Maxwellian but within recent years it has been shown[8.1] that the distribution is approximately Maxwellian for only a very small range of discharge conditions. Outside this range the distribution deviates and takes up another form. The shape of the distribution has been examined in the present investigation for variation with pressure, longitudinal discharge current, diameter of tube and location in the tube. It has also been investigated for variation with area of the reference probe and for variation in size of the measuring probe. This investigation has been undertaken for helium, helium-neon and helium-nitrogen mixtures.

8.1 Variation with pressure and discharge current.

To investigate the variation with pressure the electron energy distribution curves obtained were compared with the Maxwellian and Druyvesteyn forms at low, intermediate and high pressures. These are shown in Fig.8.1 for helium, in Fig. 8.2 for helium-neon and in Fig.8.3 for helium-nitrogen mixtures. The results for helium were obtained using the 40mm diameter discharge tube and those for helium-neon. The results for helium-nitrogen mixtures were obtained in a 80mm diameter discharge tube.In all cases it can be seen that the high energy tail becomes more attenuated as the pressure increases.

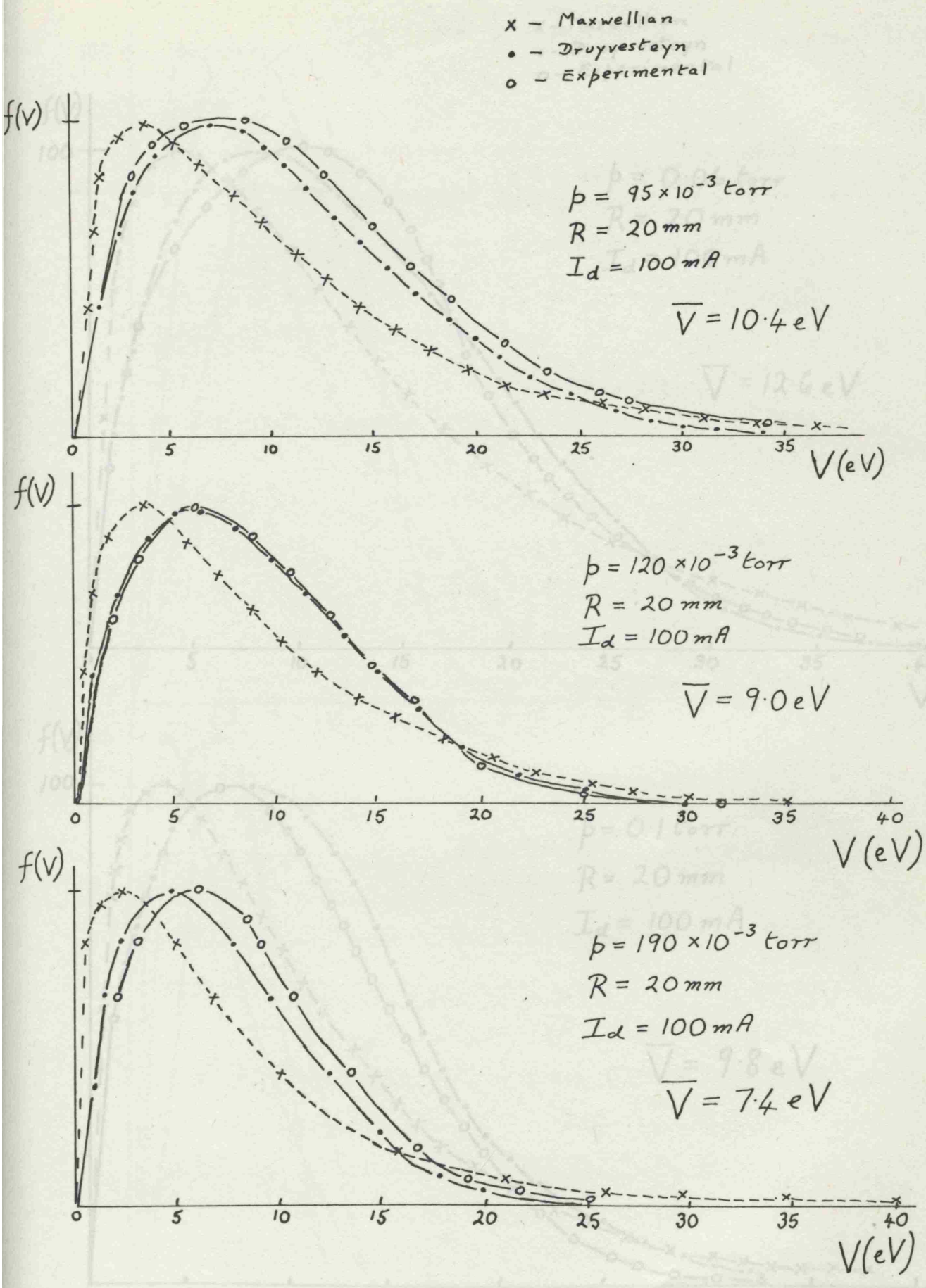

Fig. 8.1. Electron energy distribution for helium

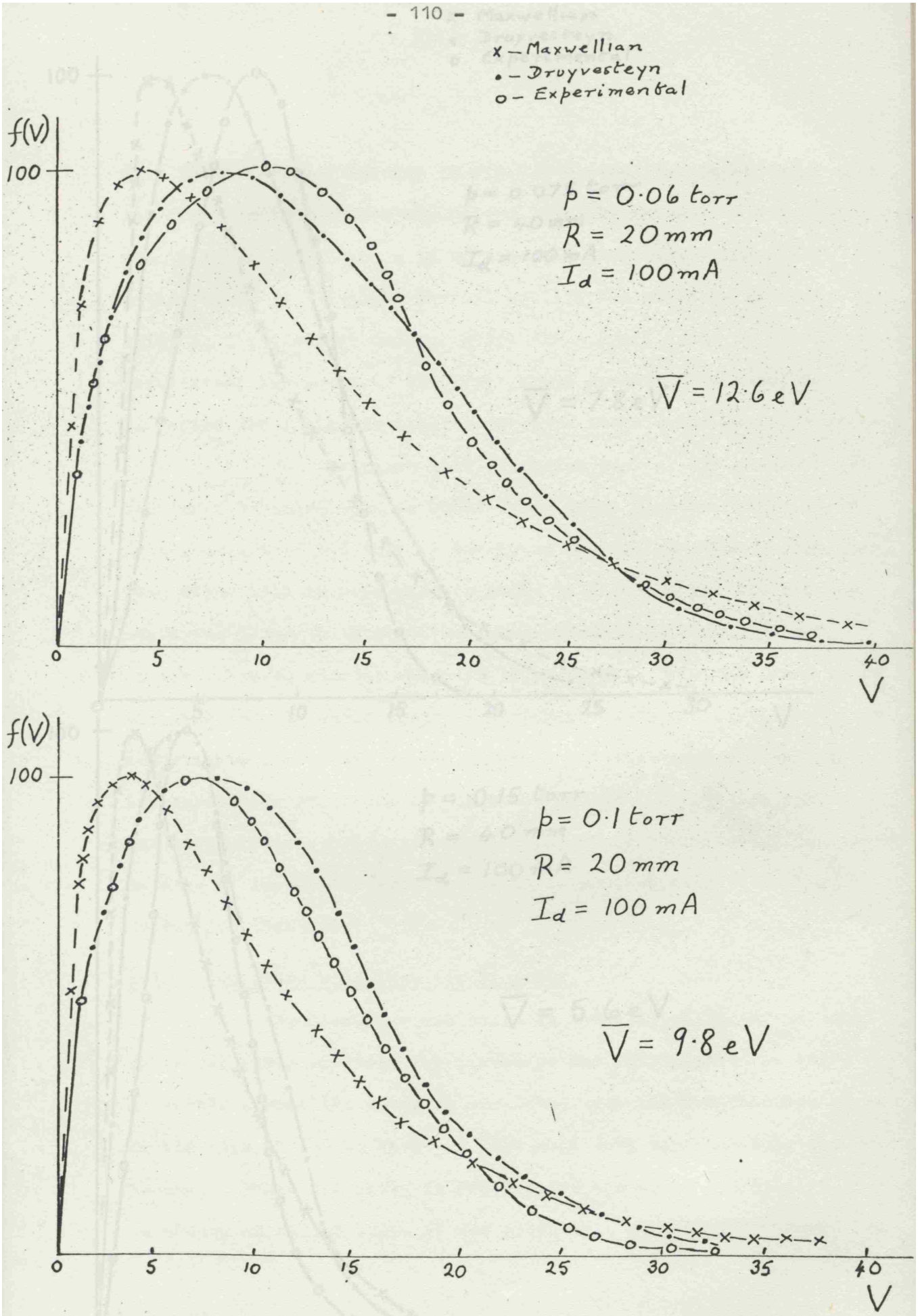

Fig. 8.2 Electron energy distribution for He-Ne (90/10)

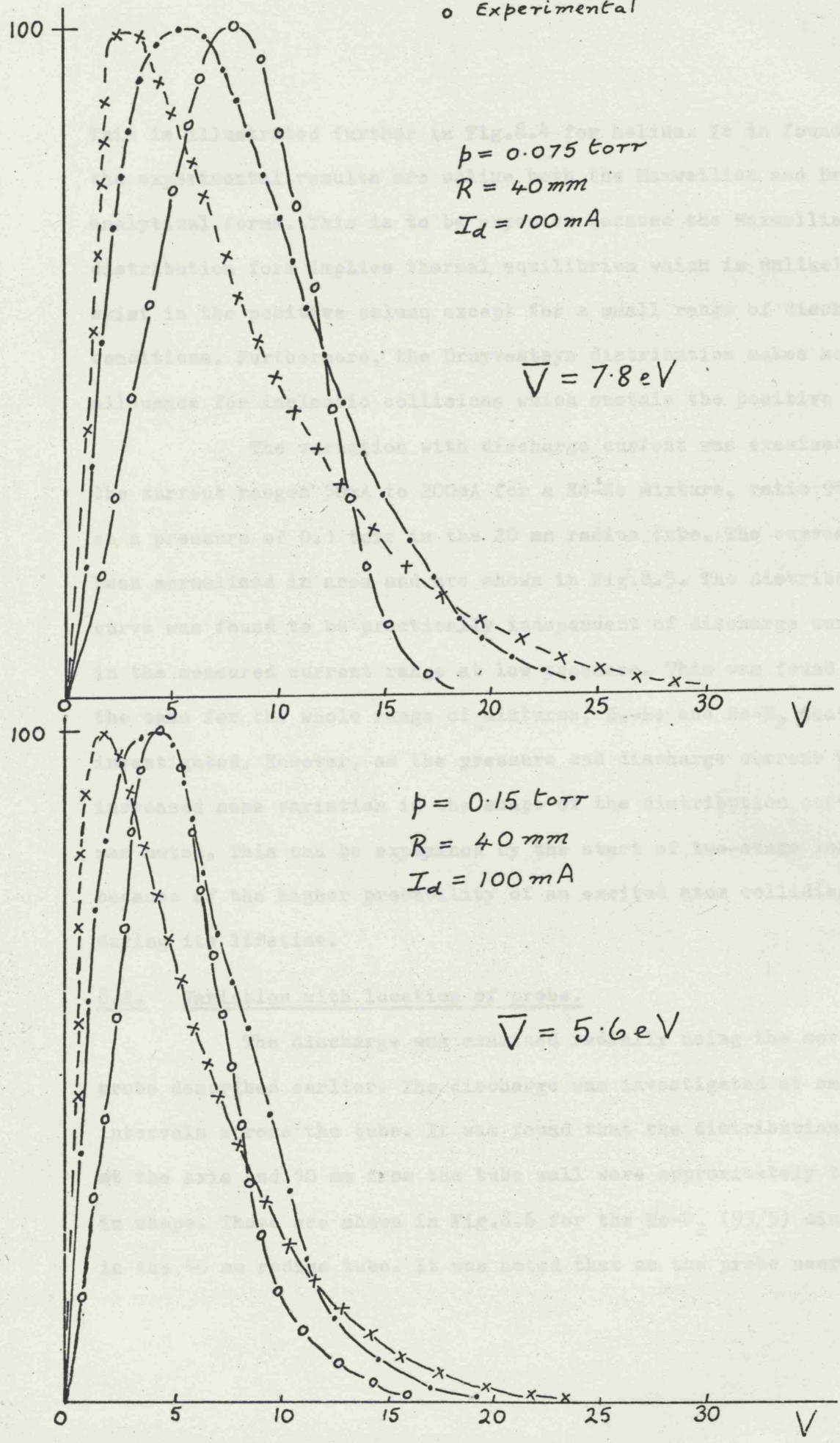

Fig. 8.3. Electron energy distribution for He–N_2 (90/10)

This is illustrated further in Fig.8.4 for helium. It is found that the experimental results are unlike both the Maxwellian and Druyvestyn analytical forms. This is to be expected because the Maxwellian distribution form implies thermal equilibrium which is unlikely to exist in the positive column except for a small range of discharge conditions. Furthermore, the Druyvesteyn distribution makes no allowance for inelastic collisions which sustain the positive column.

The variation with discharge current was examined for the current ranges 50mA to 200mA for a He-Ne mixture, ratio 90/10 at a pressure of 0.1 torr in the 20 mm radius tube. The curves have been normalised in area and are shown in Fig.8.5. The distribution curve was found to be practically independent of discharge current in the measured current range at low pressure. This was found to be the case for the whole range of mixtures, He-Ne and He-N_2 that were investigated. However, as the pressure and discharge current was increased some variation in the shape of the distribution curves was noted. This can be explained by the start of two-stage ionization because of the higher probability of an excited atom colliding during its lifetime.

8.2. Variation with location of probe.

The discharge was examined radially using the moveable probe described earlier. The discharge was investigated at small intervals across the tube. It was found that the distribution curve at the axis and 10 mm from the tube wall were approximately the same in shape. These are shown in Fig.8.6 for the He-N_2 (95/5) mixture in the 40 mm radius tube. It was noted that as the probe neared the

Fig. 8.4 Variation with pressure of electron energy distribution function in helium.

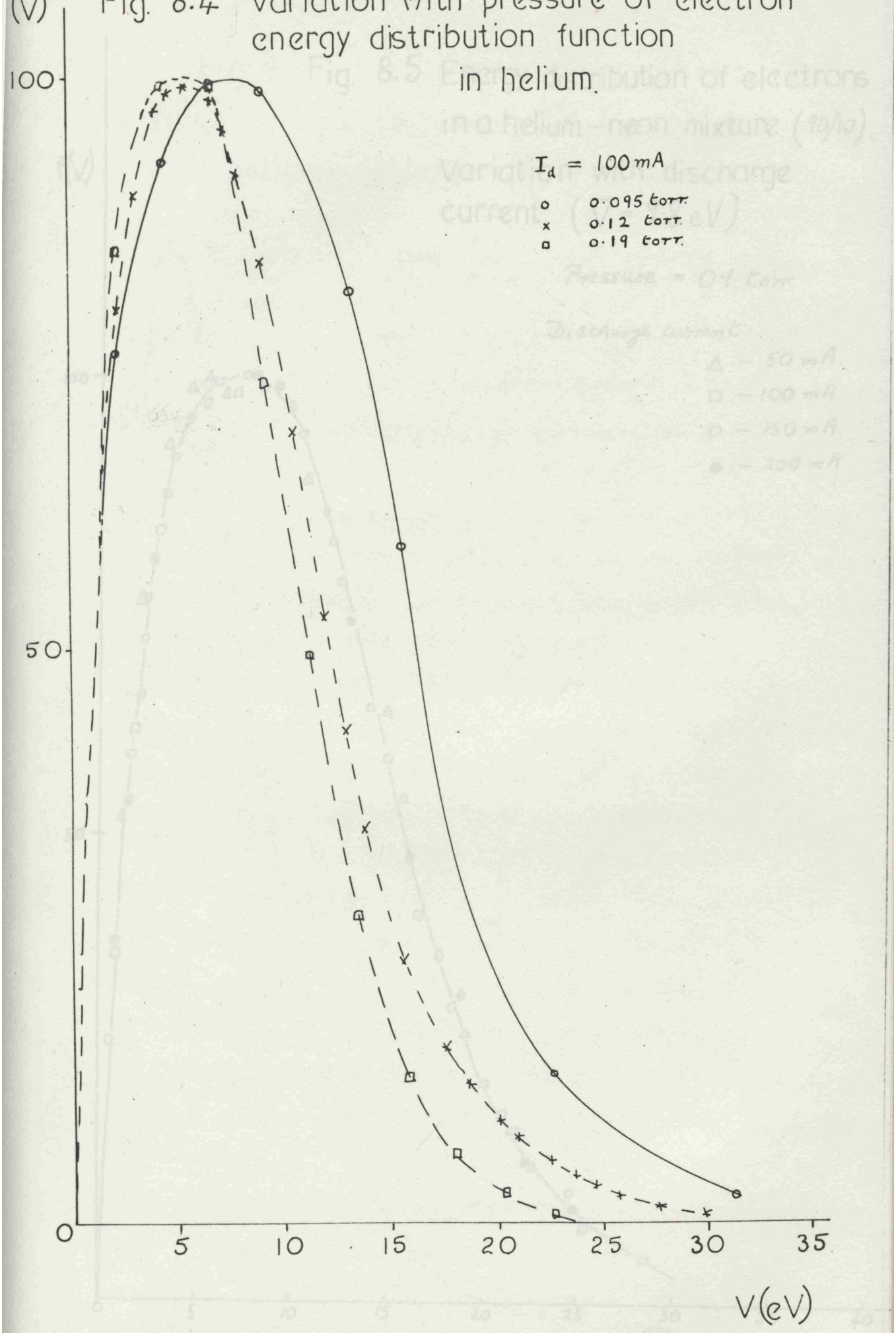

Fig. 8.5 Energy distribution of electrons in a helium–neon mixture (90/10). Variation with discharge current. ($\bar{V}$ = 9·8 eV)

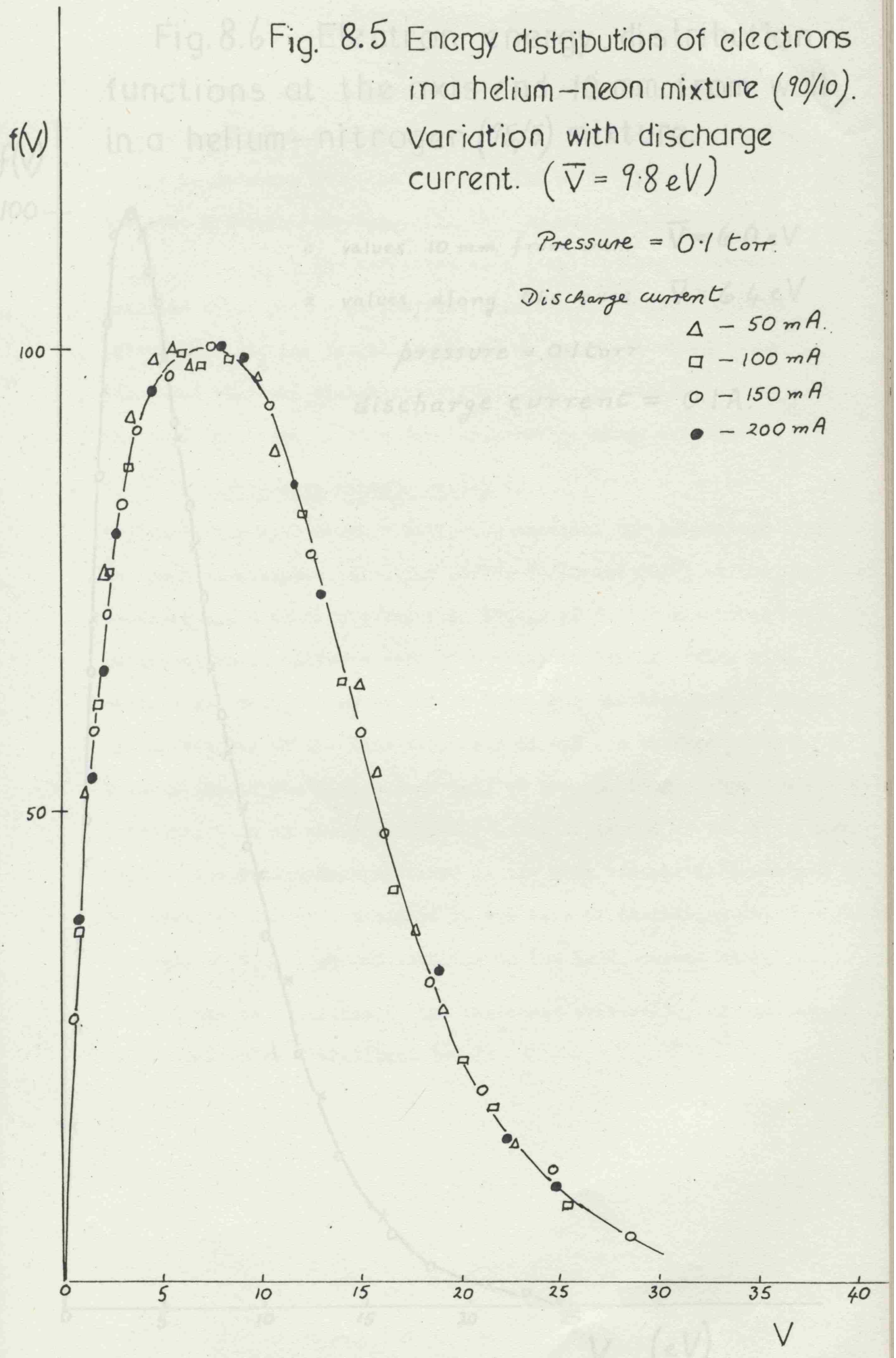

Fig. 8.6 Electron energy distribution functions at the axis and 10 mm. from wall in a helium–nitrogen (95/5) mixture.

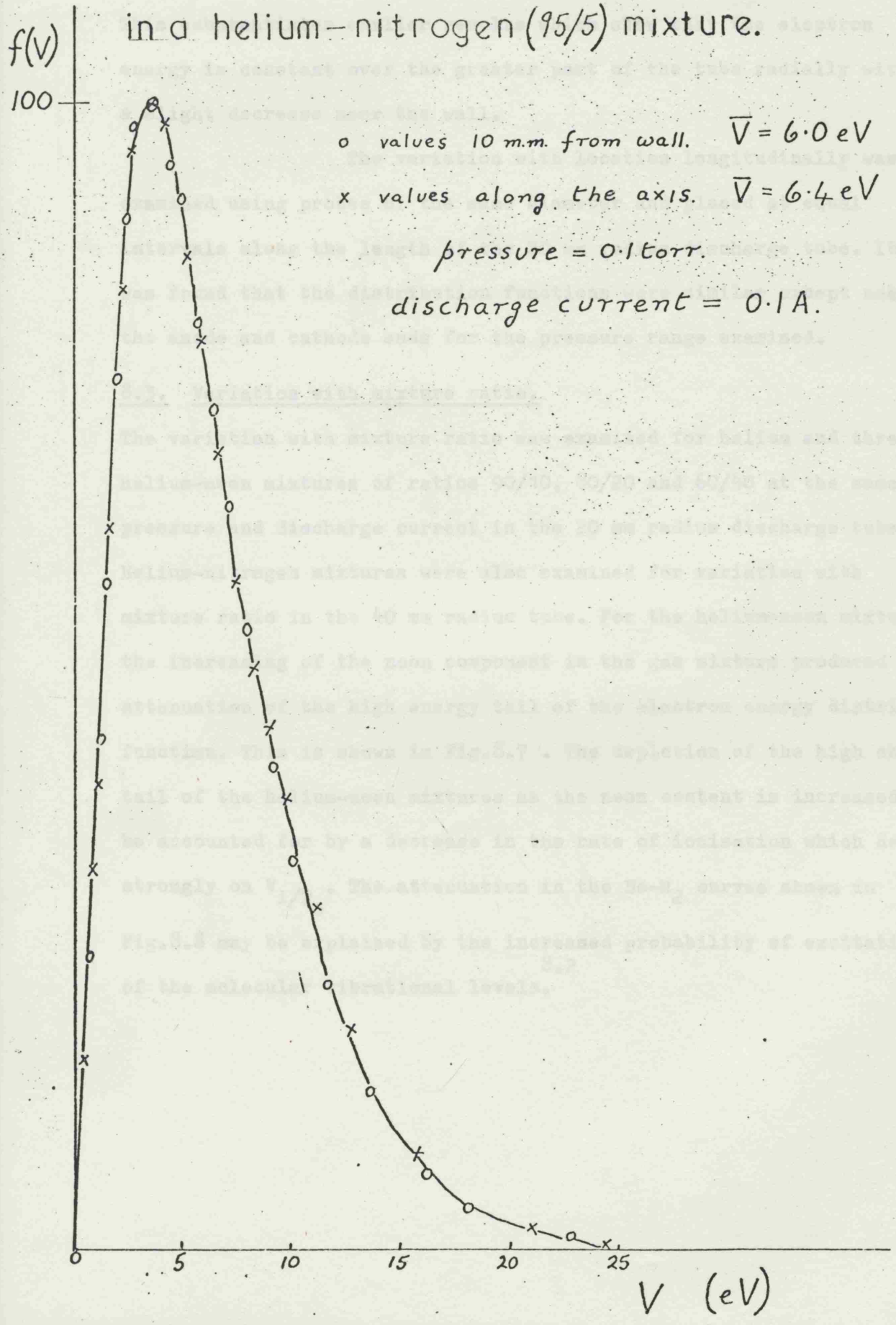

tube wall there was a slight distortion of the distribution curve This substantiates earlier results which show that the electron energy is constant over the greater part of the tube radially with a slight decrease near the wall.

The variation with location longitudinally was examined using probes of the same diameter and placed at equal intervals along the length of the 20 mm radius discharge tube. It was found that the distribution functions were similar except near the anode and cathode ends for the pressure range examined.

8.3. Variation with mixture ratio.

The variation with mixture ratio was examined for helium and three helium-neon mixtures of ratios 90/10, 80/20 and 60/40 at the same pressure and discharge current in the 20 mm radius discharge tube. Helium-nitrogen mixtures were also examined for variation with mixture ratio in the 40 mm radius tube. For the helium-neon mixture the increasing of the neon component in the gas mixture produced an attenuation of the high energy tail of the electron energy distribution function. This is shown in Fig.8.7 . The depletion of the high energy tail of the helium-neon mixtures as the neon content is increased can be accounted for by a decrease in the rate of ionisation which depends strongly on V_{i/T_e}. The attenuation in the $He-N_2$ curves shown in Fig.8.8 may be explained by the increased probability of excitation of the molecular vibrational levels.

Fig. 8.7

Variation of the experimental distribution curve with helium-neon ratio.

$p = 0.075$ torr.

$I_d = 100$mA.

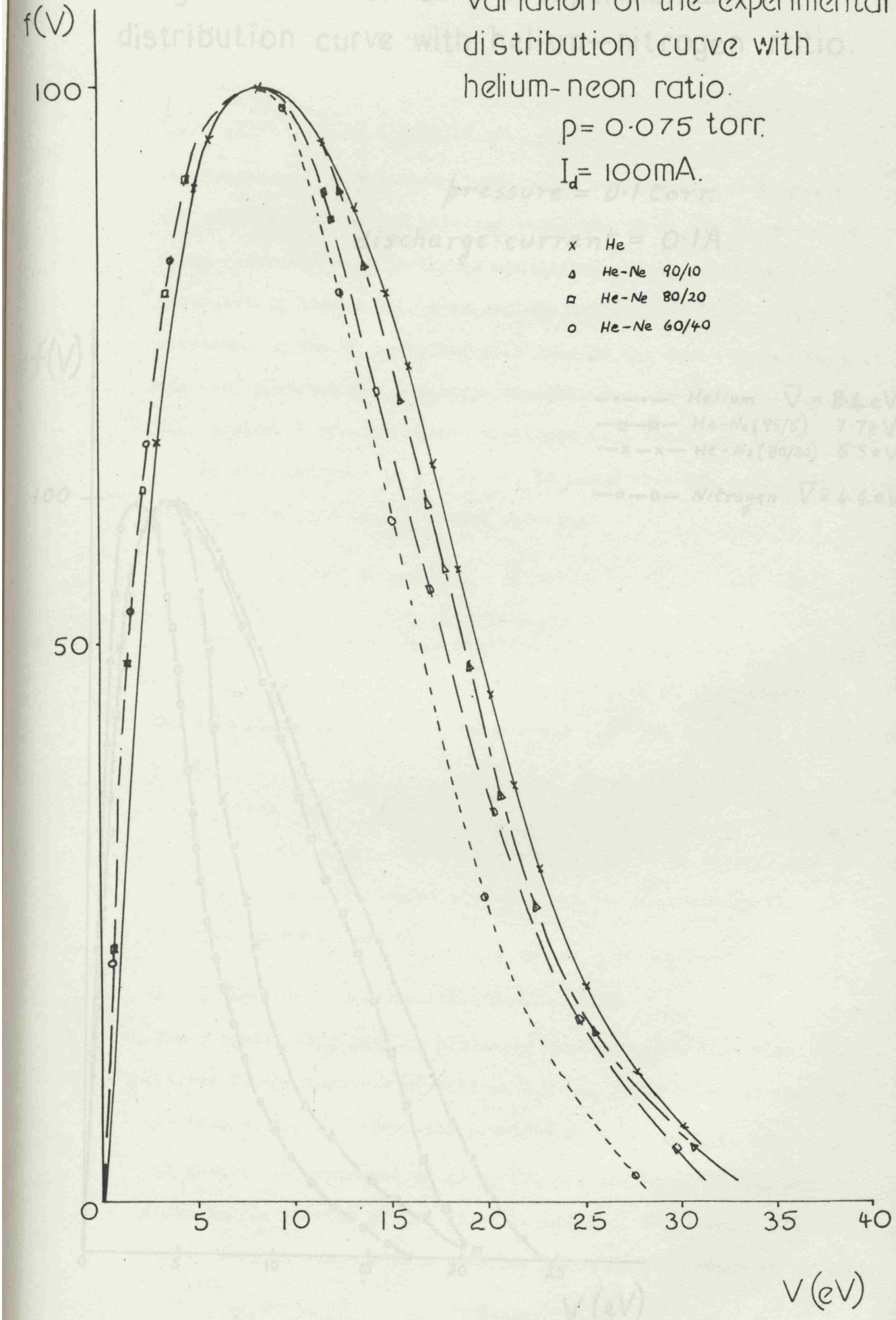

Fig. 8.8 Variation of the experimental distribution curve with helium—nitrogen ratio.

pressure = 0·1 torr.

discharge current = 0·1A.

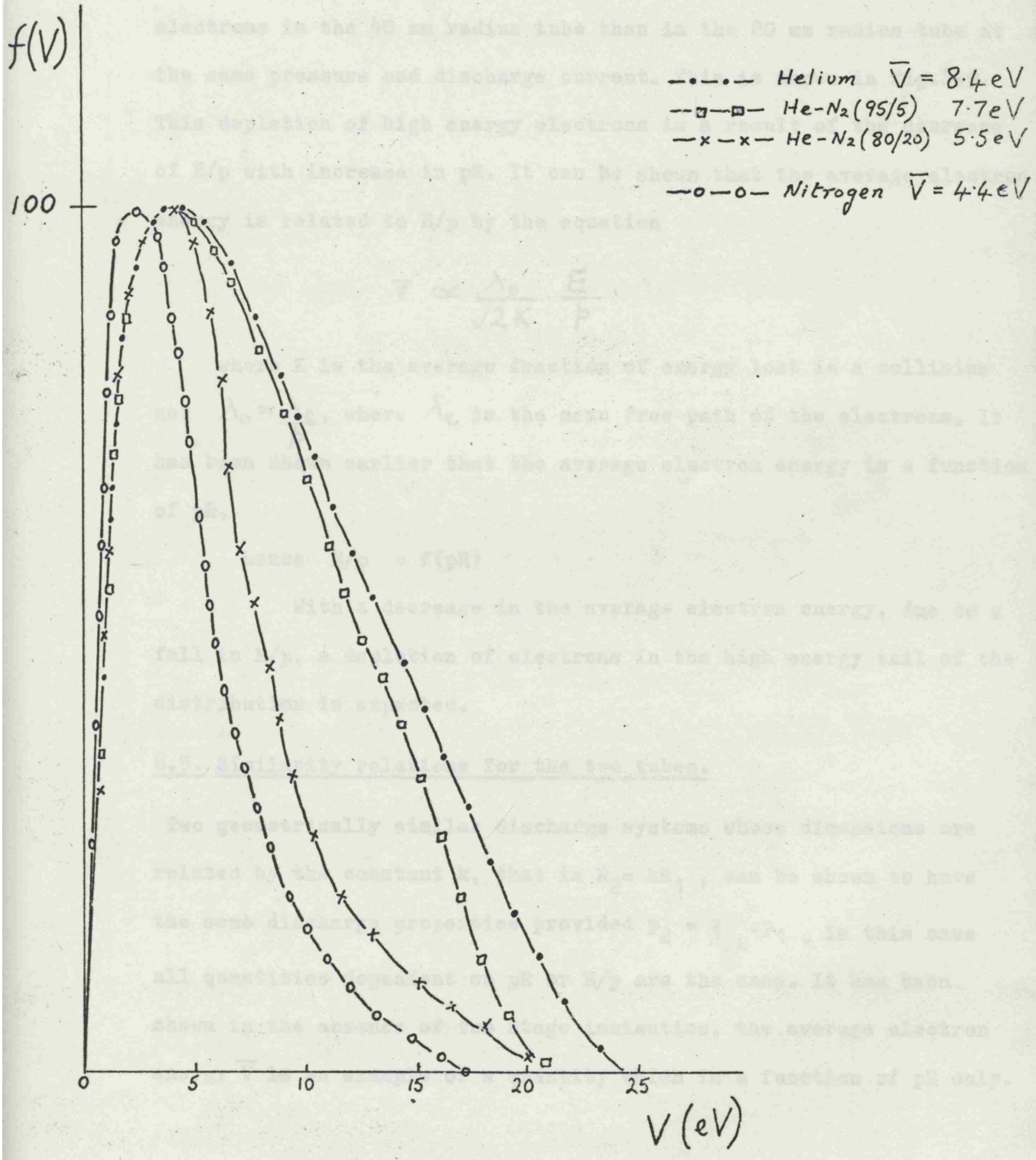

8.4. Dependence on discharge tube radius.

The dependence on discharge tube radius was investigated by comparing the distribution curves obtained using the 20 mm and 40 mm radius tubes under the same discharge conditions. It was found that the distribution curves were more rapidly depleted of high energy electrons in the 40 mm radius tube than in the 20 mm radius tube at the same pressure and discharge current. This is shown in Fig.8.9. This depletion of high energy electrons is a result of the decrease of E/p with increase in pR. It can be shown that the average electron energy is related to E/p by the equation

$$\bar{V} \simeq \frac{\lambda_o}{\sqrt{2K}} \cdot \frac{E}{p}$$

where K is the average fraction of energy lost in a collision and $\lambda_o = \frac{\lambda_e}{p}$, where λ_e is the mean free path of the electrons. It has been shown earlier that the average electron energy is a function of pR,

hence $E/p = f(pR)$

With a decrease in the average electron energy, due to a fall in E/p, a depletion of electrons in the high energy tail of the distribution is expected.

8.5. Similarity relations for the two tubes.

Two geometrically similar discharge systems whose dimensions are related by the constant k, that is $R_2 = kR_1$, can be shown to have the same discharge properties provided $p_2 = \frac{1}{k} \cdot p_1$. In this case all quantities dependent on pR or E/p are the same. It has been shown in the absence of two stage ionisation, the average electron energy $\bar{V}$ is an example of a quantity which is a function of pR only.

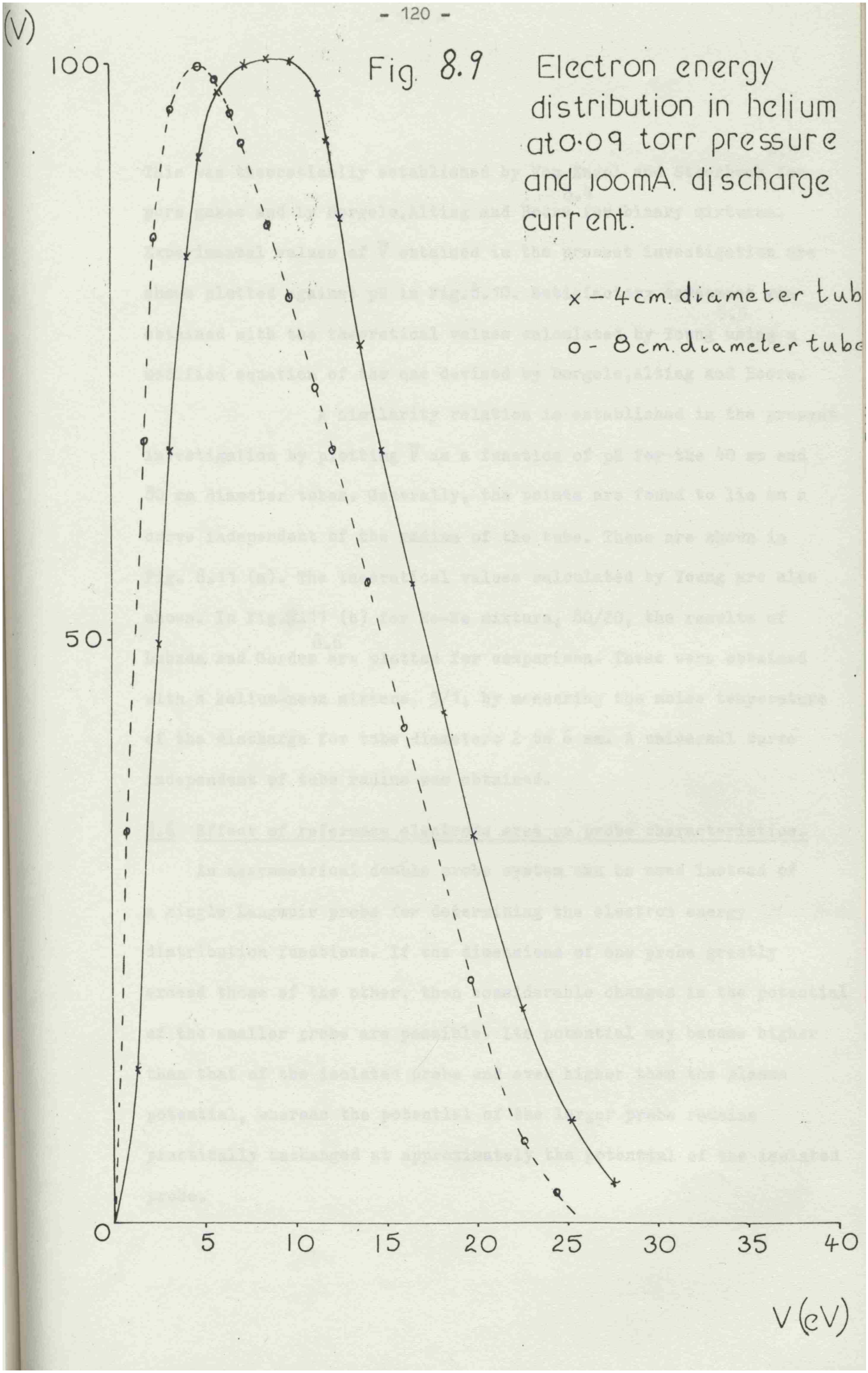

Fig. 8.9 Electron energy distribution in helium at 0·09 torr pressure and 100mA. discharge current.

x – 4cm. diameter tub

o - 8cm. diameter tube

This was theoretically established by Von Engel and Steenbeck [8.3] for pure gases and by Dorgelo, Alting and Boers [8.4] for binary mixtures. Experimental values of $\bar{V}$ obtained in the present investigation are shown plotted against pR in Fig.8.10. Satisfactory agreement was obtained with the theoretical values calculated by Young [8.5] using a modified equation of the one devised by Dorgelo, Alting and Boers.

A similarity relation is established in the present investigation by plotting $\bar{V}$ as a function of pR for the 40 mm and 80 mm diameter tubes. Generally, the points are found to lie on a curve independent of the radius of the tube. These are shown in Fig. 8.11 (a). The theoretical values calculated by Young are also shown. In Fig.8.11 (b) for He-Ne mixture, 80/20, the results of Lubuda and Gordon [8.6] are plotted for comparison. These were obtained with a helium-neon mixture, 5/1, by measuring the noise temperature of the discharge for tube diameters 2 to 6 mm. A universal curve independent of tube radius was obtained.

8.6 Effect of reference electrode area on probe characteristics.

An assymmetrical double probe system can be used instead of a single Langmuir probe for determining the electron energy distribution functions. If the dimensions of one probe greatly exceed those of the other, then considerable changes in the potential of the smaller probe are possible. Its potential may become higher than that of the isolated probe and even higher than the plasma potential, whereas the potential of the larger probe remains practically unchanged at approximately the potential of the isolated probe.

Fig. 8.10 Variation of $\overline{V}$ with pR

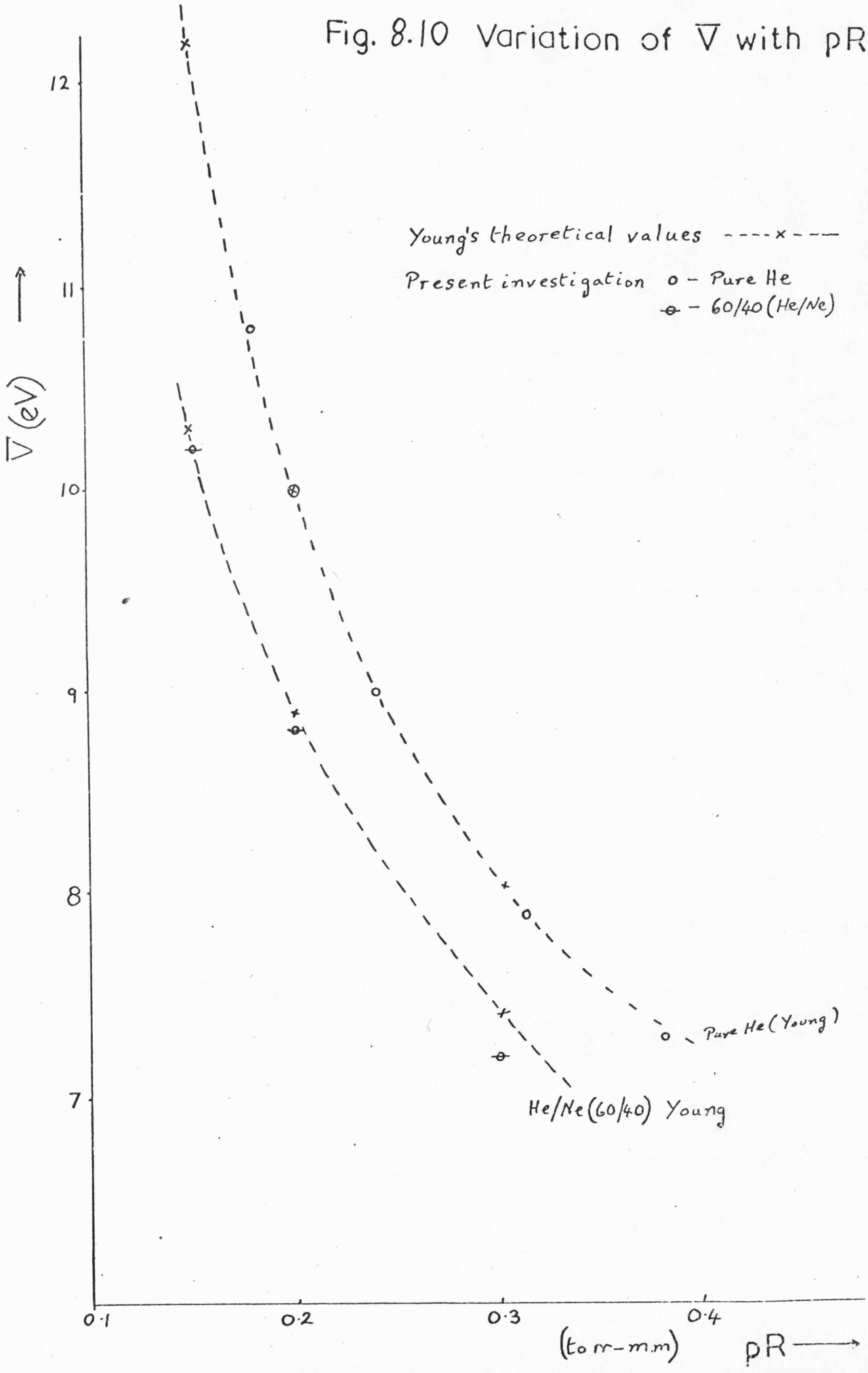

Fig. 8.11(a)

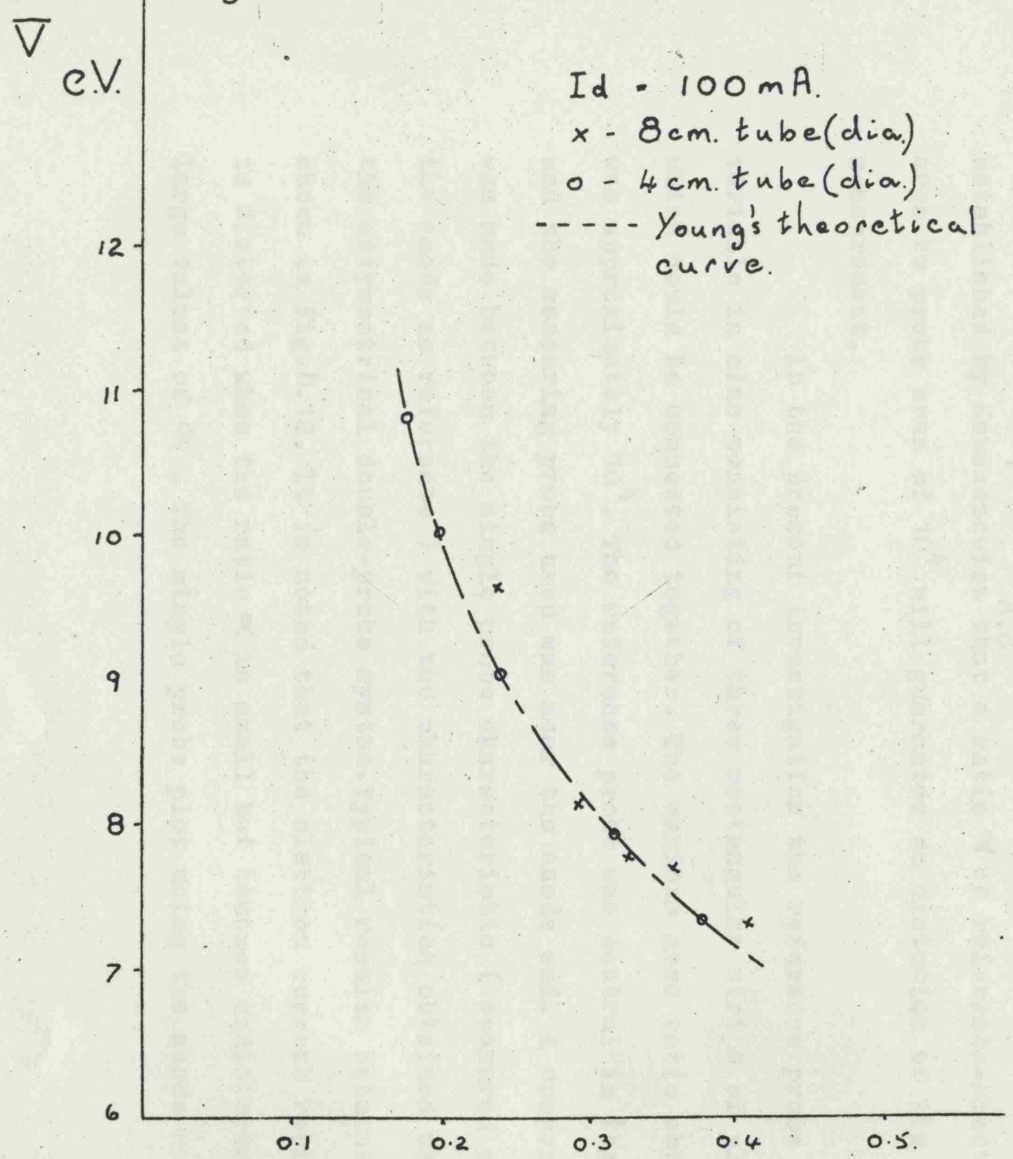

Dependence of $\overline{V}$ on pR for Helium.

Fig. 8.11(b)

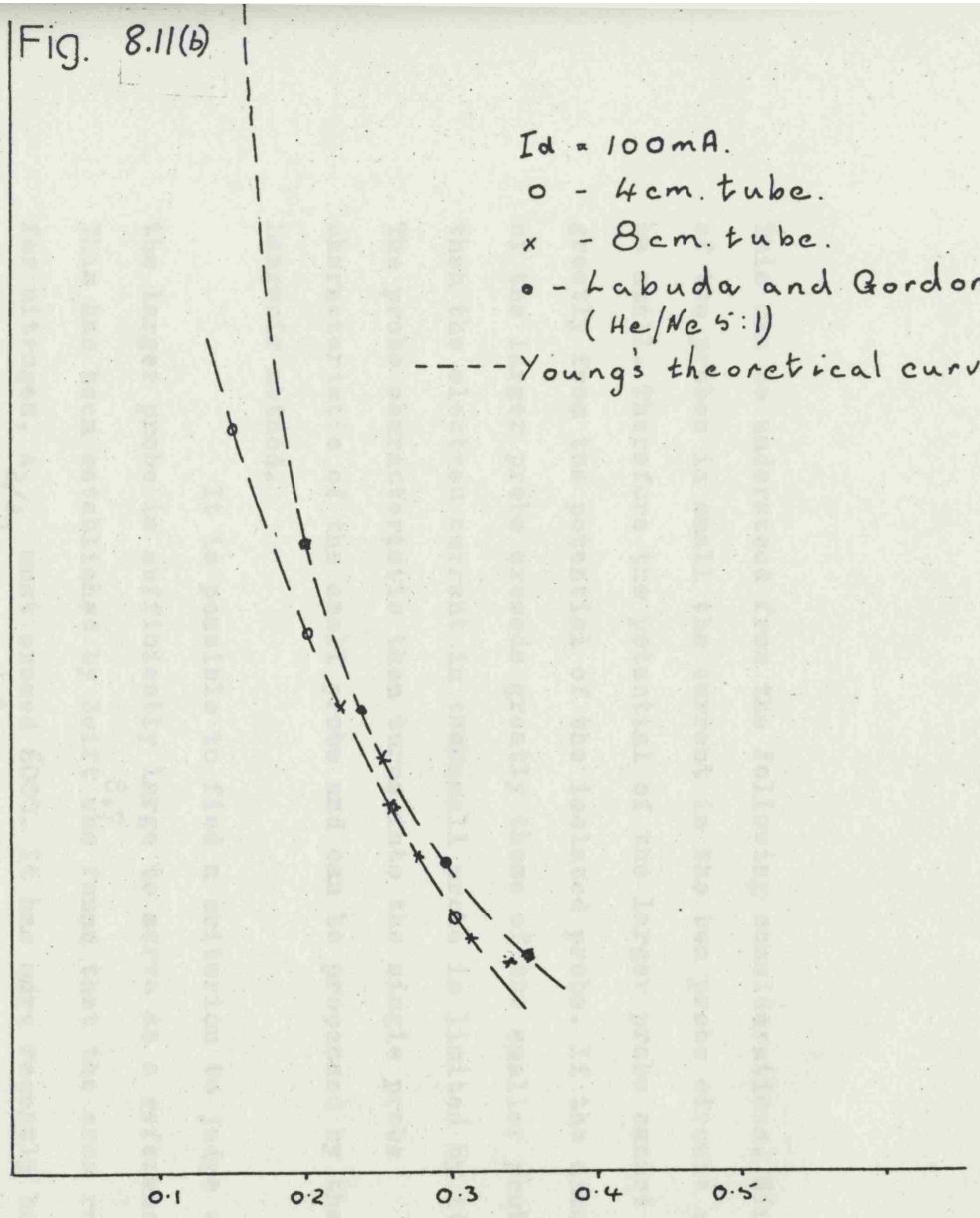

Dependence of $\overline{V}$ on pR for Helium-Neon. (80/20)

This can be understood from the following considerations. Since one of the probes is small the current in the two probe circuit should be small. Therefore the potential of the larger probe cannot differ greatly from the potential of the isolated probe. If the dimensions of the larger probe exceeds greatly those of the smaller probe, then the electron current in the small probe is limited by its size. The probe characteristic then turns into the single probe characteristic of the small probe and can be processed by the usual Langmuir method.

It is possible to find a criterion to judge whether the larger probe is sufficiently large to serve as a reference probe. This has been established by Swift[8.7] who found that the area ratio for nitrogen, A_{2/A_1} must exceed 6000. It has more recently been established by Szuszczewicz[8.8] that a ratio α of reference-electrode area to probe area of 10^4 will guarantee no distortion of the measurement.

In the present investigation the reference probe was variable in size consisting of three rectangular strips of platinum which could be connected together. The maximum area ratio obtainable was approximately 10^4. The reference probe was central in the tube and the measuring probe used was near the anode end. A comparison was made between the single probe characteristic (measured using the anode as reference) with the characteristics obtained using the assymmetrical double-probe system.Typical results obtained are shown in Fig.8.12. It is noted that the electron current response is distorted when the ratio α is small but becomes undistorted at large values of α . The single probe plot using the anode as

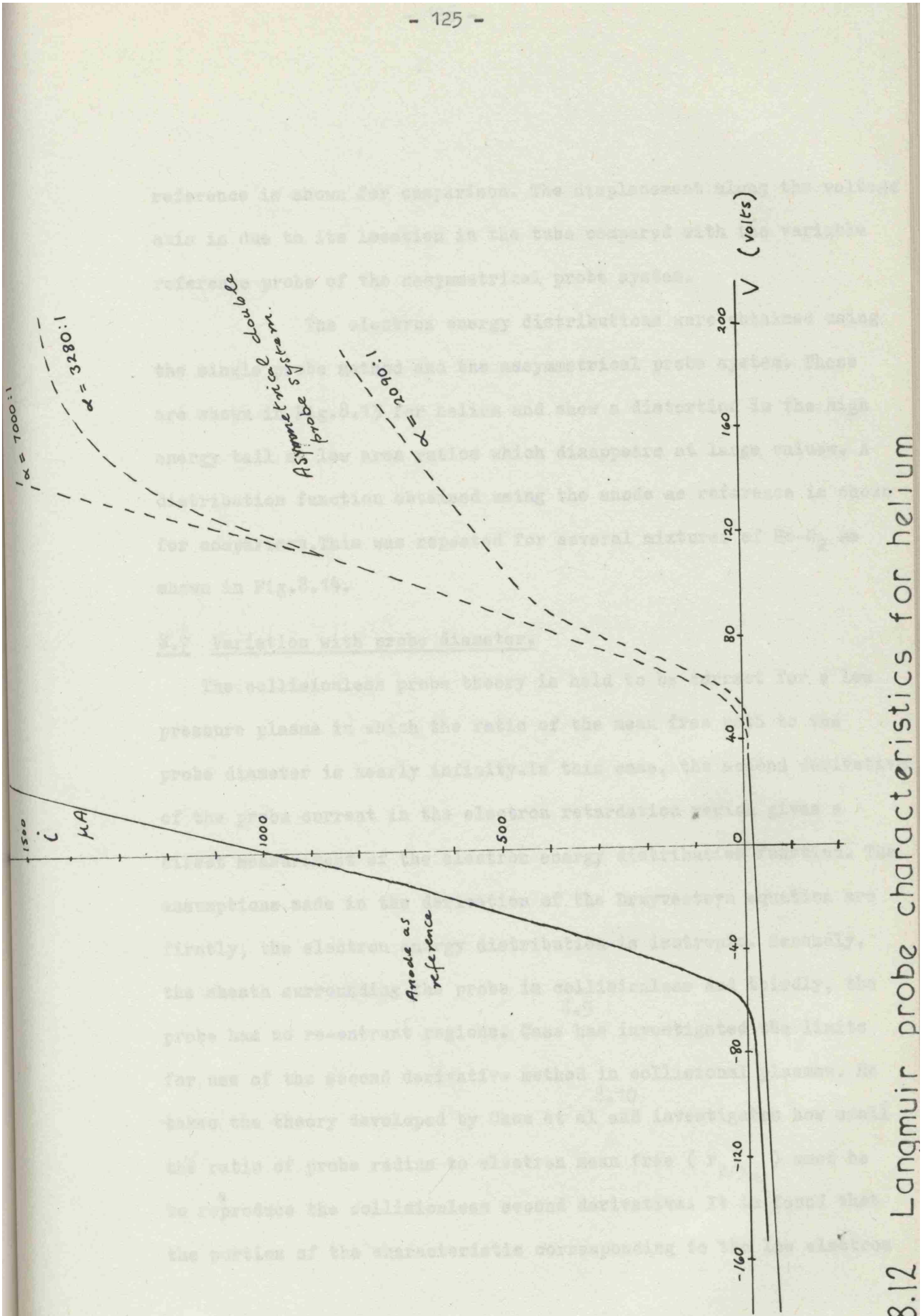

Fig. 8.12 Langmuir probe characteristics for helium

reference is shown for comparison. The displacement along the voltage axis is due to its location in the tube compared with the variable reference probe of the assymmetrical probe system.

The electron energy distributions were obtained using the single probe method and the assymmetrical probe system. These are shown in Fig.8.13 for helium and show a distortion in the high energy tail at low area ratios which disappears at large values. A distribution function obtained using the anode as reference is shown for comparison.This was repeated for several mixtures of He-N_2 as shown in Fig.8.14.

8.7 Variation with probe diameter.

The collisionless probe theory is held to be correct for a low pressure plasma in which the ratio of the mean free path to the probe diameter is nearly infinity.In this case, the second derivative of the probe current in the electron retardation region gives a direct measurement of the electron energy distribution function. The assumptions made in the derivation of the Druyvesteyn equation are firstly, the electron energy distribution is isotropic. Secondly, the sheath surrounding the probe is collisionless and thirdly, the probe has no re-entrant regions. Case [8.9] has investigated the limits for use of the second derivative method in collisional plasmas. He takes the theory developed by Chou et al [8.10] and investigates how small the ratio of probe radius to electron mean free (r_{p/λ_e}) must be to reproduce the collisionless second derivative. It is found that the portion of the characteristic corresponding to the low electron

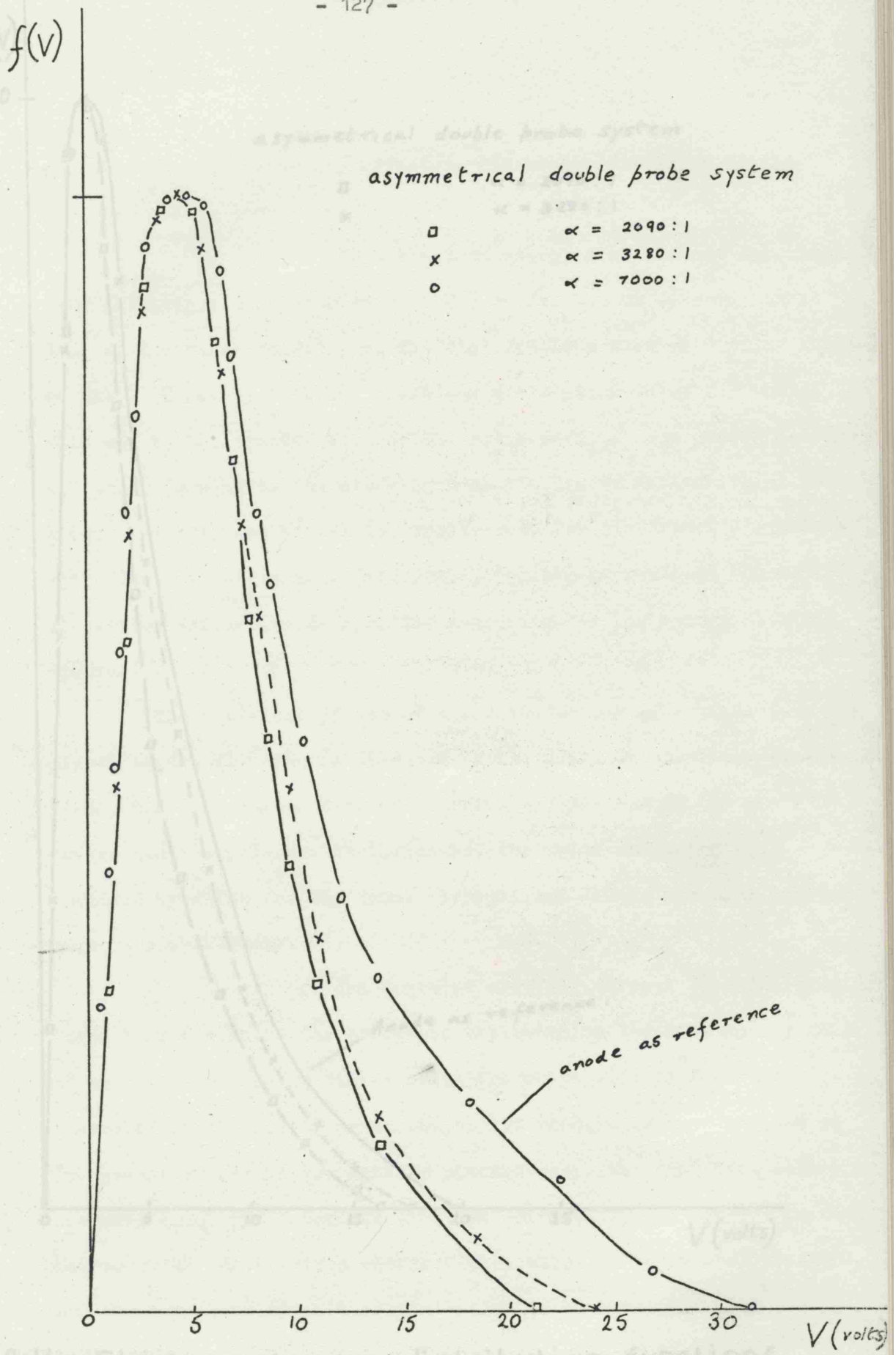

Fig. 8.13 Electron energy distribution functions using asymmetrical double probe system (helium)

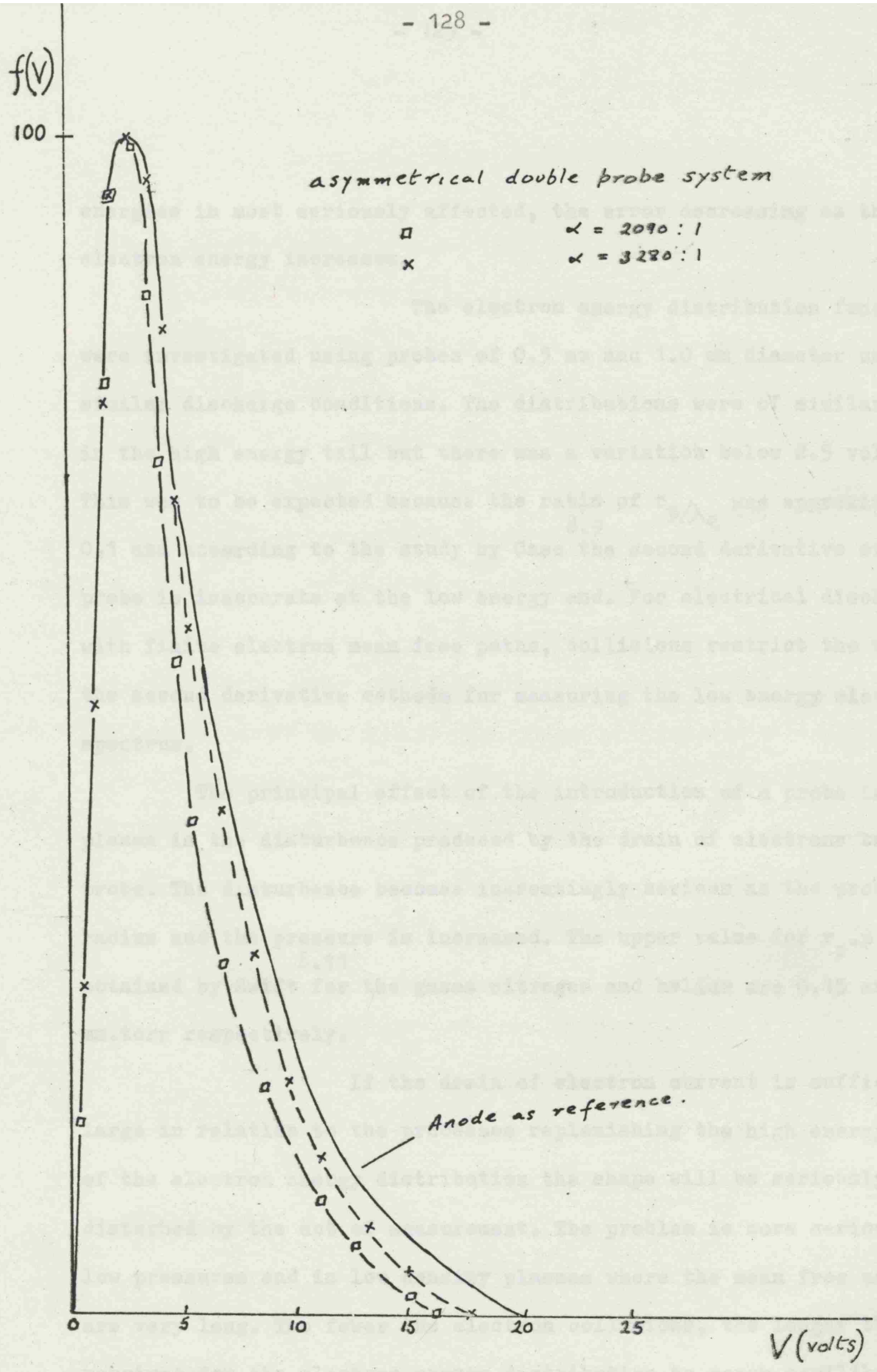

Fig. 8.14 Electron energy distribution functions using asymmetrical double probe system (helium–nitrogen 40/60)

energies is most seriously affected, the error decreasing as the electron energy increases.

The electron energy distribution functions were investigated using probes of 0.5 mm and 1.0 mm diameter under similar discharge conditions. The distributions were of similar shape in the high energy tail but there was a variation below 2.5 volts. This was to be expected because the ratio of r_p/λ_e was approximately 0.1 and according to the study by Case[8.9] the second derivative of the probe is inaccurate at the low energy end. For electrical discharges with finite electron mean free paths, collisions restrict the use of the second derivative methods for measuring the low energy electron spectrum.

The principal effect of the introduction of a probe into the plasma is the disturbance produced by the drain of electrons to the probe. The disturbance becomes increasingly serious as the probe radius and the pressure is increased. The upper value for $r_p.p$ obtained by Swift[8.11] for the gases nitrogen and helium are 0.15 and 0.3 mm.torr respectively.

If the drain of electron current is sufficiently large in relation to the processes replenishing the high energy tail of the electron energy distribution the shape will be seriously disturbed by the act of measurement. The problem is more serious at low pressures and in low density plasmas where the mean free paths are very long. The fewer the electron collisions, the longer the time required for the electron energy distribution to reach equilibrium and the more sensitive the distribution is to the perturbing influences.

In the present investigation mixtures of helium-nitrogen were used to examine the distortion of the electron energy distribution function for variation in size of the probe. It was confirmed that the high energy tail of the electron energy distribution was undisturbed by the increase in size of the probe but there was considerable distortion of the low energy end. A typical set of results are shown in Fig. 8.15 for helium-nitrogen mixture(90/10) at 100 mA discharge current and 250μ pressure. The measurements were taken with a 0.5 mm diameter probe and then with a 1.0 mm diameter probe in identical discharge conditions. The average energy of the electrons was 4.6 eV. There was a noticeable distortion of the electron energy distribution function below 2.5 eV and a slight distortion between 5 and 6.5 eV.

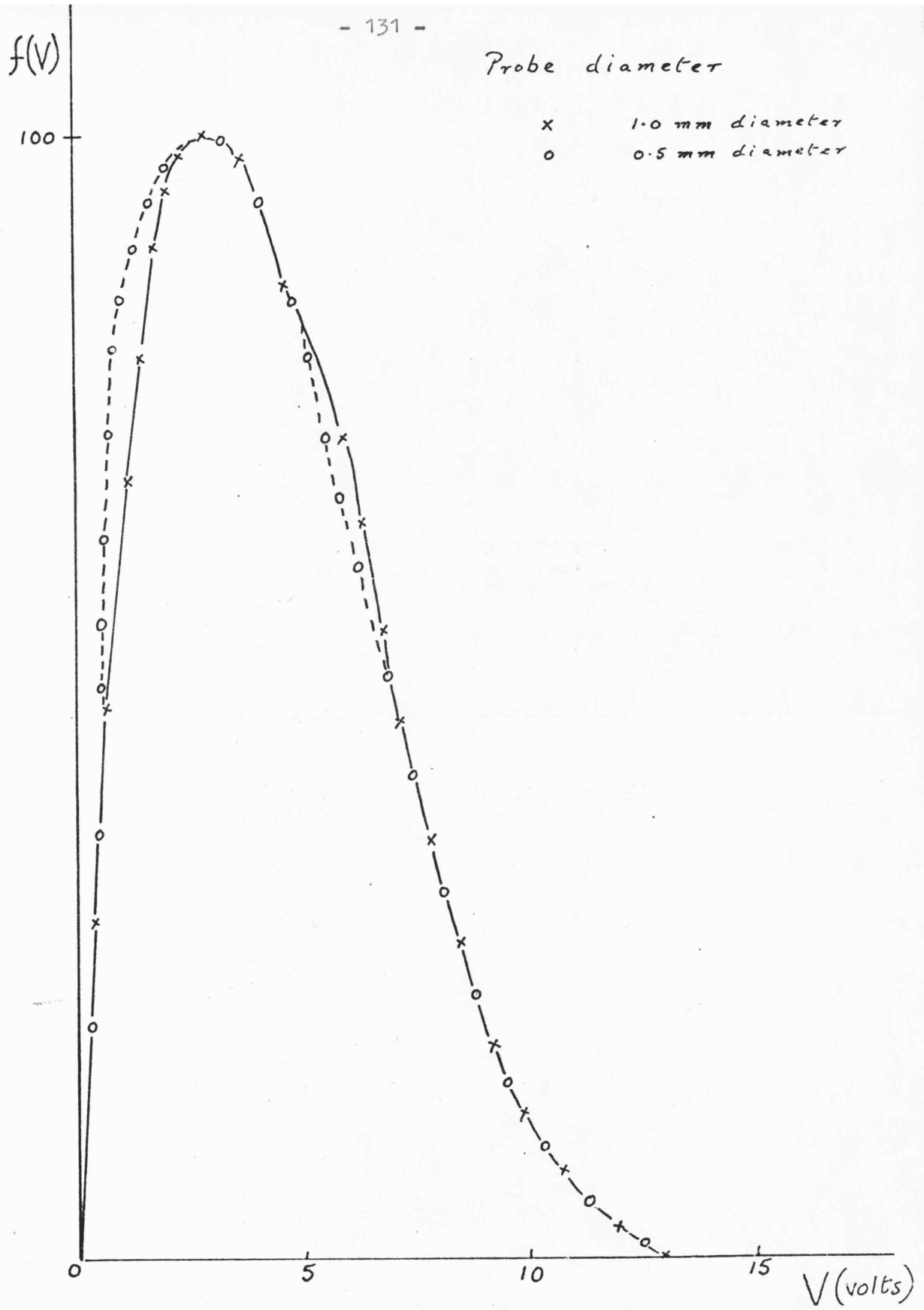

Fig. 8.15 Examination of the distortion of the electron energy distribution function for variation in size of probe.

CHAPTER 9. THE ACCURACY OF MEASUREMENT.

When considering the accuracy of the results presented in this thesis it is necessary to consider the Druyvesteyn equation

$$f(V) = B V^{\frac{1}{2}} \frac{d^2 i_e}{dV^2}$$

The accuracy of the final data depends on the error limits that can be assigned to B, a constant whose value appears difficult to determine.

$$B = \frac{2}{Ae} \left(\frac{2m}{e}\right)^{\frac{1}{2}}$$

where e is the electronic charge, m the electronic mass and A the area of the probe. The probes were carefully prepared and the area determined within an accuracy of 4%. However, there is the problem of the formation of insulating films on the probe during the investigation. The probe was kept free from contaminants by flashing red hot by electron bombardment before each run.

The accuracy of the absolute electron density and the mobilities depends not only on the accuracy of the two basic measurements of V and $\frac{d^2 i_e}{dV^2}$ but also on the accuracy of the calibration of the measuring system. This accuracy of calibration depends in turn on the accuracy of the probe area measurement, the r.m.s. value of the injected signal and the probe current. The accuracy of the two basic measurements will be considered first.

The error in V.

A switched potential divider was used which enabled the probe bias to be varied in 0.2V steps from 0 to 40V. This range covered the electron and ion saturation regions of the probe. The switched system has the advantage that exact values of bias may be repeated

easily, thus enabling the stability of the measurement with time to be checked. The d.c. bias between the probe and the anode was measured with an Advance digital voltmeter which had an impedance of 10 MΩ and did not in any way affect the probe circuit.

The location of the space potential plays an important part in determining the overall accuracy of the final result.An error of up to 0.5V may be made in the location of the space potential and this will lead to errors in the calculated values of electron density, average electron energy,drift velocity and mobility.

The error in $\frac{d^2 i_e}{dV^2}$.

The output of the detecting system has been shown to be proportional to the second harmonic component of the probe current. However, it contains an additional noise component which was measured by observing the amplifier output when no signal was introduced into the probe circuit. The second harmonic signal was many times greater than the noise signal and hence the performance of the detecting system was considered to be suitable.

Another possible error is that due to second harmonic distortion . This could come from the transformer used to introduce the a.c. signal to the probe circuit. A Radford distortion analyser was used to measure the second harmonic distortion and was found to be less than 0.2%. This would produce a distortion in the probe signal which is less than the minimum value measured by the detecting system.

The error in electron density.

The electron density is given by the expression

$$n_e = f(V).dV = \frac{Bk}{E^2} V^{\frac{1}{2}}.S.dV$$

$$= \frac{Bk}{E^2} \times \text{area under the distribution curve}$$

$$\% \text{ error in } n_e = \% \text{ error in B} + \% \text{ error in k} + 2 \times \% \text{ error in E} + \% \text{ error in area under curve}$$

The accuracy of the constant B depends solely on the probe area A. The diameter of the spherical probes were measured to an accuracy of $\pm$ 2% giving an accuracy of B to be $\pm$ 4%.

As described in Section 5.6 the detecting system was calibrated by feeding in a small sinusoidal signal. A calibration constant k corresponding to the current producing unit galvanometer deflection was calculated. The sinusoidal signal calibration accuracy was $\pm$ 2% and the galvanometer readings $\pm$ 1%. This gives the accuracy of E to be $\pm$ 2% and that of k to be $\pm$ 3%.

The area under the distribution curve can be shown to have an accuracy of $\pm$ 3% for a typical curve but higher for noisy discharges. Hence the total error involved in measuring the electron density was 14% for a normal discharge and higher errors for noisy discharges.

The error in the average electron energy.

The error in the average electron energy is affected by inaccuracies in determining the electron energy distribution function.There is uncertainty in locating the position of space potential which is

used as the zero of the electron energy distribution function. In the present investigation, the zero cross of the second derivative curve is taken as defining space potential However, it has been suggested by some workers[9.1] that the maximum of the second derivative curve is a better point to take the space potential.

Generally,throughout the present investigation, the voltage difference between the maximum and zero cross of the second derivative curve was found to be about 1 volt. However, this voltage difference was found to increase in some cases where moving striations were present. The error in the average electron energy was found for these cases. It was estimated by taking the space potential at the maximum and zero cross of the second derivative curve and calculating the average electron energy in each case. The distribution curves obtained using these two definitions of space potential are shown in Fig.9.1 for the mixture He-Ne (40/60) together with the average electron energies evaluated. The error bars shown in Fig.7.8 were obtained by using the maximum and minimum values of the average electron energy derived in this way.

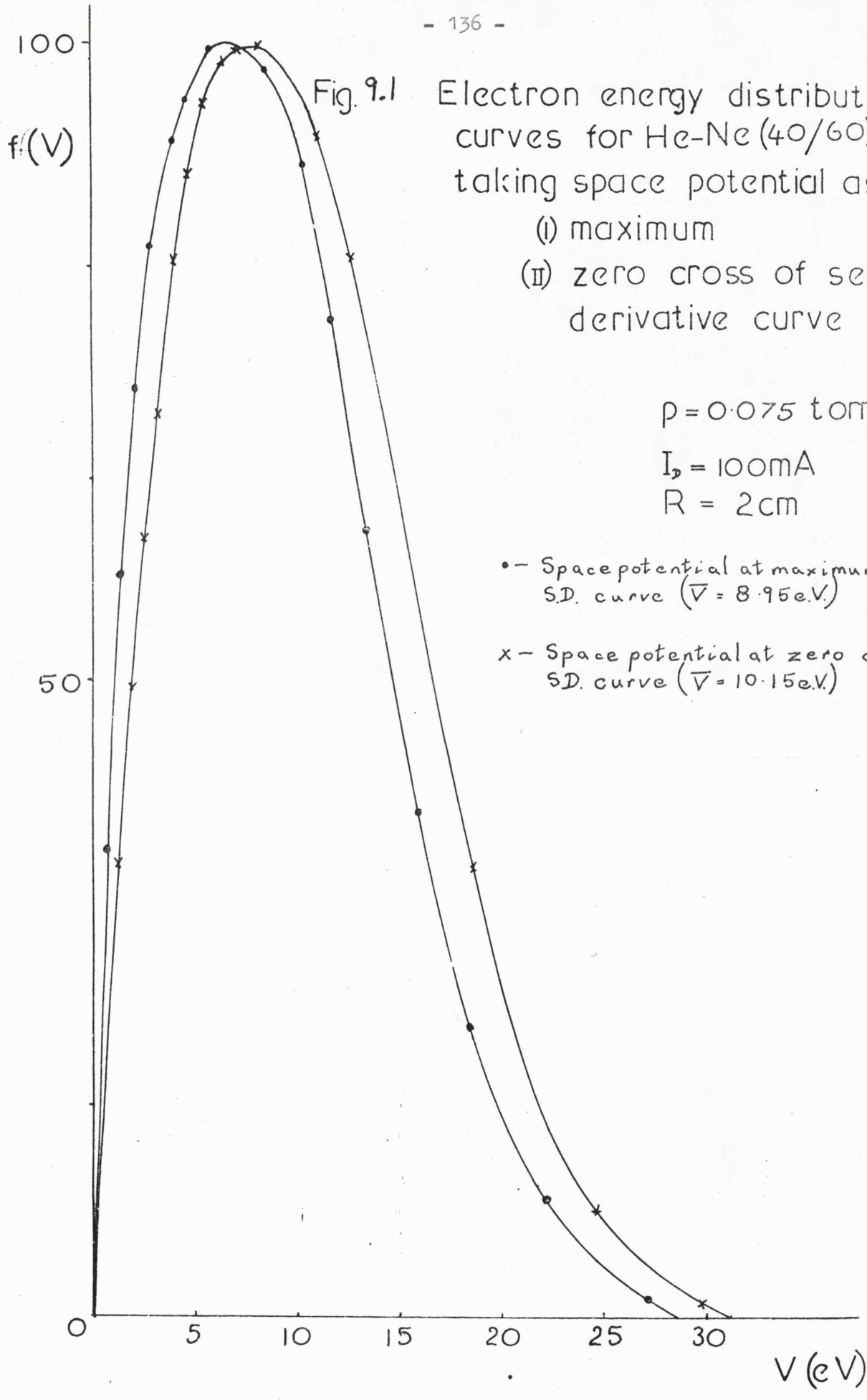

Fig. 9.1 Electron energy distribution curves for He-Ne (40/60) taking space potential as

(I) maximum

(II) zero cross of second derivative curve

$p = 0.075$ torr

$I_p = 100$mA

$R = 2$cm

• – Space potential at maximum of S.D. curve ($\overline{V} = 8.95$ e.V.)

x – Space potential at zero cross of S.D. curve ($\overline{V} = 10.15$ e.V.)

CHAPTER 10. FURTHER ANALYSIS.

10.1. Effect of a.c. amplitude on the measurement of the electron energy distribution function.

It has been shown by Kilvington et al [10.1] that the apparent form of the electron energy distribution function is dependent on the amplitude of the a.c. signal applied to the probe.

It can be shown that the application of the a.c. signal to the probe produces an a.c. component of the probe current at twice the frequency of the signal applied. This has a value given by

$$i_{2\omega} = \frac{E^2}{4}\varphi''(V) + \frac{E^4}{48}\varphi^{IV}(V) + \frac{E^6}{1536}\varphi^{VI}(V) + \ldots$$

when E is kept small then

$$i_{2\omega} = \frac{E^2}{4}\varphi''(V)$$

however at higher values there is a departure from this linear relationship between $i_{2\omega}$ and E^2 and the shape of the electron energy distribution curve is affected.

Like Kilvington et al it was established that a linear relationship did exist for Nitrogen for low values of E, but failed at higher values indicating that the higher order terms in the Taylor expression should be taken into account. Similarly, a linear relationship for helium was established for lower values of E, but failed at higher values . Examples of the curves for nitrogen and helium are shown in Fig. 10.1 and 10.2.

It will be noted that there is an upturning of the $i_{2\omega}$ against E^2 graph for nitrogen at higher values of E, but for helium a downturning of the graph is observed. The degree of departure from the E^2 law is dependent on the probe bias V.

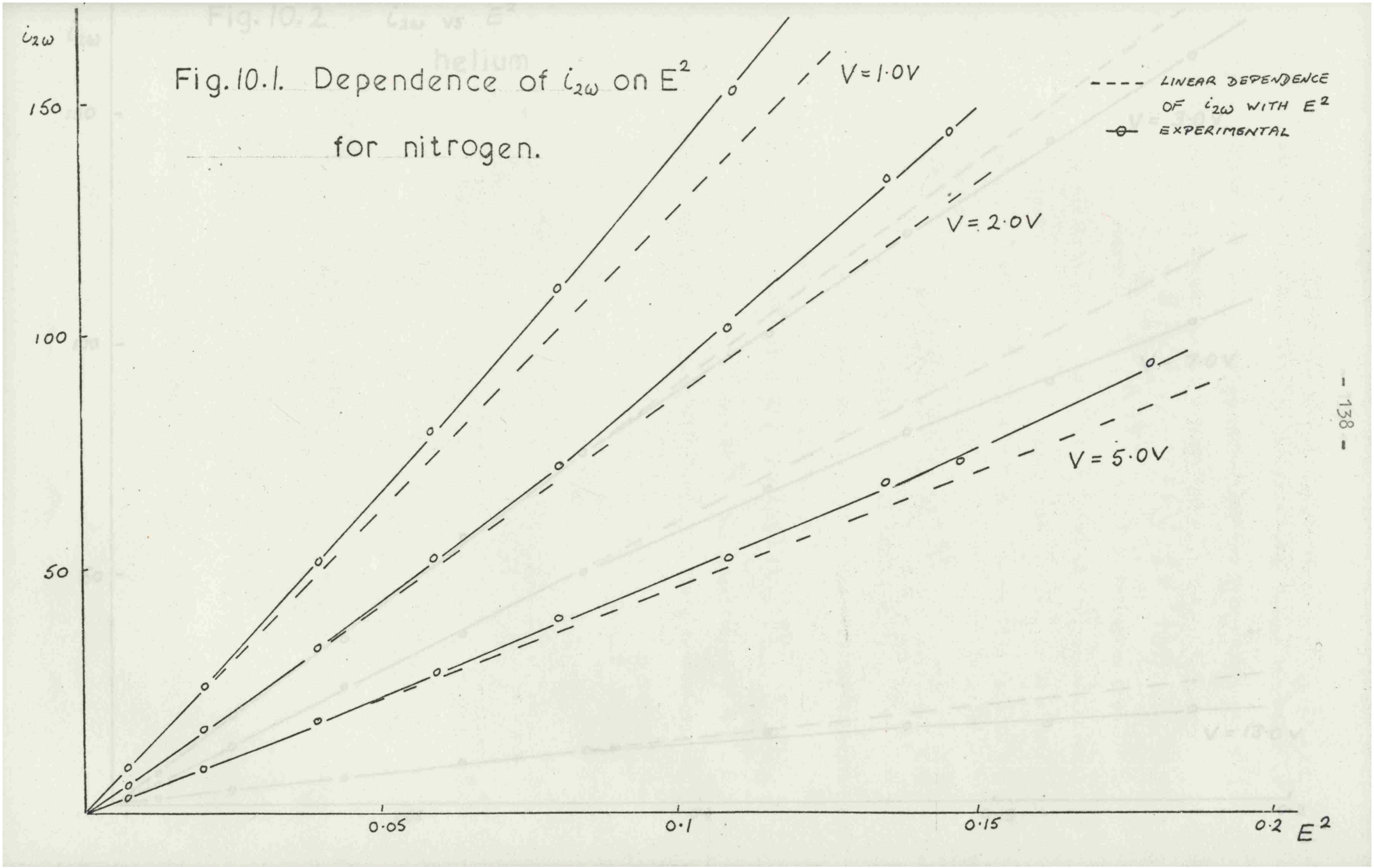
Fig. 10.1. Dependence of $i_{2\omega}$ on E^2 for nitrogen.
$i_{2\omega}$
150
100
50
V = 1·0V
V = 2·0V
V = 5·0V
LINEAR DEPENDENCE OF $i_{2\omega}$ WITH E^2
EXPERIMENTAL
0·05
0·1
0·15
0·2
E^2

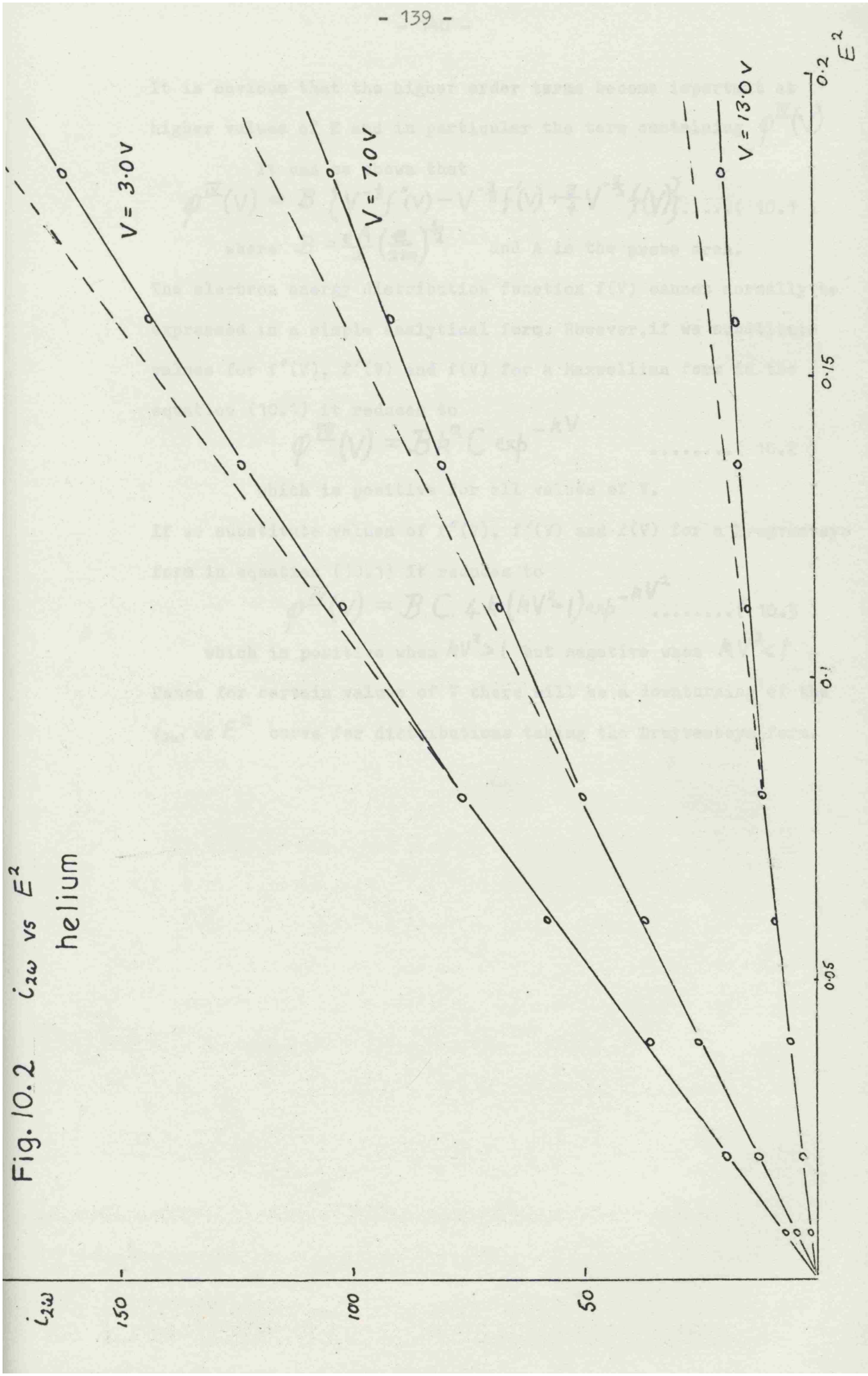

Fig. 10.2 $i_{2\omega}$ vs E^2
helium

It is obvious that the higher order terms become important at higher values of E and in particular the term containing $\varphi^{IV}(V)$

It can be shown that

$$\varphi^{IV}(V) = B\left\{V^{-\frac{1}{2}}f''(V) - V^{-\frac{3}{2}}f'(V) + \frac{3}{4}V^{-\frac{5}{2}}f(V)\right\} \quad \ldots\ldots (10.1)$$

where $B = \frac{eA}{2}\left(\frac{e}{2m}\right)^{\frac{1}{2}}$ and A is the probe area.

The electron energy distribution function f(V) cannot normally be expressed in a simple analytical form. However, if we substitute values for f''(V), f'(V) and f(V) for a Maxwellian form in the equation (10.1) it reduces to

$$\varphi^{IV}(V) = Bk^2C\exp^{-kV} \quad \ldots\ldots\ldots (10.2)$$

which is positive for all values of V.

If we substitute values of f''(V), f'(V) and f(V) for a Druyvesteyn form in equation (10.1) it reduces to

$$\varphi^{IV}(V) = B.C.4k(kV^2-1)\exp^{-kV^2} \quad \ldots\ldots\ldots (10.3)$$

which is positive when $kV^2 > 1$ but negative when $kV^2 < 1$

Hence for certain values of V there will be a downturning of the $i_{2\omega}$ vs E^2 curve for distributions taking the Druyvesteyn form.

10.2. Comparison of spherical and cylindrical probes.

As described in Chapter 4 the 40 mm diameter tube was fitted with both spherical and cylindrical probes for comparitive purposes. The first cylindrical probe had the highest length to diameter ratio and gave the best comparison with the spherical probes within its vicinity. The electron density measured with the fifth spherical probe and the first cylindrical probe are compared in Table 10.1. As can be seen from the results the ratio of the two electron densities is comparable with the ratio of the probe areas. An exact comparison is not possible because whereas the spherical probe was located at the axis, the cylindrical probe was of length 7.2mm with only its tip on the axis. Consequently, the electron density obtained by the cylindrical probe can be shown to be $0.96\ n_o$, where n_o is the density at the axis. Furthermore, the Langmuir-Druyvesteyn analysis is applicable to both spherical and cylindrical probes only when the distribution is isotropic. If there is any doubt then it is necessary to use a spherical probe. Rayment and Twiddy[10.2] have shown that the electron energy distribution in a low pressure positive column is anisotropic and this invalidates the use of all probes except spherical ones. The isotropic nature of the electron energy distribution in the present investigation was not tested.

TABLE 10.1

COMPARISON OF SPHERICAL AND CYLINDRICAL PROBES.

Gas	pressure torr	Discharge current, mA	Ratio of areas spherical/ cylindrical	Ratio of electron concentration spherical/ cylindrical
Helium	0.11	25	0.69	0.72
"	0.11	50	0.69	0.74
"	0.11	100	0.69	0.72
"	0.16	100	0.69	0.73
Helium–Neon (90/10)	0.095	100	0.69	0.72

CHAPTER 11 CONCLUSION

The present investigation was concerned with the determination of the electron energy distribution functions in mixtures of helium/neon and helium/nitrogen at relatively low pressures in the positive column of a glow discharge. From these distribution functions it was possible to determine the densities, mean energies, drift velocities and the mobilities of the electrons in the mixture A comparison of the electron mean energies with those obtained using other techniques has shown that the Langmuir probe method is both reliable and sensitive to variations in pressure, discharge current and location in the positive column. A dependence of the electron mean energy on the Rp value was confirmed.

The observations were made with mixtures which are relevant to low power laser systems. It would be of interest to extend the work to other mixtures using gas lasers. For example, an area for investigation could be the role played by foreign gases in the nitrogen/carbon dioxide system in improving the power output of the laser. There are at present a number of theories which try to explain the function of these gases. If oscillations occur in these mixtures then one of the techniques described in section 2.6 could be used for obtaining the electron energy distribution functions.

The shape of the helium/nitrogen mixture curves disagreed with both the Maxwellian and Druyvesteyn forms. This is to be expected because the Maxwell-Boltzmann distribution implies thermal equilibrium which does not exist in the positive column and the Druyvesteyn distribution makes no allowance for

inelastic collisions which sustain the positive column. The depletion of the high energy electrons as the nitrogen content is increased is probably connected with the excitation of the molecular vibrational levels. Calculations by Nighan [11.1] indicate that the high energy tail of the electron energy distribution function in nitrogen is very sensitive to the vibrational temperature. Recent experiments by Ivanov et al [11.2] support this conclusion.

The present investigation has been concerned mainly with the measurement of various parameters in mixtures of gases in the positive column of the glow discharge. However, part of the investigation was concerned with studying the operation of the probe itself and the experimental technique used to obtain the second derivative.These include the effect of the reference probe area on the probe characteristics,the variation of the characteristics with the measuring probe diameter and the effect of increasing the amplitude of the a.c. signal applied to the probe on the measurement of the electron energy distribution functions.

It has recently been shown by Berger et al [11.3] that in electron energy distribution measurements with Langmuir probes distortions appear if secondary discharge parts(anode glow, positive column) exist between the plasma surrounding the measuring probe and the reference probe. This is because the voltage applied between the probe and the reference electrode is across a resistance made up of the probe-plasma transition region and that of the plasma parts. Whereas the transition region near the probe is dependent on the applied voltage, that of the plasma

column remains the same throughout the investigation for that pressure and current. Consequently,as the probe potential approaches the plasma potential, a larger fraction of the applied voltage will be across the plasma column. This leads to systematic errors in the second derivative and a shift in the maximum of the electron energy distribution function. The error involved depends on the nature of the gas being investigated and the location of the measuring probe in relation to the reference electrode.

One of the main difficulties throughout the investigation has been the occurrence of moving striations. These were found to be present for a wide range of pressure and discharge conditions, particularly when investigating the mixtures with a high percentage of neon. Wherever possible, the gases were investigated in the absence of moving striations or where the amplitude of the moving striations were of small enough magnitude to influence only slightly the discharge properties in their path To investigate the whole range of pressures and discharge current effectively, it would be necessary to apply one of the techniques described in Section 2.6.

Apart from the errors introduced by the presence of plasma parts , the accuracy of the technique used in the investigation is dependent on a number of factors; space potential, positive ion contribution etc. The determination of space potential is discussed in Section 6.1 and it is difficult to determine with greater accuracy than $\pm$ 0.5V. It has been assumed throughout the investigation that the positive ion contribution is negligible compared with that from the electrons.

That is, the second derivitive of the circuit current is essentially the same as the second derivative of the electron current. However, it has been shown by Richards et al[11.4] that the positive ion contribution extends the tail of the distribution indefinitely. This produces a small error in the density of the electrons and a slightly larger error in the mean electron energy.

The accuracy of the detecting system itself is dependent on its ability to eliminate noise. Most of the noise was filtered out by the amplifier which allowed only the component at 992 hz to reach the phase sensitive detector output.

The discharges were investigated ,generally, in a region where the electron and ionic mean free paths were less than the tube radius, and hence the Schottky theory of the positive column is acceptable. The experimental values of the average electron energies in helium-neon mixtures were generally in agreement with those calculated using an extension of the Schottky theory for binary mixtures. Also, the measurements were taken in a region where the electron mean free path to probe radius ratio was high, and hence the Langmuir-Druyvesteyn probe theory was valid.

APPENDIX 1

DORGELO, ALTING AND BOERS THEORY FOR MIXTURES.

Dorgelo, Alting and Boers [A.1.1] found that in the positive column of a neon-argon mixture at constant pressure and discharge current, the electron temperature decreased with increase in argon pressure. Also with neon-mercury mixtures the electron temperature fell with increase in vapour pressure of mercury. Through an extension of the diffusion theory of Schottky, they were able to explain these changes.

Like Schottky, [A.1.2] they made three assumptions. Firstly, the electrons possess a Maxwellian velocity distribution with temperature T_e, which is much greater than the gas temperature. Secondly, the pressure lies in the region where the ambipolar diffusion theory can be applied. Thirdly, the ions are only formed by electron impact and disappear by recombination at the walls. No volume recombination was assumed to exist so that the ions produced per sec per unit length must balance those which disappear at the walls. They proceeded to derive a formula as follows:-

Let q_1 and q_2 be the number of ions produced per second per unit volume in gases 1 and 2 respectively. Then it follows that

$$\int_0^r q_1 r\,dr = j_1 r \quad \text{or} \quad r q_1 = j_1 + r\frac{dj_1}{dr} \qquad \text{.....(A1.1a)}$$

$$\int_0^r q_2 r\,dr = j_2 r \quad \text{or} \quad r q_2 = j_2 + r\frac{dj_2}{dr} \qquad \text{.....(A1.1b)}$$

$$\int_0^r (q_1+q_2) r\,dr = j_e r \quad \text{or} \quad r(q_1+q_2) = j_e + r\frac{dj_e}{dr} \qquad \text{.....(A1.1c)}$$

and if j is the number of ions and electrons crossing unit area per second in the radial direction, then

$$j_1 = -D_1 \frac{dn_1}{dr} + n_1 b_1 E_r \qquad \text{.....(A1.2a)}$$

$$j_2 = -D_2 \frac{dn_2}{dr} + n_2 b_2 E_r \qquad \text{.....(A1.2b)}$$

$$j_e = -D_e \frac{dn_e}{dr} - n_e b_e E_r \qquad \text{.....(A1.2c)}$$

where D is the diffusion coefficient, b is the mobility of the particle, n the particle density and E_r the radial field intensity.

Because $n_1 + n_2 \simeq n_e$ and also $j_1 + j_2 = j_e$ we can eliminate E_r from equation (A.1.2) and arrive at

$$\frac{j_1}{b_1} + \frac{j_2}{b_2} + \frac{j_e}{b_e} = \frac{-D_1}{b_1}\frac{dn_1}{dr} - \frac{D_2}{b_2}\frac{dn_2}{dr} - \frac{D_e}{b_e}\frac{dn_e}{dr} \qquad \text{.....(A1.3)}$$

Differentiating equation (A1.3) gives

$$\frac{1}{b_1}\frac{dj_1}{dr} + \frac{1}{b_2}\frac{dj_2}{dr} + \frac{1}{b_e}\frac{dj_e}{dr}$$

$$= -D_1\frac{d^2n_1}{dr^2} - D_2\frac{d^2n_2}{dr^2} - D_e\frac{d^2n_e}{dr^2} \qquad \text{.....(A1.4)}$$

Multiplying equation (A1.4) by r , adding equation (A1.3) and using equation (A1.1), one obtains

$$r\left(\frac{q_1}{b_1} + \frac{q_2}{b_2} + \frac{q_1+q_2}{b_e}\right)$$

$$= -\frac{D_1}{b_1}\left(r\frac{d^2n_1}{dr^2} + \frac{dn_1}{dr}\right) - \frac{D_2}{b_2}\left(r\frac{d^2n_2}{dr^2} + \frac{dn_2}{dr}\right) - \frac{D_e}{b_e}\left(r\frac{d^2n_e}{dr^2} + \frac{dn_e}{dr}\right) \qquad \text{.....(A1.5)}$$

Now since $T_e >> T_1$ or T_2 and $b_e >> b_1$ or b_2 and with a Maxwellian distribution we have $D_e = b_e \frac{k}{e} T_e$

then equation (A1.5) becomes

$$\frac{q_1}{b_1} + \frac{q_2}{b_2} = -\frac{k}{e} T_e \left(\frac{d^2 n_e}{d\tau^2} + \frac{1}{\tau} \frac{dn_e}{d\tau} \right) \qquad \text{.....(A1.6)}$$

The number of ions produced per unit volume per second is proportional to n_e , so $q = \nu n_e$

Putting this into equation (A1.6) gives

$$\frac{k}{e} T_e \left(\frac{d^2 n_e}{d\tau^2} + \frac{1}{\tau} \frac{dn_e}{d\tau} \right) + \left(\frac{\nu_1}{b_1} + \frac{\nu_2}{b_2} \right) n_e = 0$$

which is a Bessel equation from which it follows that

$$n_e = n_o J_o \left[\tau \left\{ \left(\frac{\nu_1}{b_1} + \frac{\nu_2}{b_2} \right) \frac{e}{kT_e} \right\}^{\frac{1}{2}} \right] \qquad \text{.....(A1.7)}$$

where n_o is the electron concentration at the tube axis.

Assuming that at the wall $n_e = 0$

Equation (A1.7) becomes

$$\frac{\nu_1}{b_1} + \frac{\nu_2}{b_2} = \frac{k}{e} T_e \left(\frac{2.4}{R} \right)^2 = \frac{2}{3} \overline{V} \left(\frac{2.4}{R} \right)^2 \qquad \text{.....(A1.8)}$$

where V is the mean energy and R is the tube radius.

The value of ν is given by

$$\nu = a p \frac{4}{\sqrt{\pi}} \left(\frac{e}{3m} \right)^{\frac{1}{2}} V_i \left[1 + \frac{4}{3} \frac{\overline{V}}{V_i} \right] \overline{V}^{\frac{1}{2}} \exp\left(-\frac{3}{2} \frac{V_i}{\overline{V}} \right) \qquad \text{...(A1.9)}$$

Following the method used by Dorgelo, Alting and Boers[A.1.1], the equations (A1.8) and (A1.9) were combined by Young[A.1.3] to give a relationship between the electron temperature and pR for binary mixtures. He arrived at an equation of the form

$$\frac{f_1 a_1 V_1^{\frac{1}{2}}}{b_1 p}\left(\frac{\kappa T_e}{e V_1}\right)^{\frac{1}{2}}\left(1+\frac{e V_1}{2\kappa T_e}\right)\exp\left(\frac{-e V_1}{\kappa T_e}\right)$$

$$+\frac{f_2 a_2 V_2^{\frac{1}{2}}}{b_2 p}\left(\frac{\kappa T_e}{e V_2}\right)^{\frac{1}{2}}\left(1+\frac{e V_2}{2\kappa T_e}\right)\exp\left(\frac{-e V_2}{\kappa T_e}\right)=\frac{4\cdot305\times10^{-8}}{(pR)^2} \quad \ldots\ldots(A1.10)$$

where a_1, a_2 are the initial slopes of the ionization efficiences; b_1, b_2 the mobilities of the positive ions; f_1, f_2 ratio of parial pressures to total pressures; V_1, V_2 the ionization potentials.

The ion mobility $b_1 = \frac{760\mu_1}{p}$ and $b_2 = \frac{760\mu_2}{p}$

where μ_1 and μ_2 are the mobilities at S.T.P. The μ's are evaluated by the application of Blanc's Law:

$$\frac{1}{\mu_1} = \frac{f_1}{\mu_{11}} + \frac{f_2}{\mu_{12}} \qquad \frac{1}{\mu_2} = \frac{f_1}{\mu_{21}} + \frac{f_2}{\mu_{22}}$$

where μ_{11} = mobility of ion 1 in gas 1, μ_{12} ion 1 in gas 2 μ_{21} ion 2 in gas 1 and μ_{22} ion 2 in gas 2.

An alternative method of evaluating the mobility constants is given by Hiraoka and Kamada[A.1.4] who used Young's equation to evaluate the electron temperatures in argon-helium mixtures.

APPENDIX 2

THEORETICAL STUDIES OF THE ELECTRON ENERGY DISTRIBUTION FUNCTION.

The calculation of the energy of electrons in a gas acted on by an electric field was first considered by Pidduck[A.2.1] and later by other workers. During this period work was restricted to the case where all the collisions made by the electrons were elastic. The effect of Ramsauer free paths was also considered.

Druyvesteyn[A.2.2] was the first to successfully attempt the derivation of a distribution law. His analysis considered electrons in elastic collision with molecules but left out the effects of inelastic collisions. He also assumed the mean free paths of the electrons were independent of energy. His treatment considered the steady velocity distribution of electrons in a current traversing a gas in a homogeneous electric field E, assuming no electron loss. He equated the energy taken from the field with the total loss of energy of the electrons giving his first equation

$$J(\epsilon).e.E = \rho(\epsilon)\left(\frac{2e}{m}\right)^{\frac{1}{2}}\left(\frac{\delta\epsilon}{\lambda}\right)$$

where $J = \frac{j}{e}$ is the number of electrons passing one cm^2 normal to the field per second, λ the electron mean free path, $\delta = \frac{2m}{M}$ where m is the electron mass and M the mass of the molecule, e the electron charge, ϵ the electron energy and $\rho(\epsilon)$ the electron energy distribution function.

As a second equation between J and ρ, he used the mobility equation[A.2.3]

$$J(\epsilon,x) = -\frac{\lambda}{3}\left(\frac{2\epsilon}{m}\right)^{\frac{1}{2}}\rho_x' - \frac{\lambda.e.E}{3}\left(\frac{2\epsilon}{m}\right)^{\frac{1}{2}}\rho_\epsilon' + \frac{\lambda.e.E}{3m}\left(\frac{m}{2\epsilon}\right)^{\frac{1}{2}}\rho$$

In the case of a steady distribution ρ_x' is zero and a

combination of the two equations gives

$$\rho(\epsilon) = C\,\epsilon^{\frac{1}{2}}\,\exp\left[\frac{-3\delta\epsilon^2}{2\lambda^2 e^2 E^2}\right]$$

$$= C\,\epsilon^{\frac{1}{2}}\,\exp\left[-0.55\frac{\epsilon^2}{\bar{\epsilon}^2}\right]$$

where C is a constant. In the derived distribution the number of fast electrons was found to be much less than that of a Maxwellian distribution at the same average energy.

A method of analysis which allowed for inelastic collisions and variable mean free paths was developed by Smit.[A.2.4] He based his approach on an equation given as

$$\tfrac{2}{3}\tfrac{m}{M}\tfrac{1}{\lambda}\bar{\epsilon}_a\epsilon^{\frac{1}{2}}\rho(\epsilon) - 2\tfrac{m}{M}\tfrac{1}{\lambda}\epsilon^{\frac{3}{2}}\rho(\epsilon) - \tfrac{4}{3}\tfrac{m}{M}\tfrac{1}{\lambda}\bar{\epsilon}_a\epsilon^{\frac{3}{2}}\frac{d\rho(\epsilon)}{d\epsilon}$$

$$+\tfrac{1}{6}E^2e^2\lambda\epsilon^{-\frac{1}{2}}\rho(\epsilon) - \tfrac{1}{3}E^2e^2\lambda\epsilon^{\frac{1}{2}}\frac{d\rho(\epsilon)}{d\epsilon}$$

$$= N_a\int_{\epsilon}^{\infty}\alpha\cdot\xi^{\frac{1}{2}}\cdot\rho(\epsilon)\cdot d\xi$$

where α is the total inelastic cross-section, N_a the concentration of gas atoms and $\bar{\epsilon}_a$ the mean energy of the gas atoms. The total inelastic cross-section measured by Maier-Leibnitz[A.2.5] was used in the calculations. Using this method he calculated the electron energy distribution functions in helium for four values of E/N up to $3\times10^{-20}\ V.m^2$. In later years, Dunlop[A.2.6] extended the calculations for helium to higher values of E/N.

The electron energy distribution function has been derived by a large number of investigators using various treatments of the Boltzmann transport equation. This has the form

$$\frac{\partial f}{\partial t} + v.\nabla r.f + a.\nabla v.f = \left(\frac{\partial f}{\partial t}\right)$$

where ∇r is the divergence in three-dimensional configuration space,

∇_v is the divergence in the corresponding three dimensional velocity space, a is the total field acceleration, f the velocity distribution function and $\left(\frac{\partial f}{\partial t}\right)_{coll}$ is the rate of loss of electrons from the elemental volume of the six dimensional hyperstate due to collisional processes.

If it is assumed that there are no spacial variations in f and the external force arises from an electric field E acting in the x- direction only then the Boltzmann equation simplifies to

$$\frac{eE}{m}\frac{\partial f}{\partial v_x} + \frac{\partial f}{\partial t} = \left(\frac{\partial f}{\partial t}\right)_{coll}$$

Here $\frac{\partial f}{\partial t}$ represents the local time rate of change caused in f by variations of E and $\left(\frac{\partial f}{\partial t}\right)_{coll}$ represents the change due to collisions with gas molecules. Solution of this equation is, in principle, then possible by introducing appropriate expressions of $\left(\frac{\partial f}{\partial t}\right)_{coll}$ and expressing f in terms of a system of spherical harmonics. A review of methods of solving this equation has been given by Allis.[A.2.7]

Heylen and Lewis[A.2.8] in their calculations took into account all collisional processes including those due to elastic, rotational and vibrational collisions. The Smit derivation, which is related to the more usual treatment based on the Boltzmann transport equation, is used as the starting point.

After some re-arrangement, the Smit equation may be written as

$$\left[2\frac{m}{M}\frac{1}{\lambda}\epsilon^{3/2} - \frac{1}{6}e^2E^2\lambda\epsilon^{-1/2}\right]\rho(\epsilon) + \frac{e^2E^2}{3}\lambda\epsilon^{\frac{1}{2}}\frac{d\rho(\epsilon)}{d\epsilon} + N_a\int_{\epsilon}^{\infty}\alpha.\xi^{\frac{1}{2}}.\rho(\epsilon).d\xi = 0$$

with the assumption that $(eE\lambda)^2 >> \frac{m}{M}\epsilon_a.\epsilon$, which is that the electrons have much greater energies than the mean gas energy ϵ_a . If $\alpha = 0$ the equation yields distributions of the Druyvesteyn type according to the form of θ_d , the cross-section for momentum transfer. This is related to λ by $\lambda = \frac{1}{N\theta_d}$. Since the momentum transfer cross-section is a function of ϵ and assuming it varies with ϵ according to the n^{th} power law then

$$\rho(\epsilon) = C\epsilon^{\frac{1}{2}} \exp\left[\frac{-3m}{(n+1)M}\left(\frac{N\theta_d.\epsilon}{eE}\right)^2\right]$$

from which, if $n = 0$ (θ_d constant) the usual Druyvesteyn form results.

Retaining the terms containing α , Heylen and Lewis went on to show that in rare gases , the electron energy distribution may be far from Maxwellian especially in the high energy tail.Here the distributions became depleted of electrons beyond the inelastic region. For molecular gases, however, they showed that the distribution should be approximately a Maxwellian form.

Coulomb collisions between electrons mutually and between electrons and ions, neglected by earlier workers, was considered by Postma. Since electrons can exchange large fractions of their energies in mutual collisions, they have large influence on the high energy tail of the distribution function and hence on the ionization and excitation rates. In his calculations of the distribution function, Postma[A.2.9] used measurements made in recent years of the cross-sections of the inelastic and elastic

electron-atoms collisions. He assumed that the energy loss of the electrons in exciting collisions was equal to the excitation energy of the first exciting state. This assumption becomes questionable at values of $\frac{E}{N} > 9\times10^{-20}\ V.m^2$ where other approximations also become doubtful. Ionizing collisions of electrons with excited atoms were neglected and over the whole region the total inelastic cross-section used by Postma was about 10% smaller than the Maier-Leibnitz curve used by Smit. A choice of suitable momentum transfer cross-section was made by comparing the electron mobilities calculated from the cross-sections with experimental values. The momentum transfer cross-section of Golden and Bandel[A.2.10] was used because it gave the best agreement between calculated and experimental values of the mobilities. Postma[A.2.11] extended his treatment of the electron energy distribution function in helium to include collisions of electrons with already excited atoms.

Hughes[A.2.12] has shown that the electron transport equation in the regime of elastic and inelastic collisions derived by Smit follows simply from an extension of a treatment given by Davidson[A.2.13] using a velocity diagram. Hughes computes the distribution of electron energies in helium and neon over the range $1\times10^{-20} \leq \frac{E}{N} \leq 12\times10^{-20}\ V.m^2$. Total cross-sections for momentum transfer in helium and neon were taken from Massey and Burhop[A.2.14] while those for ionization by electron impact were obtained from an investigation by Rapp and Englander-Golden.[A.2.15] The cross-sections for excitation by electron impact were obtained from the results of Maier-Leibnitz.[A.2.5]

ELECTRONIC DEBYE LENGTHS AT VARIOUS ELECTRON DENSITIES AND TEMPERATURES.

$$\lambda_D = \left(\frac{\epsilon_o \, k T_e}{e^2 \, n_e} \right)^{\frac{1}{2}} \text{ metres}$$

n_e (m^{-3}) \ T_e (°K)	50,000	70,000	90,000	110,000
10^{14}	1.54×10^{-3}	1.82×10^{-3}	2.07×10^{-3}	2.28×10^{-3}
10^{15}	4.87×10^{-4}	5.77×10^{-4}	6.54×10^{-4}	7.23×10^{-4}
10^{16}	1.54×10^{-4}	1.82×10^{-4}	2.07×10^{-4}	2.28×10^{-4}

REFERENCES

Chapter 1

1.1 W.S.Schottky, Physik.Zeits. 25, 342 and 635, 1924

1.2 R.M.Howe, J.Appl.Phys., 24, 881, 1953

1.3 Y.M.Kagan and V.M.Milenin, Soviet Phys.-Technical Phys., 10, 1470,1966

1.4 E.Spenke, Zeits.F.Physik, 127,221,1950

1.5 T.Killian, Phys.Rev., 35,1238,1930

1.6 M.J.Druyvesteyn, Zeits.F.Phys., 81,571,1933

1.7 A. von Engel and M.Steenbeck, Electrische Gasentladungen,Springer,Berlin, Vol. 2, Sec.14-16, 1934

1.8 L.Tonks and I.Langmuir, Phys.Rev., 34,876,1929

1.9 B.Klarfeld, Journ. of Phys., 5, 155, 1941

1.10 N.A.Karelina, Journ. of Phys., 6, 218, 1942

Chapter 2

2.1 H.Margenau, Phys.Rev., 69, 508, 1946

2.2 M.A.Biondi, Rev.Sci.Inst., 22,500, 1951

2.3 E.F.Labuda and E.I.Gordon, J.Appl.Phys.,35,1647,1964

2.4 L.J.Varnerin and S.C.Brown, Phys.Rev.,79,946,1950

2.5 P.Parzen and L.Goldstein, Phys.Rev., 79,190,1950

2.6 E.O.Johnson and L.Malter, Phys.Rev., 80,58,1950

2.7 S.Kojima and K.Takayama, J.Phys.Soc.Japan,4,349,1949

2.8 J.D.Swift,Brit.J.Appl.Phys.,2,134,1969

2.9 K.Jamanoto and T.Okuda, J.Phys.Soc.Japan,11,57,1956

2.10 S.Aisenberg, 23rd Ann.Conf.Phys.Electronics,M.I.T. 200, 1963.

2.11 M.J.Druyvesteyn, Zeits.f.Physik, 64, 791, 1930

2.12 Y.M.Kagan et al, Dokl.Akad.Nauk, U.S.S.R. 76, 215, 1951

REFERENCES (Contd.)

2.13 R.C.G.Leckey, G.S.Higginson and K.G.Emeleus, Nature, 198, 1187, 1963

2.14 J.D.Swift, Proc.5th Int.Conf. on Ionization Phenomena in Gases, 1, 343, 1961

2.15 B.W.Smithers, J.Sci. Inst., 39,21, 1962

2.16 F.W.Crawford, A.Garscadden and R.S.Palmer, Proc. 6th Int.Conf. on Ionization Phenomena in Gases, 4, 53, 1963.

2.17 R.H.Sloane and E.I.R.McGregor, Phil.Mag., 18,193,1934

2.18 R.L.F.Boyd and N.D.Twiddy, Proc.Roy.Soc.A., 250,53,1959.

2.19 R.L.F.Boyd and N.D.Twiddy, Proc.Roy.Soc.A, 259,145,1960

2.20 N.D.Twiddy, Proc.Roy.Soc.A, 262,379,1961

2.21 N.D.Twiddy, Proc.Roy.Soc.A, 275,338,1963

2.22 E.M.Friar, 23rd Ann.Conf.Phys.Electronics, M.I.T., 195, 1963

2.23 N.A.Vorob'eva et al, Sov.Phys.Tech.Phys., 8, 423, 1963

2.24 S.D.Vagner, V.A.Virolainen and Y.M.Kagan, Sov.Phys.Tech.Phys., 14, 502, 1969.

2.25 D.Thomas, Ph.D. thesis, University of London, 1965

2.26 A.I.Kilvington, R.P.Jones and J.D.Swift, J.Sci.Inst., 44, 517, 1967

2.27 S.C.M.Luijendijk and J.Van Eck, Physica, 36,49,1967

2.28 G.R.Branner, E.M.Friar and G.Medicus, Rev.Sci.Inst., 34,231, 1963.

2.29 J.M.Malyshev and V.L.Federov, Dokl.Akad.Nauk, U.S.S.R.,92,269,1953.

REFERENCES (Contd.)

2.30 M.G.Drouet, Can.J.Phys., 46, 227, 1968

2.31 S.W.Rayment and N.D.Twiddy, Nature,Lond.,216,674,1967

2.32 S.W.Rayment and N.D.Twiddy, Proc.9th Int.Conf.on Ionization Phenomena in Gases, 1969.

2.33 S.W.Rayment and N.D.Twiddy, Brit.J.App.Phys.(J.Phys.D) 2, 1747, 1969.

2.34 M.Sicha et al, Czech.J.Phys., B21,62,1971

2.35 Y.M.Kagan, N.B.Kolokolov and V.M.Milenin, Sov.Phys.Tech.Phys., 13, 1468, 1969

2.36 Y.M.Kagan et al, Sov.Phys.Tech.Phys., 16, 88, 1971

2.37 O.N.Oreshak, A.F.Stepanov and V.A.Stepanov, Sov.Phys.Tech.Phys., 16, 93, 1971.

Chapter 3

3.1 I.Langmuir and H.M.Mott-Smith, Gen.Electr.Rev.,26,731,1923.

3.2 M.J.Druyvesteyn, Zeits.f.Physik, 64,791,1930

3.3 Y.M.Kagan and V.I.Perel, Soviet Phys. USP, 6, 767, 1964

3.4 S.E.A.Landale, Proc.Cambridge Phil.Soc.,25,355,1929

3.5 G.R.Branner,E.M.Friar and G.Medicus, Rev.Sci.Inst.,34,231,1963.

3.6 R.H.Sloane and E.I.R.McGregor, Phil.Mag.,18,193,1934

Chapter 4

4.1 S.Tolansky, ' High Resolution Spectroscopy ' , p.39, Methuen, London, 1947.

4.2 D.J.Santerer, Trans.Nat.Symp.,American Vacuum Society, p.1, Pergamon Press, 1958.

REFERENCES (Contd.)

4.3 R.L.F.Boyd and N.D.Twiddy, Proc.Roy.Soc.A,250,53,1959

4.4 S.W.Rayment and Twiddy, Proc.Roy.Soc.A,340,87,1968

4.5 J.F.Waymouth,Physics of Fluids,7,1843,1964

4.6 C.T.Case, 10th Int.Conf.Ionization Phenomena in Gases, p.402, Oxford,1971.

4.7 J.D.Swift, Proc.Phys.Soc.,79,697,1962

4.8 S.L.F.Richards,G.T.Lloyd andR.P.Jones, Int. J. Electr (G.B.) 38,551,1975.

4.9 R.A.Olson and G.Medicus, J.Appl.Phys.,38,4539,1967

Chapter 5

5.1 J.M.Malyshev and V.L.Federov, Dokl.Akad.Nauk.,U.S.S.R., 92,269,1953.

5.2 Mullard Reference Manual for Transistor Circuits,p.304

5.3 A.I.Kilvington,R.P.Jones and J.D.Swift, J.Sci.Inst.,44,517,1967.

Chapter 6

6.1 G.Medicus, 5th Int.Conf.Ioniz.Phen.in Gases, 2,1397,1961.

6.2 M.A.Easley, J.Appl.Phys., 22, 1035, 1952

6.3 G.Medicus and G.Wehner, J.Appl.Phys., 23, 1035, 1952

6.4 A.Garscadden and K.G.Emeleus, Proc.Phys.Soc.,79,535,1962.

6.5 M.J.Druyvesteyn,Zeits.f.Physik,64,791,1930

6.6 A.A.Zaitsev, N.Ya.Vasil'eva and V.M.Mnev, Soviet Physics,J.E.P.T.,9,1130,1959.

REFERENCES (Contd.)

6.7 V.M.Milenin, Soviet Physics -Technical Physics, 16,654, 1971.

6.8 S.C.M.Luijendijk and J.Van Eck, Physica,36,49,1967

6.9 R.S.Hemsworth and N.D.Twiddy, 8th Int. Conf.Phen. in Ionized Gases, Vienna, 1967.

6.10 J.D.Swift, Brit.J.Appl.Phys.,16,837,1965.

Chapter 7

7.1 W.S.Schottky, Physik Zeits, 25, 342 and 635, 1924

7.2 E.Spenke, Zeits.f.Physik, 127,221,1950

7.3 J.S.Townsend and V.A.Bailey, Phil.Mag., 46, 657, 1923

7.4 R.A.Nielsen, Phys.Rev., 117,1411,1936

7.5 J.C.Bowe, Phys.Rev., 117, 1411,1960

7.6 J.A.Hornbeck, Phys.Rev., 83,374,1951

7.7 A.V.Phelps, J.L.Pack and L.S.Frost, Phys.Rev., 117, 470, 1960.

7.8 K.Takayama, Rev.Electr.Commun.Lab., 10,100, 1962

7.9 J.M.Anderson, Physics of Fluids, 7, 1517, 1964

7.10 J.L.Pack and A.N.Phelps, Phys.Rev., 121, 798, 1961

7.11 M.Sugawara and C.J.Chen, J.Appl.Phys.,41,3442,1970

7.12 W.Verweig, Philip Res.Rep.Suppl.,No.2,1961

7.13 H.M.J.Kinderdijk and J.Van Eck, 8th Int.Conf.Ioniz.Phen. in Gases, p.481,1967.

7.14 N.A.Karelina, Journ. of Physics,6,218,1942

7.15 H.B.Dorgelo, H.Alting and J.Boers, Physic. Haag 2, 959,1935

REFERENCES (Contd.)

7.16 R.T.Young, J.Appl.Phys.,2324,1965

7.17 E.F.Labuda and E.I.Gordon, J.Appl.Phys., 35, 1647, 1964

7.18 L.Tonks and I.Langmuir, Phys.Rev.,34,876,1929

Chapter 8

8.1 R.W.Callis and D.T.Tuma, I.E.E.E. Trans on Plasma Science Vol. PS-2, 283, 1974.

8.2 W.L.Nighan, Phys.Rev., 42,1989,1970

8.3 A.von Engel and M.Steenbeck, Electrische Gasentladungen, Springer,Berlin,vol 2 , sec.14-16,1934.

8.4 H.B.Dorgelo,H.Alting and J.Boers, Physic Haag, 2,959,1935

8.5 R.T.Young, J.Appl.Phys.,2324,1965

8.6 E.F.Labuda and E.I.Gordon, J.Appl.Phys., 35,1647,1964

8.7 J.D,Swift, Brit.J.Appl.Phys.(J.Phys.D) 2, 134, 1969

8.8 E.P.Szuszczewicz, J.Appl.Phys.,43,874,1972

8.9 C.T.Case, 10th Int.Conf.Ioniz.Phen. in Gases,402,1971

8.10 Y.S.Chou,L.Talbot and D.R.Willis, Phys.Fluids,9,2150,1966

8.11 J.D.Swift, Proc.Phys.Soc.,79,697,1962

Chapter 9

9.1 N.A.Vorob'eva, Y.M.Kagan and V.M.Milenin, Sov.Phys.Tech.Phys., 8, 423, 1963.

Chapter 10

10.1 A.I.Kilvington, R.P.Jones and J.D.Swift, J.Sci.Inst., 44, 517, 1967.

10.2 S.W.Rayment and N.D.Twiddy, Proc.Roy.Soc.A., 340, 87, 1968.

REFERENCES (Contd.)

Chapter 11

11.1 W.L.Nighan, Phys. Rev., 42, 1989, 1970

11.2 Y.M.Ivanov et al, High Temperature(U.S.A.) Vol.13,433,1975.

11.3 E.Berger and A.Heisen, J.Phys.D., 8, 629, 1975

11.4 S.L.F.Richards, R.P.Jones and G.Lloyd, Int.J.Electronics, 38, 551, 1975.

Appendix 1

A.1.1 H.B.Dorgelo,H.Alting and J.Boers, Physic Haag, 2, 959, 1935.

A.1.2 W.S.Schottky, Physik Zeits, 25, 342 and 635, 1924

A.1.3 R.T.Young, J.Appl.Phys., 2324, 1965

A.1.4 K.Hiraoka and H.Kamada, Jap.J.Appl.Phys.,10,339,1971.

Appendix 2

A.2.1 F.B.Pidduck, Proc.Roy.Soc.A., 88, 296, 1913
Proc.Lond.Math.Soc., 15, 89, 1915.

A.2.2 M.J.Druyvesteyn and F.M.Penning, Rev.Mod.Phys., 12, 88, 1940
Physica 3, 65, 1936.

A.2.3 G.Herz, Z.Phys., 32, 298, 1925

A.2.4 J.A.Smit, Physica, 3, 543, 1937

A.2.5 H.Maier-Leibnitz, Z.Phys., 95, 499-523, 1935

A.2.6 S.M.Dunlop, Nature, Lond., 164,452,1949

A.2.7 W.P.Allis, Encyclopaedia of Physics, Springer-Verlog,Vol.XX1, 404, 1956.

A.2.8 A.E.D.Heylen and T.J.Lewis, Proc.Phys.Soc.Lond., A 271, 531-50,1963.

A.2.9 A.J.Postma, Physica, 43, 581-595, 1969

A.2.10 D.E.Golden and H.W.Bandel, Phys.Rev.,A14,138,1965.

REFERENCES (Contd.)

A.2.11 A.J.Postma, Physica, 45, 609-618, 1970

A.2.12 M.H.Hughes, J.Phys.B., Vol.3, 1544, 1970

A.2.13 P.M.Davidson, Proc.Phys.Soc., B.67, 159-61, 1954

A.2.14 H.S.W.Massey and E.H.S.Burhop,
Electronic and Ionic Impact Phenomena,
2nd. Edn., Vol.1, Oxford,Clarendon Press,
1969.

A.2.15 D.Rapp and P.Englander-Golden,
J.Chem.Phys., 43,1464,1965.

Determination of the average electron energy in the positive column of an He–Ne glow discharge

E E MAINWARING† and J D SWIFT‡
† Bristol Polytechnic, Ashley Down Road, Bristol, BS7 9BU
‡ University of Bath, Claverton Down, Bath, BA2 7AY

MS received 30 March 1972

Abstract. Measurements of the average electron energy in the positive column of an He–Ne glow discharge are reported. A Langmuir probe second-derivative method was used for discharge currents from 20 to 200 mA with a 4 cm radius tube and a gas pressure of 0·06 Torr. Electron energy distribution functions for He–Ne mixtures were determined and from these the average electron energies calculated. The experimental values obtained are shown to give reasonable agreement with a modified version of the Schottky theory.

1. Introduction

An understanding of He–Ne lasers requires that one knows the average electron energy and electron density in He–Ne mixtures as a function of the pressure and the discharge current. A symmetrical double-probe technique has been used (Belousova *et al* 1968) for determining these parameters, but this can be unsatisfactory when the electron energy distribution function is nonmaxwellian. The difficulty can be overcome by deriving the actual form of the electron energy distribution function and from this determining the average electron energy and the electron density. To obtain this information, a Langmuir probe second-derivative method has been used in the positive column of an He–Ne discharge for discharge currents from 20 to 200 mA with a 4 cm radius tube at a gas pressure of 0·06 Torr. This paper describes the technique and some of the results obtained.

2. Measuring technique

The form of the electron energy distribution function $f(V)$ was determined from the following equation (Druyvesteyn 1930):

$$f(V)=BV^{1/2}\frac{\mathrm{d}^2 i_e}{\mathrm{d}V^2} \tag{1}$$

where V is the potential difference between the probe and the plasma, i_e is the electron current to the probe at a retarding potential V, and B is a constant that depends on the area of the probe. The second derivative is determined by introducing a sinusoidal voltage of small amplitude into the probe circuit. It can be shown (Branner *et al* 1963)

that the second harmonic $i_{2\omega}$ of the probe current is related to the second derivative by the equation

$$i_{2\omega}=\frac{E^2}{4}\frac{\mathrm{d}^2 i_e}{\mathrm{d}V^2} \tag{2}$$

where E is the amplitude of the applied sinusoidal voltage. This second harmonic is filtered from the other harmonics of the probe current and amplified. The circuit used is similar to that described in an earlier paper (Kilvington *et al* 1967). A phase-sensitive detector (Brookdeal, type 411) is used to improve the signal-to-noise ratio and yields more accurate measurements of the second-derivative for weak signals in the high-energy part of the distribution function.

3. Vacuum system and discharge tube

The vacuum system was a circulatory flow type constructed entirely of glass except for stainless steel isolation valves which could be outgassed at 450 °C. The system was bakeable and was evacuated to 10^{-7} Torr prior to introducing the spectroscopically pure gases (BOC Grade X). The discharge tube was 8 cm in diameter and 80 cm long. A tungsten filament served as the cathode and a nickel disc as the anode (2·5 cm diameter). The probe was a platinum sphere of 0·5 mm diameter placed near the axis of the discharge tube and 22 cm from the anode.

4. Results

In order to plot the electron energy distribution function it is essential to identify space potential as accurately as possible. In these experiments it was taken as the potential at which $\mathrm{d}^2 i_e/\mathrm{d}V^2=0$. It was shown by Milenin (1971) that the amplitude of the noise reaching the probe has a maximum value at the space potential when no space-charge sheath occurs. He found the noise maximum coincided with the zero of the second-derivative curve. In the present investigation it was found in general that the difference between the maximum of the second-derivative curve and the zero cross was less than 1 V However, in the presence of moving striations, which were detected using a photomultiplier, this difference increased to several volts. All measurements were taken in the absence of moving striations except for the case of pure neon.

A typical electron energy distribution curve is shown in figure 1. This is more attenuated at high energies than a maxwellian distribution. The average electron energy was calculated from the distribution function by applying the equation

$$\bar{V}=\frac{\int_0^\infty Vf(V)\,\mathrm{d}V}{\int_0^\infty f(V)\,\mathrm{d}V}. \tag{3}$$

The average energy of the electrons for various He–Ne mixtures are shown in figure 2 for a pressure of 0·06 Torr and a 100 mA discharge current in a 4 cm radius discharge tube. The average energy is seen to decrease approximately linearly as the percentage of neon increases. It was found that the average electron energy was independent of the discharge current over the range 20–200 mA and electron density was proportional to current over the same range.

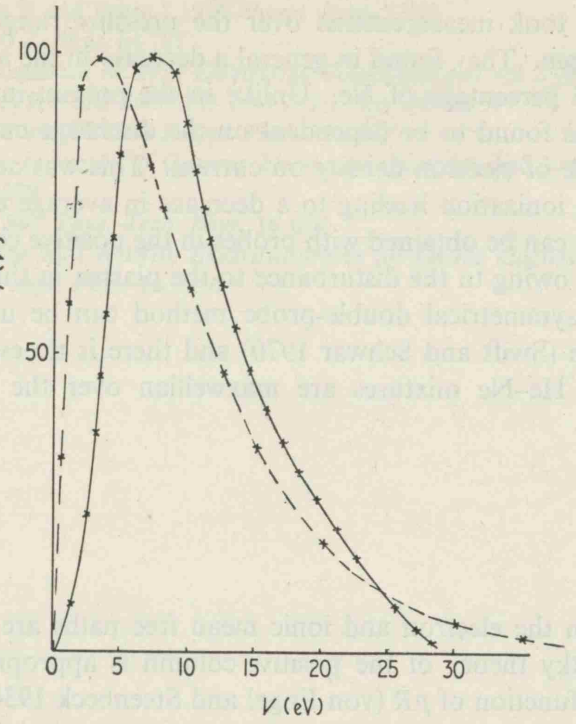

Figure 1. Electron energy distribution function for He–Ne, ratio 9 : 1 at 0·06 Torr and 100 mA. The broken line indicates the maxwellian distribution function for the same mean energy.

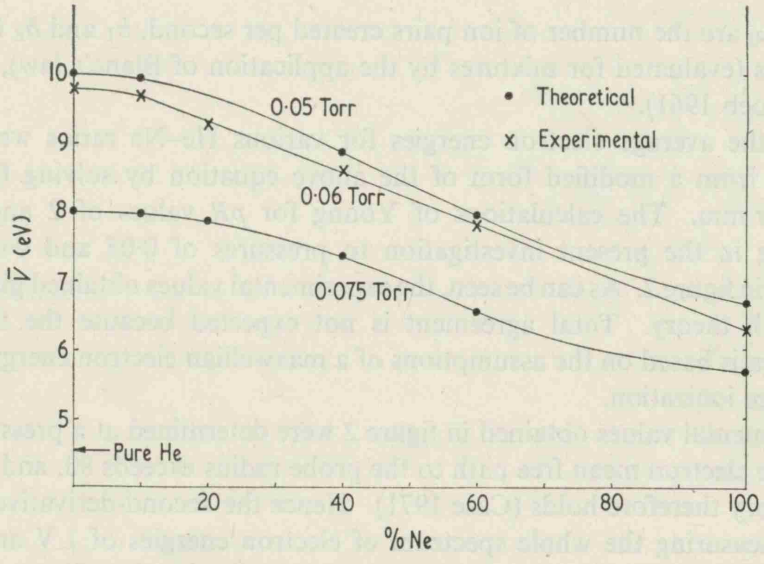

Figure 2. Average energy of electrons as a function of He–Ne ratios measured at 0·06 Torr and 100 mA, for a tube of radius 4 cm.

Labuda and Gordon (1964) measured the average electron energy and density using a noise method for tube radii in the range 1 to 3 mm and with discharge currents of 5–100 mA. Like us, they observed a linear dependence of electron density on discharge current and showed that the average electron energy was a function of pR up to 2·5 Torr mm where cumulative ionization becomes significant.

Belousova *et al* (1968) took measurements over the pressure range 0·35–1·4 Torr using tube radii 1·5 to 7·5 mm. They found in general a decrease in the average electron energy with increase in the percentage of Ne. Unlike in the present investigation, the average electron energy was found to be dependent on the discharge current and there was a nonlinear dependence of electron density on current. This was accounted for by the presence of cumulative ionization leading to a decrease in average electron energy. However, unreliable results can be obtained with probes in the positive column when the radius of the tube is small, owing to the disturbance to the plasma in the vicinity of the probe. Furthermore, the symmetrical double-probe method can be unreliable for a nonmaxwellian distribution (Swift and Schwar 1970) and there is no evidence that the distribution functions for He–Ne mixtures are maxwellian over the pressure range chosen.

5. Discussion

In the present investigation the electron and ionic mean free paths are both less than $R/5$, and hence the Schottky theory of the positive column is appropriate. This was extended to obtain $\bar{V}$ as a function of pR (von Engel and Steenbeck 1934). This theory was further extended to a binary mixture (Dorgelo *et al* 1935), enabling the average electron energy to be calculated from an equation of the form

$$\frac{\alpha_1}{b_1}+\frac{\alpha_2}{b_2}=\tfrac{2}{3}\bar{V}\left(\frac{2{\cdot}4}{R}\right)^2 \tag{4}$$

where α_1 and α_2 are the number of ion pairs created per second, b_1 and b_2 the mobilities of positive ions (evaluated for mixtures by the application of Blanc's law), and R is the tube radius (Loeb 1961).

Values of the average electron energies for various He–Ne ratios were calculated (Young 1965) from a modified form of the above equation by solving for pR values of 1 to 9 Torr mm. The calculations of Young for pR values of 2 and 3 Torr mm (corresponding in the present investigation to pressures of 0·05 and 0·075 Torr) are shown plotted in figure 2. As can be seen, the experimental values obtained give reasonable agreement with theory. Total agreement is not expected because the theory of the positive column is based on the assumptions of a maxwellian electron energy distribution and single-stage ionization.

The experimental values obtained in figure 2 were determined at a pressure for which the ratio of the electron mean free path to the probe radius exceeds 80, and the collisionless probe theory therefore holds (Case 1971). Hence the second-derivative method can be used for measuring the whole spectrum of electron energies of 1 V and above and gives a direct measurement of the electron energy distribution function.

References

Belousova I M, Danilov O B and El'kina I A 1968 *Sov. Phys.–Tech. Phys.* **12** 1229

Branner G R, Friar E M and Medicus G 1963 *Rev. sci. Instrum.* **34** 231

Case C T 1971 *Proc. 10th Int. Conf. on Phenomena in Ionized Gases, Oxford* (Oxford : Donald Parsons) p 402

Dorgelo H B, Alting H and Boers J 1935 *Physic. Haag* **2** 959
Druyvesteyn M 1930 *Z. Phys.* **64** 781
von Engel A and Steenbeck M 1934 *Elektrische Gasentladungen* vol 2 (Berlin: Springer-Verlag) §§14–6
Kilvington A I, Jones R P and Swift J D 1967 *J. sci. Instrum.* **44** 517
Labuda E F and Gordon E I 1964 *J. appl. Phys.* **35** 1647
Loeb L B 1961 *Basic Processes of Gaseous Electronics* (Berkeley and Los Angeles: University of California Press) p 129
Milenin V M 1971 *Sov. Phys.–Tech. Phys.* **16** 654
Swift J D and Schwar M J R 1970. *Electrical probes for plasma diagnostics* (London: Iliffe) p 147)
Young R T 1965 *J. appl. Phys.* **36** 2324

1.1.1

THE MOBILITIES OF ELECTRONS IN HELIUM AND HELIUM-NEON MIXTURES

E.E.MAINWARING + and J.D.SWIFT ++
+ Bristol Polytechnic, Ashley Down Rd.Bristol,England
++ University of Bath, Claverton Down, Bath, England.

roduction

purpose of this paper is to report values of the electron mobilities helium and helium-neon mixtures determined in the range = 2 x 10^{-20} to 2 x 10^{-19} V.m^2 (E is the value of the electric ld intensity and N the gas number density) Electron energy distribution ctions for the gases were determined using a Langmuir probe second ivative method and from these the drift velocities and reduced mobilities culated. Takayama (I) has measured the drift velocity of electrons in ium and in neon using the principle of the Hall effect. Anderson(2) d microwave cavity techniques for measurements in the same gases. se techniques usually have poor space resolution since they measure an rage electron density, whereas Langmuir probe techniques measure the sity at a point.

hod

principle of the measurement of the drift velocities and hence their uced mobilities in the present investigation is as follows. The surements were made in the positive column of a glow discharge. The itive ion contribution to the discharge current is negligible and ce the discharge current may be expressed as

$$I_d = 1.36\, e.V_d.\, n_o.\, R^2 \quad \text{.....(1)}$$

re the e is the electronic charge, V_d the drift velocity, n_o the ctron density at the axis, R the tube radius. The above expression based on the Schottky theory of the positive column which assumes mobility equation holds good and that only single stage ionisation urs. A radial distribution of electron density falling to zero at walls is also assumed. The Schottky theory has been tested by ious workers who have confirmed the theoretical dependence of the ctron density in the radial direction from the tube axis. The radial tribution of the electron density is given by the equation

$$n(r) = n_o.\, J_o\, \frac{2.405\, r}{R} \quad \text{---------(2)}$$

cont/.....

re J_o is a Bessel function of zero order. If two stage ionisation is en into account, it has been shown by Spenke (3) that the resulting tribution curve for the electron density drops down more quickly from axis of the tube. The drift velocities were calculated from equation using electron density values determined from the electron energy tribution curves obtained for the various gases. The reduced electron dility is defined as

$$\mu' = \frac{V_d}{E/p} \quad \text{------(3)}$$

re V_d is the drift velocity, E the field strength and p the pressure the temperature of the glow discharge tube (300°K).

form of the electron energy distribution curves were determined from equation by Druyvesteyn (4)

$$f(V) = BV^{\frac{1}{2}} \frac{d^2 i_e}{dV^2} \quad \text{--------(4)}$$

re V is the potential difference between the probe and the plasma, the electron current to the probe at retarding potential V, and B is a tant that depends on the area of the probe. The second derivative is rmined by introducing a sinusoiial voltage of small amplitude into the e circuit. It has been shown by Brenner et al (5) that the second onic, $i_{2\omega}$ of the probe current is related to the second derivative he equation.

$$i_{2\omega} = \frac{v^2}{4} \frac{d^2 i_e}{dV^2} \quad \text{--------(5)}$$

e v is the amplitude of the applied sinusodal voltage. The second onic is filtered from the other harmonics of the probe current and ified.

ase sensitive detector is used to improve the signal to noise ratio yields more accurate measurements of the second derivative for weak als in the high energy tail of the distribution curve.

ratus

investigation was carried out in a pyrex tube of 4 cm diameter and 80 cm . A tungsten filament was used as the cathode and a nickel disc as the e. Spherical platinum probes of 0.5 mm diameter were positioned at 7 cm rvals along the length of the tube and were placed near the axis. The m system and electronic detection apparatus is similar to that described lously (6). Spectroscopically pure gases obtained from the British Oxygen any were used in the investigation.

ts and Discussion

dical electron energy distribution curve for helium-neon (80/20) is shown g 1. The area under the distribution curve was computed using

cont/.....

computer ICL1902A, programmed using the Fortran system. The electron density at the axis was obtained from this area and used to obtain the drift velocity and reduced mobility.

The reduced mobilities observed for helium and helium-neon mixtures as a function of E/N are shown in Fig 2. The results are compared with those obtained by other workers for the pure gases helium and neon.

There are several inherent errors in the probe technique used in the present investigation. Foremost amongst these is the exact determination of space potential which is used as the origin of the electron energy distribution curve. In an ideal case the second derivative of the probe current vanishes at the space potential. However, in practice, in the region of space potential secondary effects occur which prevent this abrupt fall to zero. These secondary effects include contamination of the probe surface, emission from the probe by impinging particles and the presence of oscillations (moving striations) in the discharge. In the present investigation moving striations were detected, using a photomultiplier, for many of the helium-neon mixtures and for pure neon. Measurements were taken in regions of pressure and discharge current where moving striations were known to be absent. The space potential was taken as the potential at which the second derivative crossed the zero axis $\left(\text{i.e. } \frac{d^2 i_e}{dV^2} = 0\right)$

In the absence of moving striations it was found that the difference between the maximum and zero cross of the second harmonic was less than 1 volt, which gives an error of less than 10% in the values of the reduced mobility.

The mobility values determined in the present investigation for helium were generally 30% higher than those obtained by Anderson (2) using microwave techniques. The difference is only partly explained by the difficulties in determining the space potential as discussed above. However, microwave techniques generally have poor space resolution and give an average value of the electron density across the discharge tube. This could be a contributory factor in the discrepancy between the results obtained by the probe technique used in the present investigation with those obtained by microwave techniques.

REFERENCES

(1) K.Takayama, Rev. Elect.Commun.Lab., 10, 100, 1962
(2) J.M.Anderson, The Physics of Fluids, 7, 1517, 1964.
(3) E.Spenke, Zeits F. Physik, 127, 221, 1950
(4) M.J.Druyvesteyn, Zeits, F.Physik, 64, 791, 1930
(5) G.R.Branner, E.M.Friar and G Medicus. Rev.Sci.Inst.,34,231, 1963.
(6) E.E.Mainwaring and J.D.Swift, Journal of Physics D, 5,1433, 1972.

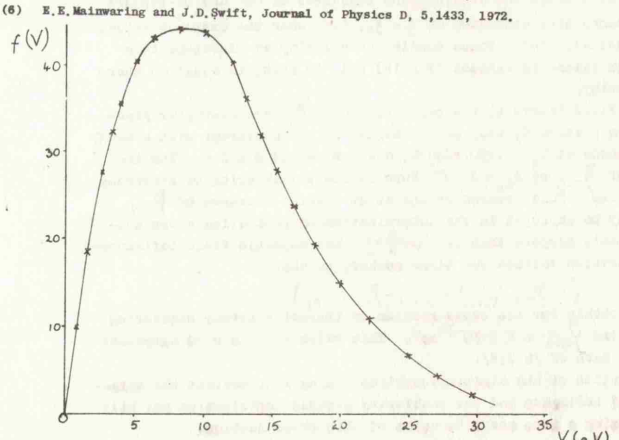

Fig. 1. Electron energy distribution for He-Ne (80/20) at 75 x 10^{-3} torr and 100 mA discharge current.

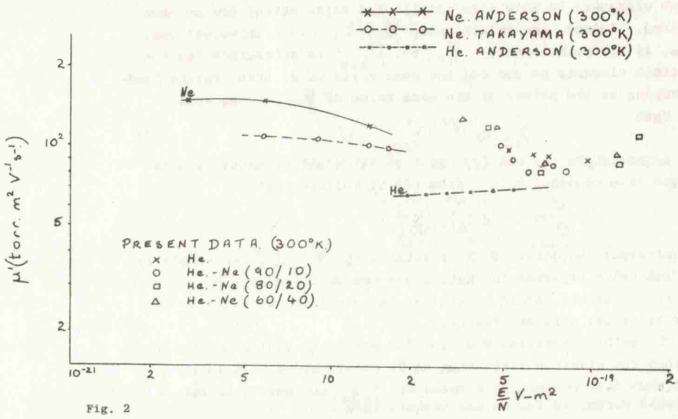

Fig. 2

The reduced electron mobilities in helium and helium-neon mixtures as a function of E/N.

1.1.2

MEASUREMENTS OF CROSS SECTIONS FOR THERMAL ELECTRON SCATTERING ON Cs AND Ba ATOMS

by V.I.Babanin, Yu.A.Dunaev, A.S.Mustafaev, V.I.Sitnov, A.Ya.Ender

A.F.Ioffe Physical Technical Institute, USSR Academy of Sciences, Leningrad, USSR

Measurement of the scattering cross sections at thermal energies of electrons has proved a very difficult task. In the present report a method is described which uses some peculiarities of the transverse magnetic field influence upon the current in a thermionic converter with an operating mode intermediate between collisionless and collisional modes.

The thermionic converter with Cs-Ba vapours, is used whose main feature is that work function of its cathode can be varied in a wide range by varying Ba-vapour pressure, while ions are produced as a result of Cs-vapour surface ionisation.

The transverse magnetic field influence on a converter operating in the collisionless (Knudsen) mode was studied in /1-5/. In /1/ as distinct from /5/ it is shown that this influence results in the change of the saturation current value, and this effect is employed for investigation of a thermionic plasma and a converter cathode in the collisionless mode /3/. If Ba-vapour pressure is increased while cathode temperatures and Cs-vapour pressures remain constant cathode work function and compensation ratio, γ, decrease monotonously.

$$\gamma = \frac{n_{i+(0)}}{n_{e+(0)}} \qquad (1)$$

Here $n_{i+(0)}$ ($n_{e+(0)}$) concentration of ions (electrons) produced on the cathode. Under these conditions one observes typical maximum points on the curve "saturation current vs. Ba-vapour pressure (Fig.1a) and minimum points on the curve "saturation current ratio ξ vs. S-parameter" (ξ is a ratio of the current in the presence of the transverse magnetic field, j_H, to the corresponding current in the absence of the field, j, "S" is a parameter proportional to the magnetic field strength). From the analysis demonstrated, in /4/ it follows that the extremum points mentioned above are attained at $\gamma = \gamma_0 = 0.405$, i.e. at the transition from the overcompensated to the undercompensated mode. At $\gamma = \gamma_0$ a cathode sheath potential drop becomes minimal and has a value of 0.345 kT/e. During experiments reported here which were carried out at different pressures of Cs- and Ba-vapours measurements were conducted at $\gamma = \gamma_0$, i.e. when the extremum values were attained. Under these conditions velocity of electrons in a converter plasma is minimal (Fig.1b) and, in fact, is equal to thermal velocity.

In Fig.2 (curve 1) the relationships "ξ_{min} vs. Cs-vapour pressure" are presented; they were obtained in the converter with a tungsten cathode at T_k = 1850-2000°K, d = 0.8 mm and S = 2.4. The increase of ξ_{min} at $P_{Cs} > 2\cdot10^{-2}$ Torr is due to scattering of electrons on Cs atoms. This process brings about a large increase of ξ_{min} which may be employed in the determination of scattering cross-section. Let's suppose that at $Kn = \frac{d}{\lambda} = 1$ the magnetic field influences the saturation current two times weaker, so that

$$(1-\xi_{min}(_{Kn=1})) = \tfrac{1}{2}(1-\xi_{min}(_{Kn=\eta_1}))$$

then we obtain for the cross-section of thermal electron scattering on Cs atoms $Q_{eCs} = 2.6\cdot10^{-14}$ cm^2. This value is in a good agreement with the data of /6,7,8/.

Solution of the kinetic equations taking into account the magnetic field influence and the scattering process contribution may help in obtaining a more accurate value of this cross section.

The method described above may be successfully used for measurement of cross-section ratios in experiments involving vapours of different elements; in this case complicated calculations are no more required. Indeed, the relationship $\xi_{min}(Kn)$ is a universal one, hence, if the relationship "ξ_{min} vs. P_{a_1}/P_{a_2}" is determined for two different elements at one and the same value of S, then, taking Knudsen values at the points of the same value of ξ_{min} to be equal, will have

$$Q_{ea_1} n_a^{(1)} d^{(1)} = Q_{ea_2} n_a^{(2)} d^{(2)} \qquad (2)$$

Here superscripts (1) and (2) refer to different elements, and n_a denotes atom concentration. From (2) it follows that

$$\frac{Q_{ea_1}}{Q_{ea_2}} = \frac{n_a^{(2)} d^{(2)}}{n_a^{(1)} d^{(1)}} = \frac{P_a^{(2)} d^{(2)}}{P_a^{(1)} d^{(1)}} \qquad (3)$$

The universal character of the relationship $\xi_{min}(Kn)$ can be easily verified using experimental data since the relationships $\xi_{min}(P_a)$ for different elements should be similar and displaced relative to each other along the axis of pressures.

The method described was used for measuring ratios of the cross sections for electron scattering on Cs and Ba atoms. It is to be noted that data concerning a value of Q_{eBa} are not to be met in published works, as far as the authors know.

To obtain the relationship $\xi_{min}(P_{Ba})$ a thermionic converter with a tantalum cathode was used because in this case, due to lower adsorption energies of Ba-vapours on tantalum, value of the compensation ratio $\gamma = \gamma_0$ is attained at such higher Ba-vapour pressures in comparison with the thermionic converter having the tungsten cathode; this effect becomes quite prominent at higher cathode temperatures, as is illustrated by Fig.3, which shows the saturation current as a function of P_{Ba} for different cathode temperatures, solid curves referring to the tungsten cathode, dotted curves to the tantalum one. In this case, in order to exclude the influence of scattering processes, measurements were conducted at d = 0.1 mm. The relationships $\xi_{min}(P_{Ba})$ are presented in Fig.2 (curve 2). It is seen that the curves $\xi_{min}(P_{Cs})$ and $\xi_{min}(P_{Ba})$ are nearly identical as to their shape. This is illustrated by tabular values as well - see the table below containing pressure ratio values at different levels of ξ_{min}

ξ_{min}	0.4	0.45	0.5	0.55	0.6
P_{Cs}/P_{Ba}	0.122	0.13	0.122	0.124	0.12

In the experiments the interelectrode distance ($d^{(1)} = d^{(2)}$) was 0.8 mm. Hence, one obtains on the average $Q_{eBa}/Q_{eCs} = P_{Cs}/P_{Ba} = 0.124$

Using a value of Q_{eCs} which was obtained in the experiment (it proves to be the same as in /6-8/) the authors determined

$$Q_{eBa} = 3.2\cdot10^{-15}\,\text{cm}^2$$

References

1. A.Ya.Ender, Zh.Tekh.Fiz. (USSR), 3, 551 (1970).
2. Yu.G.Korosov, A.Ya.Ender, Zh.Tekh.Fiz., 11, 2412 (1971).
3. V.I.Babanin, Yu.A.Dunaev, A.S.Mustafaev, V.I.Sitnov, A.Ya.Ender, Zh.Tekh.Fiz., 8, 1662 (1972).
4. V.I.Babanin, A.S.Mustafaev, V.I.Sitnov, A.Ya.Ender, Zh.Tekh.Fiz. 10, 2144 (1972).
5. A.Schock, J.Appl.Phys., 31, 1978 (1960).
6. G.A.Dushev, Thesis, Inst. for Research on Semiconductors, USSR Academy of Sciences, Leningrad, 1967.
7. V.Ya.Kulik, P.P.Kulik, V.A.Riabyi, Teplofiz.Vys.Temp., 10, 715, (1972).
8. L.P.Harvis, J.Appl.Phys., 34, 2958 (1963).

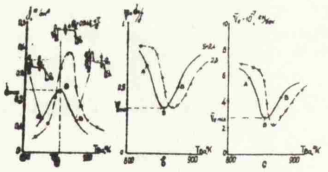

Fig. 1 Dependencies of the electron current, j, (a), the saturation current ratio, ξ, (b) and the average electron velocity in a plasma, V_e, (c) on T_{Ba} at T_e=1850°K(solid curves) and T_e=1920°K (dotted curves); $P_{Cs}=2\cdot10^{-4}$ Torr .

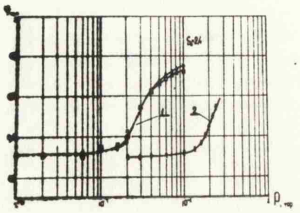

Fig.2 Dependence of ξ_{min} on the filling gas pressure 1-Cs; 2-Ba; T_e = 1850; Δ -1920; o-2000°K; d=0,8mm.

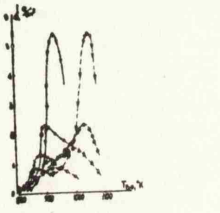

Fig.3 Dependence of the electron saturation current density j on T_{Ba} for the tungsten cathode (solid curves) and tantalum cathode (dotted curves); $P_{Cs}=10^{-4}$Torr. T_e=1100°K; T_e o-1650; o-1800; o-1850; o-2000; T-2100°K; d=0,1mm.

ELECTRON ENERGY DISTRIBUTION FUNCTIONS IN HE-NE AND HE-N_2 MIXTURES.

E.E. Mainwaring and J.D. Swift

Introduction

The electron energy distribution function is a significant characteristic of the positive column. An understanding of lasers and other devices requires that one should determine the shape of the high energy tail of the distribution function and its variation with pressure and discharge current.
For a long time it was thought that the electron energy distribution in the positive column was Maxwellian. However, it has been shown that the distribution is only Maxwellian for a very small range of discharge conditions. Outside this range the distribution deviates and in some cases takes up an approximately Druyvesteyn form.
To obtain this information, a Langmuir probe second-derivative method has been used in an He-Ne discharge for currents from 20 to 200mA with a 20mm radius tube at pressures between 0.06 Torr and 0.25 Torr. A He-N_2 discharge has also been investigated in a 40mm radius tube for pressures in the range 0.05 Torr to 0.25 Torr. This discharge tube carried a movable probe for investigating the variation of the electron energy distribution functions radially.

Experimental set-up and measuring technique

The electron energy distribution function was determined using the Druyvesteyn equation [1] . The second derivative of the probe current with respect to the probe voltage was found using a similar circuit to that described previously [2] . The probes were platinum spheres of 0.5mm diameter and were located on the axis at equal intervals along the length of the tube. The movable probe used for radial measurements in the 40mm radius tube employed a permanent magnet for controlling it. The mixtures were prepared by the British Oxygen Company, Special Gases Department and were analysed using chromatographic techniques.

Results

The variation with pressure of the shape of the electron energy distribution functions was examined for both mixtures. These are shown in Fig.1 for He-Ne and in Fig.2 for He-N_2. Also shown are the Maxwellian and Druyvesteyn distribution functions at the same mean energy. For both mixtures the high energy tail becomes more attenuated as the pressure increases and has a similarity in some cases with the Druyvesteyn form.

E.E. Mainwaring: Physics Department, Bristol Polytechnic
(now with City of Liverpool Education Department)

J.D. Swift : School of Physics, University of Bath.

The variation with discharge current was examined for the current range 50mA to 200mA for a He-Ne mixture, ratio 90/10 at a pressure of 0.1 Torr in the 20mm radius discharge tube. The curves have been normalised in area and are shown in Fig.3. The distribution curve was found to be practically independent of the discharge current in the measured current range at low pressures. This was also found to be the case for all mixtures examined.

The variation with mixture ratio was examined for helium and three helium-neon mixtures of ratios 90/10, 80/20 and 60/40 at the same pressure and discharge current. The investigation was carried out in a 20mm radius discharge tube and the distribution functions obtained are shown in Fig. 4. Helium-nitrogen mixtures were also investigated for variation with mixture ratio. For the helium-neon mixture the increasing of the neon component in the gas mixture produced an attenuation of the high energy tail of the electron energy distribution function. An attenuation of the high energy tail with increase in percentage of nitrogen was also found for the helium-nitrogen mixtures.

The variation with location longitudinally was examined using probes of the same diameter and placed at equal intervals along the length of the discharge tube. It was found that the distribution functions were similar except near the anode and cathode ends for the pressure range examined. The discharge was also examined radially and it was found that the distribution function at the axis and 10mm from the tube wall were approximately the same in shape. These are shown in Fig.5 for a helium-nitrogen (95/5) in a 40mm radius discharge tube.

The dependence on tube radius was investigated by comparing the distribution curves obtained using the 20mm and 40mm radius tubes under the same discharge conditions. It was found that the distribution curves were more rapidly depleted of high energy electrons in the 40mm tube than in the 20mm tube at the same pressure and discharge current. This is shown in Fig.6 for a helium-neon mixture. This depletion of high energy electrons is a result of a decrease of E/p with increase in pR.

It can be shown that the average electron energy is related to E/p by the equation

$$\bar{V} \simeq \frac{\lambda_o \, (E/p)}{(2K)^{1/2}}$$

where K is the average fraction of energy lost in a collision and $\lambda_o = \lambda e/p$ where λ_e is the mean free path of the electrons. It can also be shown that the average electron energy is a function of pR

Hence

$$E/p = f(pR)$$

With a decrease in average electron energy due to a fall in E/p a depletion of electrons in the high energy tail of the distribution function is expected.

A similarity relation is established in the present investigation by plotting $\bar{V}$ as a function of pR for the 20mm and 40mm radius tubes. Generally the points were found to lie on a curve independent of the radius of the tube. The results are shown in Fig. 7 for a helium-neon mixture. The theoretical values calculated by Young [3] are plotted for

comparison. The experimental values of Lubuda and Gordon [4] for a helium-neon mixture (5/1) are also shown. These were obtained by measuring the noise temperature of the discharge for tube diameters 2 to 6mm. A universal curve independent of the tube radius was obtained.

Conclusions

The shape of the electron energy distribution curves, obtained for the helium-neon and helium-nitrogen mixures, disagreed with both the Maxwellian and Druyvesteyn forms. This is to be expected because neither distribution law allows for the effects of inelastic collisions.

References

[1] M.J. DRUYVESTEYN, ZEITS F. PHYSIK, 64, 791, 1930

[2] E.E. MAINWARING AND J.D. SWIFT, JOURNAL OF PHYSICS,D, 5, 1433, 1972

[3] R.T. YOUNG, J. APPL, PHYS. 36, 2324, 1965

[4] E.F. LABUDA AND E.I. GORDON, J. APPL. PHYS, 35, 1647, 1964.

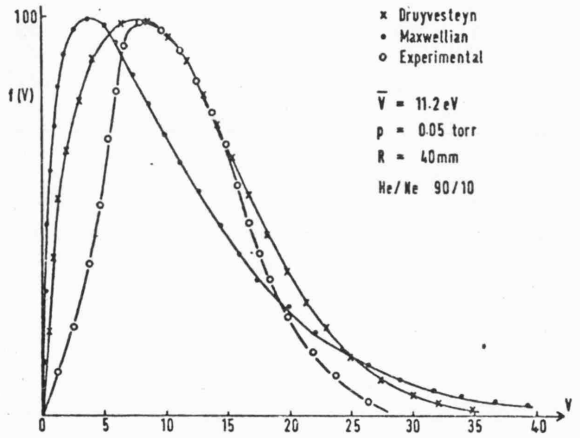

Figure 1. Electron energy distribution in the positive column in He/Ne (90/10).

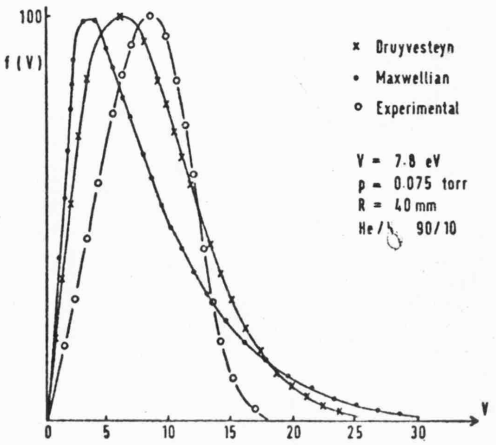

Figure 2. Electron energy distribution in the positive column in He/N_2 (90/10).

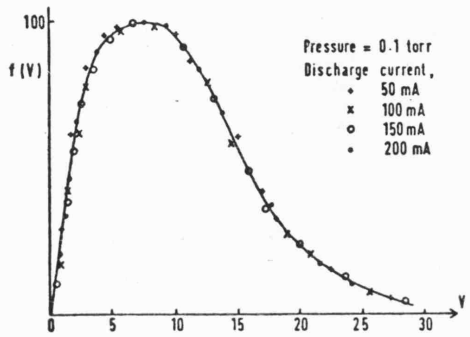

Figure 3. Electron energy distribution in a He-Ne mixture (90 / 10), variation with discharge current. $\overline{V}$ = 9.8 eV.

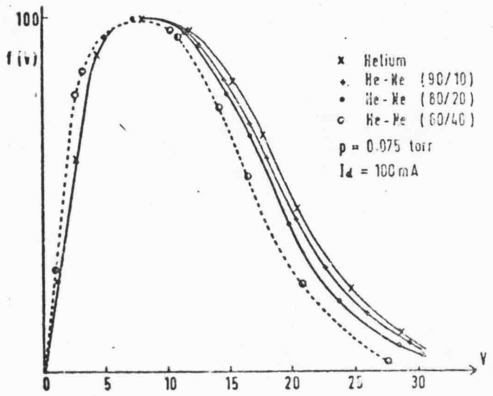

Figure 4. Variation of the experimental distribution curve with helium-neon ratio.

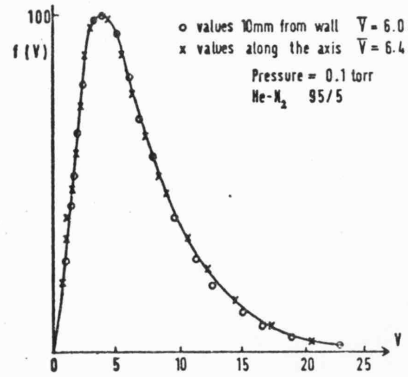

Figure 5. Electron energy distribution functions at the axis and near the wall.

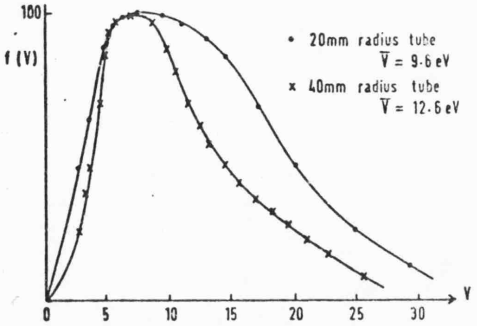

Figure 6. Electron energy distribution in helium-neon, ratio 9:1 at 0.06 torr pressure and 100mA discharge current.

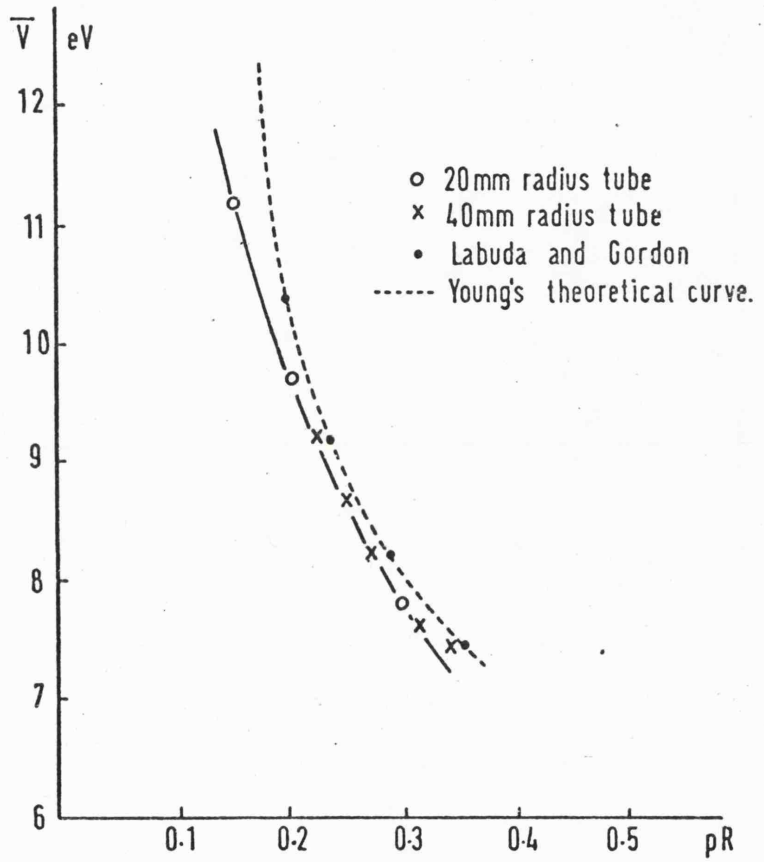

Figure 7. Dependance $\overline{V}$ on pR for helium-neon (80/20).